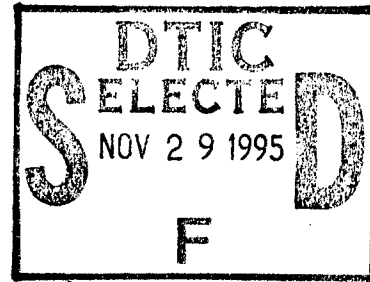


SEMICONDUCTOR LASER ARRAY COOLER DEVELOPMENT

Geoffrey O. Campbell

**Saddleback Aerospace
26012 Marguerite Pkwy, No. 133
Mission Viejo, CA 92691**



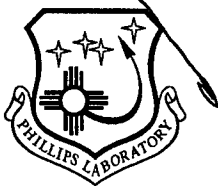
March 1994

Final Report

Distribution authorized to DoD components only; Proprietary Information; March 1994. Other requests for this document shall be referred to AFMC/STI.

WARNING - This document contains technical data whose export is restricted by the Arms Export Control Act (Title 22, U.S.C., Sec 2751 et seq.) or The Export Administration Act of 1979, as amended (Title 50, U.S.C., App. 2401, et seq.). Violations of these export laws are subject to severe criminal penalties. Disseminate IAW the provisions of DoD Directive 5230.25 and AFI 61-204.

DESTRUCTION NOTICE - For classified documents, follow the procedures in DoD 5200.22-M, Industrial Security Manual, Section II-19 or DoD 5200.1-R, Information Security Program Regulation, Chapter IX. For unclassified, limited documents, destroy by any method that will prevent disclosure of contents or reconstruction of the document.



**PHILLIPS LABORATORY
Space and Missiles Technology Directorate
AIR FORCE MATERIEL COMMAND
KIRTLAND AIR FORCE BASE, NM 87117-5776**

19951127 073

DTIC QUALITY INSPECTED 8

UNCLASSIFIED



AD NUMBER

AD-B205 228

NEW LIMITATION CHANGE

TO

DISTRIBUTION STATEMENT A -
Approved for public release; Distribution unlimited.

Limitation Code: 1

FROM

DISTRIBUTION STATEMENT -

Limitation Code:

AUTHORITY

Janet E. Mosher, Phillips Lab., Kirtland AFB, N. M.

THIS PAGE IS UNCLASSIFIED

PL-TR-94-1090

This final report was prepared by Saddleback Aerospace, Mission Viejo, CA under Contract F29601-93-C-0039 Job Order, 9991SBIR, with Phillips Laboratory, Kirtland Air Force Base, New Mexico. The Laboratory Project Officer-in-Charge was Larry Crawford, (VTPT).


When Government drawings, specifications, or other data are used for any purpose other than in connection with a definitely Government-related procurement, the United States Government incurs no responsibility or any obligation whatsoever. The fact that the Government may have formulated or in any way supplied the said drawings, specifications, or other data, is not to be regarded by implication, or otherwise in any manner construed, as licensing the holder, or any other person or corporation; or as conveying any rights or permission to manufacture, use, or sell any patented invention that may in any way be related thereto.

This report has been authored by a contractor of the United States Government. Accordingly, the United States Government retains a nonexclusive royalty-free license to publish or reproduce the material contained herein, or allow others to do so, for the United States Government purposes.


This report contains proprietary information and shall not be either released outside the government, or used, duplicated or disclosed in whole or in part for manufacture or procurement, without the written permission of the contractor. This legend shall be marked on any reproduction hereof in whole or in part.


If your address has changed, if you wish to be removed from the mailing list, or if your organization no longer employs the addressee, please notify PL/VTPT, 3550 Aberdeen Ave SE, Kirtland AFB, NM 87117-5776 to help maintain a current mailing list.

This report has been reviewed and is approved for publication.


LARRY CRAWFORD
Project Officer

FOR THE COMMANDER


DAVID KRISTENSEN, Lt Col, USAF
Chief, Space Power and Thermal
Management Division


HENRY L. PUGH, JR., Col, USAF
Director of Space and Missiles Technology

DO NOT RETURN COPIES OF THIS REPORT UNLESS CONTRACTUAL OBLIGATIONS OR NOTICE ON A SPECIFIC DOCUMENT REQUIRES THAT IT BE RETURNED.

The following notice applies to any unclassified (including originally classified and now declassified) technical reports released to "qualified U.S. contractors" under the provisions of DoD Directive 5230.25, Withholding of Unclassified Technical Data From Public Disclosure.

NOTICE TO ACCOMPANY THE DISSEMINATION OF EXPORT-CONTROLLED TECHNICAL DATA

1. Export of information contained herein, which includes, in some circumstances, release to foreign nationals within the United States, without first obtaining approval or license from the Department of State for items controlled by the International Traffic in Arms Regulations (ITAR), or the Department of Commerce for items controlled by the Export Administration Regulations (EAR), may constitute a violation of law.
2. Under 22 U.S.C. 2778 the penalty for unlawful export of items or information controlled under the ITAR is up to two years imprisonment, or a fine of \$100,000, or both. Under 50 U.S.C., Appendix 2410, the penalty for unlawful export of items or information controlled under the EAR is a fine of up to \$1,000,000, or five times the value of the exports, whichever is greater; or for an individual, imprisonment of up to 10 years, or a fine of up to \$250,000, or both.
3. In accordance with your certification that establishes you as a "qualified U.S. Contractor", unauthorized dissemination of this information is prohibited and may result in disqualification as a qualified U.S. contractor, and may be considered in determining your eligibility for future contracts with the Department of Defense.
4. The U.S. Government assumes no liability for direct patent infringement, or contributory patent infringement or misuse of technical data.
5. The U.S. Government does not warrant the adequacy, accuracy, currency, or completeness of the technical data.
6. The U.S. Government assumes no liability for loss, damage, or injury resulting from manufacture or use for any purpose of any product, article, system, or material involving reliance upon any or all technical data furnished in response to the request for technical data.
7. If the technical data furnished by the Government will be used for commercial manufacturing or other profit potential, a license for such use may be necessary. Any payments made in support of the request for data do not include or involve any license rights.
8. A copy of this notice shall be provided with any partial or complete reproduction of these data that are provided to qualified U.S. contractors.

D E S T R U C T I O N N O T I C E

For classified documents, follow the procedures in DoD 5200.22-M, Industrial Security Manual, Section II-19 or DoD 5200.1-R, Information Security Program Regulation, Chapter IX. For unclassified, limited documents, destroy by any method that will prevent disclosure of contents or reconstruction of the document.

DRAFT SF 298

1. Report Date (dd-mm-yy) March 1994		2. Report Type Final		3. Dates covered (from... to) 12-93 to 2-94		
4. Title & subtitle Semiconductor Laser Array Cooler Development				5a. Contract or Grant # F29601-93-C-0039		
				5b. Program Element # 62601F		
6. Author(s) Geoffrey O. Campbell				5c. Project # 9991		
				5d. Task # SB		
				5e. Work Unit # 1R		
7. Performing Organization Name & Address Saddleback Aerospace 26012 Marguerite Pkwy, No. 133 Mission Viejo, CA 92691				8. Performing Organization Report #		
9. Sponsoring/Monitoring Agency Name & Address Phillips Laboratory 3550 Aberdeen Ave SE Kirtland AFB, NM 87117-5776				10. Monitor Acronym		
				11. Monitor Report # PL-TR-94-1090		
12. Distribution/Availability Statement Distribution authorized to DoD components only; Proprietary Information; March 1994. Other requests shall be referred to AFMC/STI.						
13. Supplementary Notes This report is published in the interest of STINFO exchange. The established procedures for editing reports were not followed for this technical report.						
14. Abstract Progress in the development of Semiconductor Laser Diode Arrays (SLDAs) has resulted in high efficiency, compact devices suitable for use in a variety of applications. As these devices are driven to operation at increasing power levels, heat dissipation problems can limit the peak power, lasing line stability, and/or the lifetime of the array. Already, SLDAs currently being fabricated have heat dissipation requirements that cannot be met by conventional heat sink or cold plate technology. New, more effective heat dissipation technologies are required.						
15. Subject Terms Semiconductor Laser Diode Arrays, heat dissipation, array, heat sink						
Security Classification of				19. Limitation of Abstract	20. # of Pages	21. Responsible Person (Name and Telephone #)
16. Report Unclassified	17. Abstract Unclassified	18. This Page Unclassified	Limited			

**GOVERNMENT PURPOSE LICENSE RIGHTS
(SBIR PROGRAM)**

Contract Number: F29601-93-C-0039

**Contractor: Saddleback Aerospace
Mission Viejo, CA**

For a period of four (4) years after delivery and acceptance of the last deliverable item under the above contract, this technical data shall be subject to the restrictions contained in the definition of "Limited Rights" in DFARS clause at 252.227-7013. After the four-year period, the data shall be subject to the restrictions contained in the definition of "Government Purpose License Rights" in DFARS clause at 252.227-7013. The Government assumes no liability for unauthorized use or disclosure by others. This legend shall be included on any reproduction thereof and shall be honored only as long as the data continues to meet the definition on Government purpose license rights.

PREFACE

This Final Report documents work performed by Saddleback Aerospace for the USAF/Phillips Laboratory during a Phase I SBIR effort. The technical monitor for the program was Ms. Mary Corrigan of PL/VTPT, who was assisted by Dr. Donald Gluck of The Aerospace Corporation. The Program Manager and Principal Investigator for the contract was Mr. Geoffrey O. Campbell. Thanks are due Dr. David G. Paquette (AMITA) and Dr. Gluck for their technical assistance.

Metric units have been used throughout the text, except for pressure, where the psi (lb/in²) is used.

Accession For	
NTIS CRA&I	<input checked="" type="checkbox"/>
DTIC TAB	<input checked="" type="checkbox"/>
Unannounced	<input type="checkbox"/>
Justification	
By	
Distribution/	
Availability Codes	
Dist	Avail and/or Special
E-4	

CONTENTS

<u>Section</u>		<u>Page</u>
1.0	INTRODUCTION	1
2.0	SURVEY OF THE LITERATURE	6
	2.1 MICROCHANNEL TEST DATA REVIEW	7
	2.2 ANALYSIS/OPTIMIZATION OF MICROCHANNEL DESIGNS	20
3.0	DESIGN REQUIREMENTS	25
	3.1 DESCRIPTION OF THE SLDA COOLING PROBLEM	27
	3.2 PHASE I DESIGN GOALS	28
4.0	ANALYTIC TRADE STUDIES	30
	4.1 1D MICROCHANNEL SIZING STUDIES	30
	4.2 2D MICROCHANNEL FLOW STUDIES	39
	4.3 2D FACEPLATE/HEAT SPREADER DESIGN STUDIES	44
5.0	PROTOTYPE MODEL DESIGN AND FABRICATION	52
	5.1 PROTOTYPE MODEL DESIGNS	52
	5.2 FABRICATION PROCESS OVERVIEW	56
	5.3 FABRICATION OF THE PROTOTYPE MODELS	58
6.0	TESTING OF THE PROTOTYPE MODELS	63
	6.1 FLOW PERFORMANCE TESTING	64
	6.2 THERMAL PERFORMANCE TESTING	65
7.0	CONCLUSIONS AND RECOMMENDATIONS	69
	REFERENCES	72

FIGURES

<u>Figure</u>		<u>Page</u>
1.	Saddleback Aerospace microchannel cooling concept.	3
2.	Phase I microchannel cooler during exposure to 500 W/cm ² heat flux.	2
3.	Conventional microchannel construction.	6
4.	Thermal spreading phenomenon.	9
5.	LLNL diamond carrier mounting configuration.	11
6.	Side-mounting of laser diodes on wafer coolers.	12
7.	Heat transfer and pressure drop results from Reference 10.	16
8.	Comparison of electronics cooling techniques.	26
9.	Phase I design requirements - 1D SLDA configuration.	29
10.	1D calculations of temperature drop across the microchannel faceplate	31
11.	1D heat spreader sizing analysis.	32
12.	Comparison of silicon and copper microchannel performance.	35
13.	Performance of 25 μ m microchannels with 100 μ m secondary fins.	36
14.	Performance of 25 μ m microchannels with 50 μ m secondary fins.	37
15.	Performance of 25 μ m microchannels with 25 μ m secondary fins.	38
17.	Streamlines for simple microchannel with 1/4 aspect ratio.	40
18.	Streamlines for simple microchannel with 1/2 aspect ratio.	42
19.	Thermal profiles for copper faceplate for several copper thicknesses.	46
20.	Thermal profiles for copper faceplate with isotropic diamond heat spreader.	48
21.	Thermal profiles for copper faceplate with CVD diamond heat spreader.	50
22.	Sketch of impingement microchannel prototype design (inlet foil).	54
23.	Flow concept for inlet, outlet and spacer foils.	55

FIGURES (concluded)

<u>Figures</u>		<u>Pages</u>
24.	Laminated foil microchannel fabrication process.	57
25.	Microchannel section of etched foils (approximately 32X).	61
26.	Soldering fixtures used in the Phase I study.	62
27.	The three microchannel models fabricated in this program.	62
28.	Model holders for flow and thermal performance testing.	63
29.	Pressure drop performance of prototype models.	64
30.	Thermal performance of impingement prototype.	66
31.	Heat transfer coefficient as a function of mass flow rate.	67

1.0 INTRODUCTION

Progress in the development of Semiconductor Laser Diode Arrays (SLDAs) has resulted in high efficiency, compact devices suitable for use in a variety of applications. As these devices are driven to operation at increasing power levels, heat dissipation problems can limit the peak power, lasing line stability, and/or the lifetime of the array. Already, SLDAs currently being fabricated have heat dissipation requirements that cannot be met by conventional heat sink or cold plate technology. New, more effective heat dissipation technologies are required.

One of the most promising emerging thermal management approaches is the use of "microchannel" cooling, wherein cooling is provided by hundreds of miniature passages. Microchannels have excellent heat transfer capabilities; typically a microchannel cooler can achieve a 20X decrease in thermal resistance as compared with a conventional water-cooled heatsink. These gains are due to: 1) the large heat transfer area/unit volume, 2) the large convective heat transfer coefficients due to the small hydraulic radius of the channels, and 3) reduced thermal resistance of the plate assembly due to the thin face sheet.

There are issues associated with current microchannel designs, however. The micro-machining and anisotropic etching techniques used to create microchannels restrict design choices and limit the attainable channel aspect ratio. The geometry resulting from the etching process also complicates the design of the inlet and outlet manifolds. The current approaches have resulted in delicate structures, with questionable suitability for practical use. These issues are responsible for the relatively slow development of the microchannel concept; while the first work was done as early as 1980, it was until 1991 that a complete prototype cooling system was developed.

Saddleback investigated an alternative microchannel fabrication approach in the Phase I SBIR effort reported here. This approach offers greater design versatility, improved thermal performance, and improved strength over the microchannel concepts considered previously.

The concept is sketched in Figure 1, which depicts an array of laser diode bars mounted on a diamond heat spreading layer, which is in turn mounted to the microchannel cooler. The cooler itself is fabricated from a stack of thin ($50\mu\text{m}$) copper foils, which have been soldered together to form a solid structure. Each foil is photochemically etched with a detailed pattern to form the microchannels and the inlet and outlet supply manifolding. In the figure, the main and secondary manifolds are etched all the way through the foil, the microchannel section is etched halfway through, and the unetched cylinders left in each microchannel are used as heat transfer augmentation fins.

Three prototype coolers similar to the design shown in Figure 1 were fabricated in the Phase I program, and one of the coolers was tested to a heat flux of 500 W/cm^2 . A photograph of the cooler during exposure to this heat flux is presented in Figure 2. The figure shows the model, held in an insulated test fixture, with its front face immersed in the $1400\text{ }^\circ\text{C}$ flame of a propane torch. This prototype cooler was exposed to ten of these tests, with no change in its exterior appearance or internal flow characteristics, and with a maximum surface temperature of $60\text{ }^\circ\text{C}$.

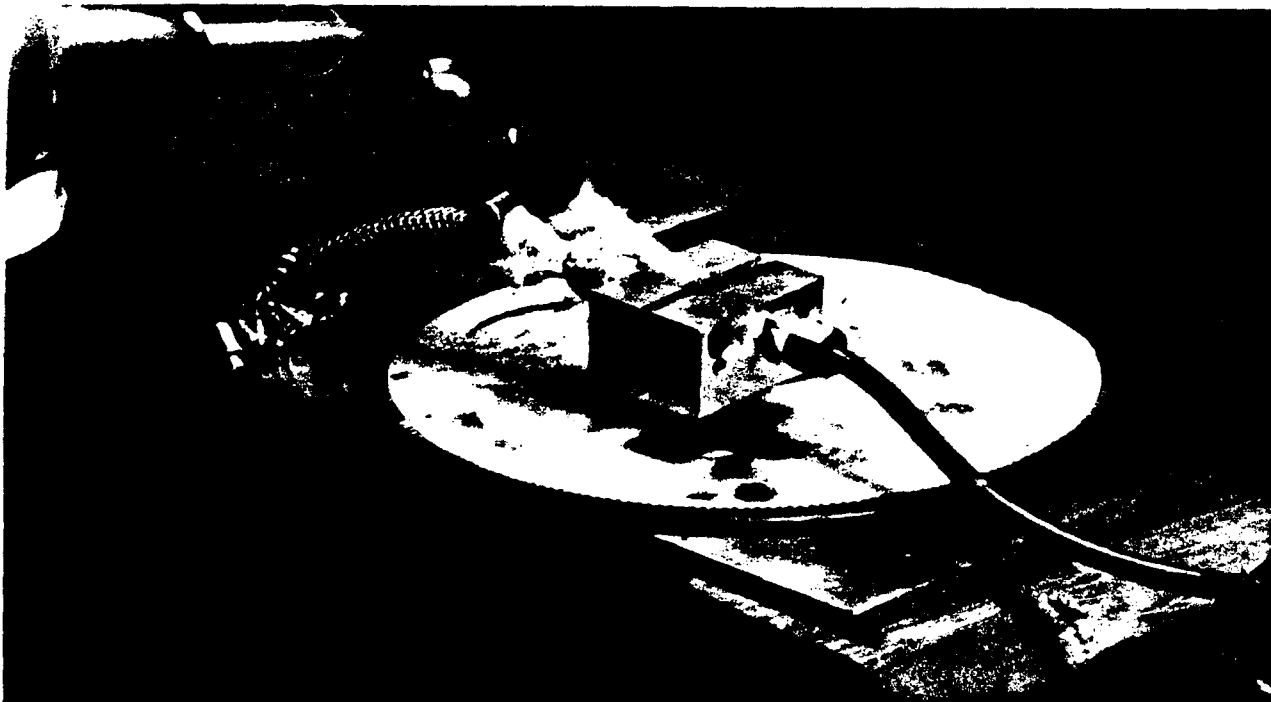


Figure 2. Phase I microchannel cooler during exposure to 500 W/cm^2 heat flux.

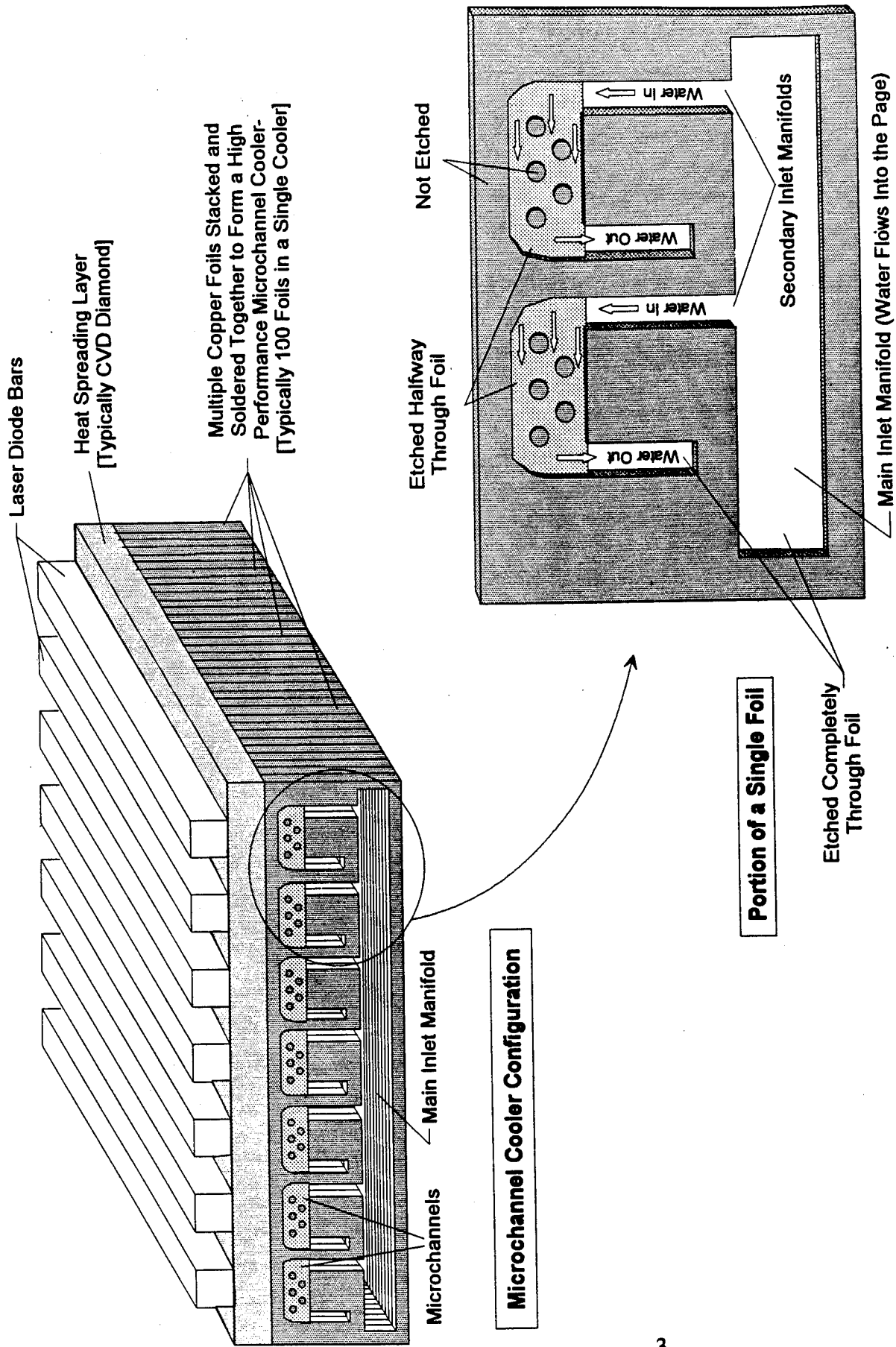


Figure 1. Saddleback Aerospace Microchannel Cooling Concept

The figure of merit for microchannel performance is the thermal resistance between the microchannel surface and the coolant, so for comparison purposes a list summarizing the configurations and thermal resistance values of previously tested microchannel coolers has been compiled (Table 1). There is some ambiguity in the definition of thermal resistance for many of the tested configurations, so the table shows two bounding values of thermal resistance for each cooler (this issue is discussed further in Sections 2 and 6). The Phase I data from the Figure 2 test indicated that the Saddleback prototype model had a thermal resistance of $0.083 \text{ }^\circ\text{C}/(\text{W}/\text{cm}^2)$. Of the table entries, only the Lawrence Livermore National Laboratory (LLNL) $25\mu\text{m} \times 150\mu\text{m}$ design appears to have reported superior performance to the Saddleback prototype.

The thermal resistance value for the Saddleback prototype was nearly the lowest ever measured for a single-phase forced convection cooling system. It does not, however, represent the ultimate capability of this approach. Fabrication difficulties are suspected to have significantly degraded the flow and heat transfer performance of the Phase I prototypes. When these difficulties have been resolved, the Saddleback microchannel coolers should have roughly half the thermal resistance of even the LLNL design.

In summary, the Phase I study demonstrated a new microchannel cooling concept, which offers many advantages over previous concepts. Major features of this concept include rugged construction, compact packaging, and extremely low thermal resistance. The Saddleback cooler appears to be well suited for the task of cooling high power laser diode arrays, particularly in military shock and vibration environments. The Phase I also laid the groundwork for future research, identifying areas where the analytic and manufacturing methodologies require improvement.

Table 1. Summary of microchannel test results for various investigators

Investigating Agency	Material	Channel Width	Channel Height	Channel Length	Flow Rate/Channel	Pressure Drop	Heat Flux Average (Local)	Local Thermal Resistance ($^{\circ}\text{C}\text{-cm}^2/\text{W}$)	Average Thermal Resistance ($^{\circ}\text{C}\text{-cm}^2/\text{W}$)
LLNL	Si ¹	25 μ	150 μ	1400 μ	0.014 g/s	50 psi	635 W/cm ² (2700 W/cm ²)	0.014	0.059
	Si ³	25 μ	200 μ	1850 μ	0.0175 g/s	55 psi	300 W/cm ² (1860 W/cm ²)	0.014	0.88
	Si ²	50 μ	200 μ	4000 μ	0.155 g/s	50 psi	111 W/cm ²	0.094	0.094
MIT/LL	InP ⁴	160 μ	160 μ	9525 μ	0.018 g/s	25 psi	68 W/cm ² (677 W/cm ²)	0.100	0.99
	InP ⁴	220 μ	165 μ	9700 μ	0.033 g/s	50 psi	114 W/cm ² (1059 W/cm ²)	0.072	0.67
	Si ⁵	100 μ	400 μ	10000 μ	0.5 g/s	70 psi	25 W/cm ² (500 W/cm ²)	0.040	0.8
N. C. State	Cu ⁶	5870 μ	1000 μ	100000 μ	31.5 g/s	16 psi	13 W/cm ² (42 W/cm ²)	0.35	1.13
	Cu ⁶	5870 μ	100 μ	100000 μ	3.15 g/s	41 psi	13 W/cm ² (42 W/cm ²)	0.40	1.29
Perkin Elmer	Si ⁷	36 μ	420 μ	10000 μ	0.013 g/s	45 psi	18 W/cm ² (600 W/cm ²)	0.009	0.28
Cornell (w/LLNL)	Si ⁸	40 μ	400 μ	3200 μ	0.027 g/s	50 psi	15.75 W/cm ² (100 W/cm ²)	0.05	1.97
NTT	Al ₂ O ₃ ⁹	800 μ	400 μ	86000 μ	0.46 g/s	?	6.0 W (24 W/cm ²)	8.0	32
	Cu ¹⁰	?	?	10000 μ	5.6 g/s/cm ²	~ 80 psi	125 W/cm ²	0.125	0.125
McDonnell Douglas	BeO ¹⁰	?	?	10000 μ	5.6 g/s/cm ²	20 psi	125 W/cm ²	0.26	0.26
Sunstrand (Jet Imp.)	Cu ¹⁰	100 μ Foils w/200 μ Jet Orifices		Jet Orifices	5.6 g/s/cm ²	~ 80 psi	125 W/cm ²	0.29	0.29
	Cu ¹⁰	100 μ Foils w/Larger Jet Orifices		Jet Orifices	5.6 g/s/cm ²	35 psi	125 W/cm ²	0.19	0.19
Saddleback Aerospace	Cu	25 μ	225 μ	600 μ	0.012 g/s	45 psi	490 W/cm ²	0.083	0.083

2.0 SURVEY OF THE LITERATURE

The concept of microchannel cooling for the thermal management of semiconductor devices was first introduced in Reference 11, and expanded upon 12. In these papers the authors noted that since the thermal resistance between a coolant passage wall and the bulk coolant drops with decreasing channel width, a heat exchanger with very thin passages and very thin passage walls could provide large heat transfer coefficients and large heat transfer areas per unit heated area. The concept is shown in Figure 3, where the configuration and fabrication are illustrated.

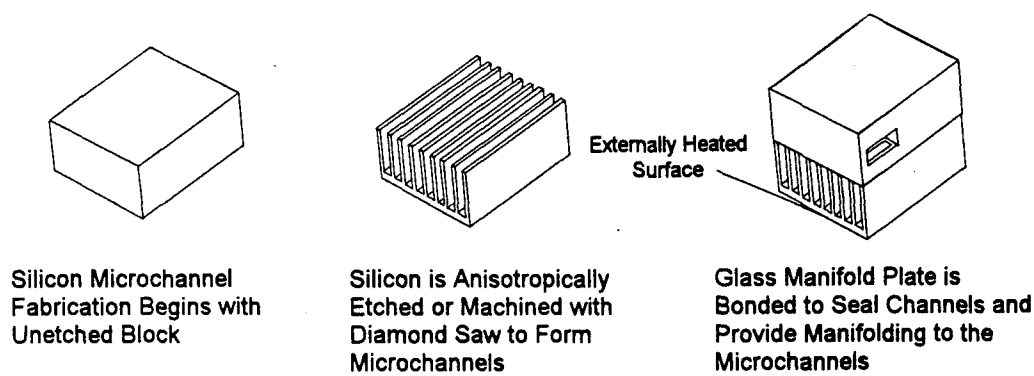


Figure 3. Conventional microchannel construction.

The authors also pointed out that such a structure could be fabricated using the anisotropic etching properties of silicon. The atomic planar density of silicon varies significantly with crystalline direction, so that the etch rates in the 100 plane and the 110 plane are approximately an order of magnitude larger than the rate in the 111 plane. This permits the etching of deep grooves in silicon, with depth-to-width ratios of from 10 to 20 (in practice, for thin channels, ratios of 8 - 10 are the maximum that can be achieved). Using this approach, the authors were able to construct 3 prototype microchannel assemblies, which were then tested to 790 W/cm^2 in a successful demonstration of their heat dissipation capability.

Although the concept of microchannel cooling was first formalized in Ref. 11, it should be noted that the concept of using small etched or machined channels for high heat flux cooling has existed for over 30 years. Allison Gas Turbines, for instance, began producing Lamilloy® for cooling turbine blades in the early sixties. Aerojet first developed etched metal "platelets" for rocket injectors, later adapting the technology for cooling reentry vehicle nosetips in the late-60's. These efforts have continued through the last decade. Reference 13 reports a variety of micro-heat exchanger development efforts by companies such as 3M, Rolls-Royce, Heatric Pty Ltd., Messerschmidt-Bolkow-Blohm, and Doty Scientific, which all have arisen independently from microchannel cooling researches.

In the specific area of microchannel research, however, the initial work reported in Ref. 11 gave rise to a variety of subsequent efforts, resulting in the generation of a scattered body of literature. This literature was reviewed recently, in a fairly comprehensive survey (Ref. 14). The predominate groups covered in the review were Stanford/Livermore, MIT Lincoln Laboratory, North Carolina State University, Auburn University, NTT (Japan), and Tohoku University (Japan). During the course of the Phase I effort Saddleback obtained most of the original sources reviewed in Ref. 14. The results of Saddleback's review are presented in the following sections. The sections are divided into those studies in which microchannel coolers were actually fabricated and tested, and those studies which concentrated mainly on design studies or analytic model development. The focus is largely on those coolers which were actually tested, since these provide a basis for comparison with the Phase I test results.

2.1 MICROCHANNEL TEST DATA REVIEW

There are several difficulties in interpreting the reported results in the literature. Most of these difficulties stem from the fact that the studies were focussed on optimizing and demonstrating the performance of the laser diode or diode array, rather than testing the microchannel performance itself. That is, many of the cited experiments were designed to measure laser performance parameters such as wavelength stability and output power, with

reduced emphasis on obtaining quality measurements of the microchannel cooler thermal performance. This renders some of the most outstanding results suspect.

For instance, the only absolutely reliable means of determining the heat flux absorbed by the coolant is to measure the coolant inlet and outlet temperatures, and the coolant flow rate. While all investigators cited in Table 1 reported measurements of the coolant inlet temperature and flow rate, the best performers (LLNL, MIT/LL and Perkin Elmer) apparently did not measure the coolant outlet temperature. Instead, they inferred the absorbed heat flux by subtracting the laser power output from the electrical input power. This can be a dangerous practice, since the waste heat flux can find a variety of dissipation paths, leading one to underpredict the value of thermal resistance. This situation is aggravated by the fact that no attempt was made to eliminate conduction or convection losses around the periphery of the model.

A second example is the test configuration. Almost all of the experiments listed in the table were performed for cases where the heated area on the cooler was much smaller than the cooled surface area. This allows thermal spreading, i.e., once the heat enters the cooler faceplate, it can spread laterally in one or two dimensions, as shown in Figure 4. The thermal resistance concept is really designed for 1D heat flows, and does not give a realistic indication of the intrinsic heat transfer performance of a cooler when thermal spreading occurs - the thermal resistance of a cooler can vary by factors greater than 3 simply by changing the effective size of the heated footprint. Unfortunately, this is usually the only performance indicator given in the literature.

In the Table, the local values of the heat flux and thermal resistance are based on the area of the heat source, while the average values are based on the surface area of the cooler. Thus, the local values will be too high, and the average values will be too low - these values are provided in order to bound the actual value. The actual value might typically be expected to be about 3 times larger than the local value. For instance, the local thermal resistance reported by Lawrence Livermore National Laboratory (LLNL, Ref. 1) shown in the first row

of the table is $0.014 \text{ }^\circ\text{C-cm}^2/\text{W}$. This value, however, is based on an area of 0.03 cm^2 (the footprint of the heat source), rather than the total surface area of the microchannel cooling section, which would give an average thermal resistance of $0.059 \text{ }^\circ\text{C-cm}^2/\text{W}$. In an attempt to account for thermal spreading, we obtained an estimated equivalent thermal resistance of about $0.048 \text{ }^\circ\text{C-cm}^2/\text{W}$. The testing by McDonnell Douglas Electronics Corporation (MDEC), Sunstrand Corporation, Saddleback Aerospace, and LLLNL (3rd row of the table), were conducted with the heat flux distributed over the entire front face (as in Figure 1), to prevent heat spreading effects from distorting the test results.

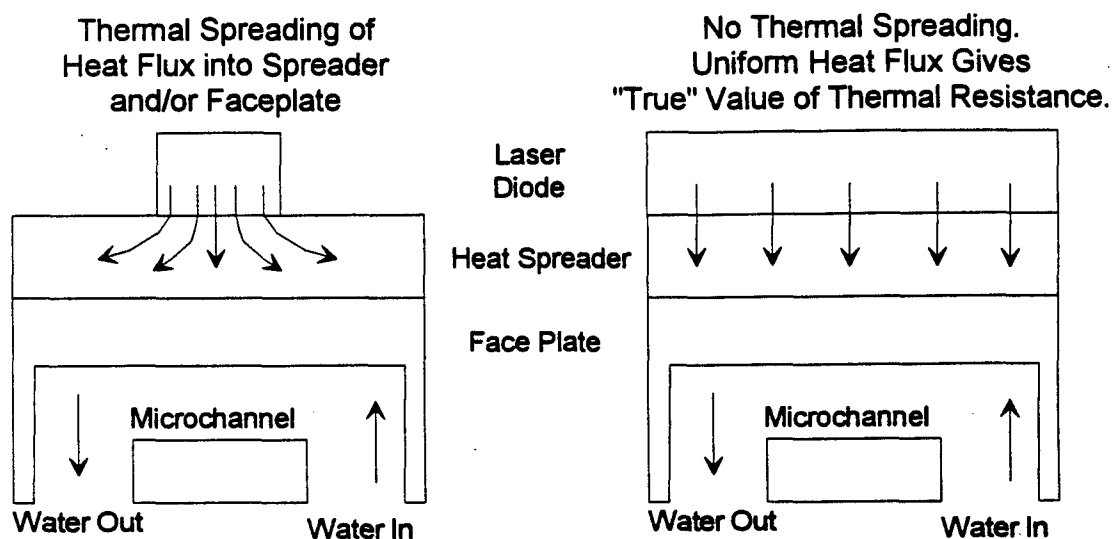


Figure 4. Thermal spreading phenomenon.

Stanford University/Lawrence Livermore National Laboratory. The Reference 2 author carried his work to Lawrence Livermore after graduating in 1984. Since that time Lawrence Livermore has been the most prolific source of published microchannel research. Much of the silicon machining, bonding and manifolding technology was developed at Livermore in the mid- to late-80's. The result of this work has been the fabrication of the first complete microchannel-cooled laser diode assembly (Reference 15). This assembly had a linear array of 42 cooling modules, with a $330 \text{ }\mu\text{m} \times 1.8 \text{ cm}$ laser diode bar mounted on each module.

They have actually used this assembly to pump an Nd:YAG slab laser to an output of 1 kW (Ref. 16.).

Most of the LLNL work has been directed toward cooling of SLDAs (Refs. 1 - 3, 15), although one reference concentrates on the cooling of RF power transistors (Ref. 17). Most of the work has also been conducted with silicon microchannels of 25 μm width, with heights ranging from 150 - 225 μm , with fin widths of 25 μm , and with faceplate thicknesses from 125 - 175 μm . These microchannels have been used to dissipate local heat fluxes as high as 2.7 kW/cm², although the average heat fluxes over the cooler face are much smaller.

LLNL has investigated several mounting approaches, two of which are discussed here. The first, shown in Figure 5, shows an array of laser diodes, each mounted on a diamond chip carriers which are in turn mounted to the silicon cooler. This arrangement was described in Reference 18 to provide a measured thermal resistance of 0.04 °C/(W/cm²), although there appear to be some anomalies. First, only one diode/carrier assembly was tested on the cooler, so thermal spreading effects could be assumed to be important. The authors estimated that the thermal resistance if the cooler were covered with diode/carrier assemblies would increase to 0.09 °C/(W/cm²). The second anomaly was that a relatively large copper electrode was placed on the side of the diode opposite the diamond carrier. The electrode was mounted firmly to both the diode and the silicon microchannel structure, and so provided an additional thermal conduction path not considered in the calculation of thermal resistance (this is probably a 10% - 20% error).

This configuration was revisited in Reference 2, where 3 diodes were sandwiched between 4 diamond carriers to form a small array. In this case 50 μm x 200 μm microchannels were used. The diodes were then driven at 8 kHz with a 40% duty cycle. The thermal resistivity was given as 0.094 °C/(W/cm²), and this value should require only minimal correction for thermal spreading effects (heating footprint = 0.14 cm², while the total cooled area = 0.4 cm²), although some questions concerning the time-averaging of the thermal resistance remain.

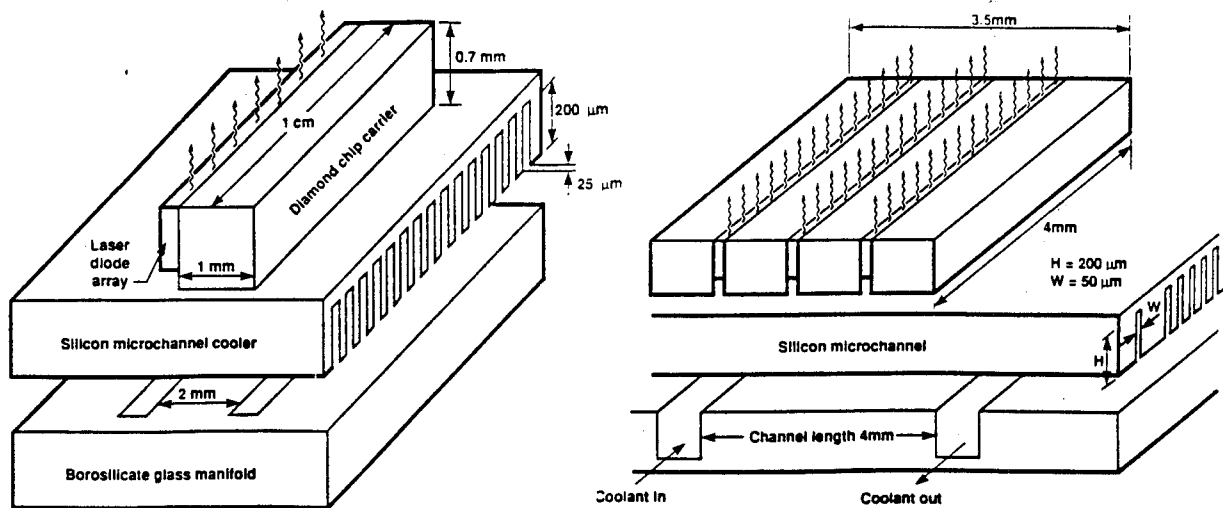


Figure 5. LLNL diamond carrier mounting configuration

The most recent mounting approach used by LLNL is depicted in Figure 6. In this figure, the diodes are shown mounted on small cooling wafers, which are stacked together to form a 1D array. Each wafer is formed by three layers, the first is a $381\ \mu\text{m}$ thick silicon wafer with the microchannels and with the inlet manifold pattern for the microchannels. The etched side of the wafer is bonded to a $787\ \mu\text{m}$ borosilicate glass spacer plate, which has through-holes in key areas to allow inlet outlet flows to pass through the spacer plate. A second silicon wafer (again, $381\ \mu\text{m}$ thick) has the return manifold pattern etched on its face, and its etched side is bonded to the opposite side of the spacer plate. The entire assembly is thus 1.55 mm thick.

This mounting scheme was also used by McDonnell-Douglas Electronics Corporation, as discussed below. Its advantage is that defective diodes or wafer coolers can easily be replaced in the array. There are two disadvantages with this approach, as well. The first is that the wafer thickness limits the proximity of adjacent array elements. The second is the entire assembly has a large dedicated manifolding/coolant routing volume, which may restrict usage in military systems.

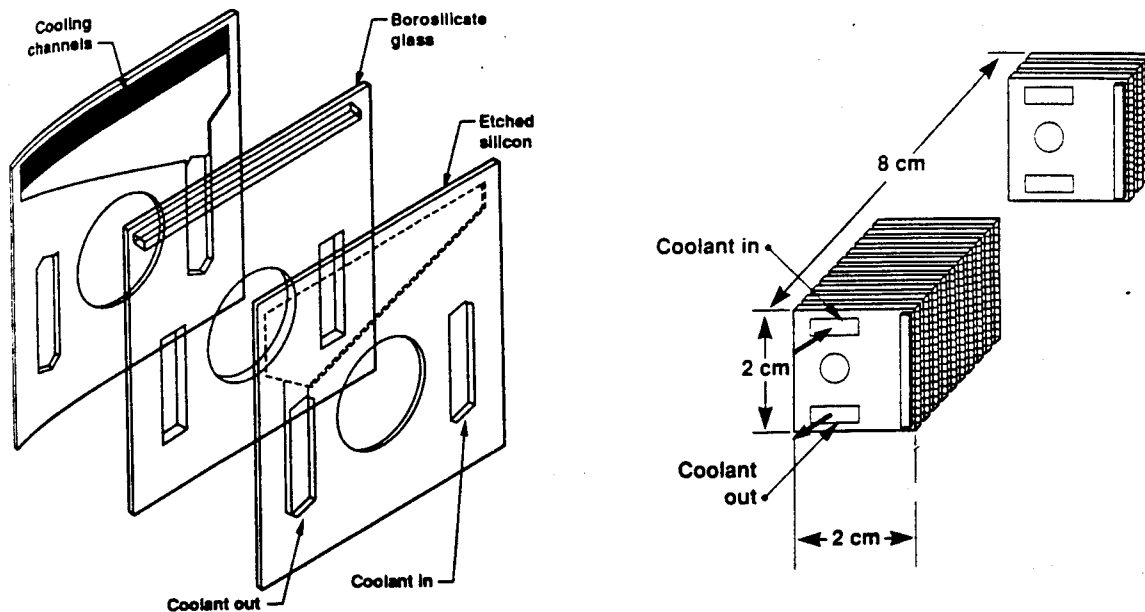


Figure 6. Side-mounting of laser diodes on wafer coolers.

MIT/Lincoln Laboratory. The work reported in Reference 4 included the fabrication and testing of 2 microchannel structures fabricated from Indium Phosphide. InP has a thermal conductivity of about 0.6 W/cm/K, versus about 1.5 W/cm/K for silicon and about 4 W/cm/K for copper. It was selected as the heat sink material due to the prospect that microchannels might be built directly into the back side of InP chips. The channels machined into these two structures were $160\ \mu\text{m} \times 160\ \mu\text{m}$ and $220\ \mu\text{m} \times 165\ \mu\text{m}$, respectively. These low aspect ratios were selected for ease of manufacture, and because the target thermal resistance for these coolers was comparatively high.

The models were tested with four $0.0625\ \text{cm}^2$ resistors on the roughly $1.12\ \text{cm}^2$ cooled surface. Thus thermal spreading effects would be important in these experiments. The local thermal resistance results, listed in Table 1, are surprisingly low given the low material conductivity and the large size and low aspect ratio of the channels. The author mentions that because one power supply was used to power all four resistors, the power to any particular resistor varied, making the analysis of the data more difficult. No apparent

attempt was made to measure outlet water temperatures, to confirm the average power dissipation values.

MIT/LL also fabricated silicon microchannel coolers, as described in Reference 5. The microchannels were $100\ \mu\text{m} \times 400\ \mu\text{m}$, with a $175\ \mu\text{m}$ faceplate. A $0.04165\ \text{cm}^2$ laser diode array was mounted in the middle of the $0.8\ \text{cm}^2$ cooler. The cooler had large pressure losses despite the relatively large size of the passages - this was due to the long lengths (1 cm) of the channels, which had to traverse the entire cooler. The local thermal resistance of $0.04\ ^\circ\text{C}/(\text{W}/\text{cm}^2)$, as reported in Table 1, is significantly low due to thermal spreading effects.

An updated silicon microchannel design was tested in Reference 20, which describes a means of alternating the water flow in adjacent channels to reduce thermal gradients in the cooler. An experiment to evaluate this design was conducted, and this experiment provided a fairly uniform heat flux over the entire cooled surface (the edges of the cooler were allowed to conduct into a brass holder). Unfortunately, the channel dimensions are not given, although it is noted that there were 33 channels per centimeter. This suggests that the channel widths were $100 - 150\ \mu\text{m}$. The cooled area was $1\ \text{cm} \times 2.3\ \text{cm}$, with the channels running in the lengthwise direction.

Two experiments were run, one with a water flow rate of $15.8\ \text{g/s}$ (and a pressure drop of $10.6\ \text{psi}$), and the second with a water flow rate of $28\ \text{g/s}$ (and a pressure drop of $36\ \text{psi}$). These pressure drop values indicate that the passages were substantially larger than in previous studies. The low flow rate experiment yielded a thermal resistance of $0.14\ ^\circ\text{C}/(\text{W}/\text{cm}^2)$, while the high flow rate test had a value of $0.11\ ^\circ\text{C}/(\text{W}/\text{cm}^2)$. These values are substantially higher than most reported in the literature. This is due to the 1D test configuration (which eliminates thermal spreading effects) and to the larger size of the passages.

Perkin Elmer Corporation. The Reference 6 paper describes a silicon microchannel cooler built to cool a 2D surface-emitting diode laser array. They report a thermal resistance of

only $0.009 \text{ }^\circ\text{C}/(\text{W}/\text{cm}^2)$ for their test configuration - the lowest reported by any investigator. As will be discussed below, however, it is suspected that this value is far lower than it should be - even accounting for thermal spreading effects. Details of their experiment are given below.

The 4×10 regular rectangular laser diode array was composed of $10 \text{ } \mu\text{m} \times 800 \text{ } \mu\text{m}$ gain-guided stripes on $380 \text{ } \mu\text{m} \times 1300 \text{ } \mu\text{m}$ centers, embedded in a monolithic wafer. The wafer was bonded to a copper sheet ($900 \text{ } \mu\text{m}$ thick), which was soldered in turn to the copper-plated surface of the silicon microchannel cooler. The array area was 0.16 cm^2 , compared to a total cooler size of 2.7 cm^2 . The diamond-sawed silicon microchannels were $36 \text{ } \mu\text{m}$ wide and $420 \text{ } \mu\text{m}$ deep, with $64 \text{ } \mu\text{m}$ primary fins and a $190 \text{ } \mu\text{m}$ faceplate.

Tests were conducted at continuous wave operation with reported heat loads as high as $600 \text{ W}/\text{cm}^2$. It is not clear how this number is calculated, since the heated area footprint is never specified. In addition, the heat load was calculated assuming that all of the resistive power losses occurred in the active region, but at one point in the report it is noted that resistive heating in the gold wires on the "top" side of the array (the side away from the cooler) was sufficient to melt the wire bonds. This suggests that not all (and maybe not even most) of the waste heat was generated in the active region, and that other heat transfer mechanisms (radiation, surface convective cooling, lateral conduction) could be responsible for dissipating a substantial portion of the waste power.

The tested configuration can be expected to have had very large thermal spreading effects, first in the wafer itself, then in the $900 \text{ } \mu\text{m}$ copper block, and finally in the silicon faceplate. Due to the stacked layers, thermal spreading will have been more significant in this configuration than in any other reviewed in this report. The authors measured a thermal resistance of $0.038 \text{ }^\circ\text{C}\text{-cm}^2/\text{W}$ based on the wavelength shift of the laser, and claimed that $0.029 \text{ }^\circ\text{C}\text{-cm}^2/\text{W}$ of this resistance was due to the conductive resistance between the active layer and the copper block. This leaves $0.009 \text{ }^\circ\text{C}\text{-cm}^2/\text{W}$ as the resulting thermal resistance from the copper block/laser array interface to the coolant. The authors mention that this is a

much smaller value than they had expected, and attribute the difference to thermal spreading. It should be noted, however, that the 1-D thermal resistance of just the copper block and the silicon faceplate is: $(0.09 \text{ cm})/(3.9 \text{ W/cm-K}) + (0.0190 \text{ cm})/(1.4 \text{ W/cm-K}) = 0.0366 \text{ }^\circ\text{C-cm}^2/\text{W}$, which is nearly as large as the entire thermal resistance the authors measured.

For these reasons, the thermal resistance values quoted by the authors should not be used for comparison purposes until more data becomes available. The measured pressure drop - 45 psi for a channel length of 10000 μm - is reasonable and consistent with the results of other investigators, most notably Cornell (see Table 1).

McDonnell-Douglas Electronics Company. References 10 and 21 discuss the design and testing of "wafer thin coolers" intended for cooling GaAs laser diode bars. The updated design discussed in the Reference 21 paper has similarities to the stacked silicon coolers built by LLNL - a major difference being that MDEC has built its coolers using copper sheets. The higher conductivity through the wafer thickness allows MDEC to use two rows of microchannels, one on either side of the centerline of the wafer. As in the case of LLNL, MDEC mounts the laser diodes on the sides of the wafer coolers, and stacks wafers to form an array (as in Figure 6).

Each 1 mm thick cell is comprised of 3 copper or beryllium foils; two outer 125 μm foils, and an inner 0.75 mm foil. The inner foil is etched on both sides with 250 μm deep microchannels, machined using electrical discharge machining. While the width of the channels was not given, Saddleback estimates that it is probably about 100 μm , with fins of the same width. This design had not been tested as of the writing of the Reference 21 paper. The earlier paper (Ref. 10) describes a prototype version of this design, which was thicker (1.8 mm), but probably had microchannels of the same dimensions (although they may have been up to twice as deep). Several prototype designs were fabricated in copper and BeO, and tested to 125 W/cm^2 .

In contrast to many of the experiments reviewed in this report, the MDEC experiments represent thorough, reliable heat transfer measurements. Their experimental results are shown below in Figure 7, which is adapted from Figure 11 of Reference 10. The CHIC designs shown in the Figure were actually fabricated by Sunstrand, and are described in the next subsection. As shown, the MDEC Double Pass design demonstrated a thermal resistance as low as $0.125 \text{ }^\circ\text{C}/(\text{W}/\text{cm}^2)$. The linear behavior of the Figure 7 curves indicates a laminar flow condition, with a linear drop in caloric resistance (due to temperature rise in the coolant) as the flow rate increases. This is consistent with MDEC's design flow condition of $\text{Re} = 500$.

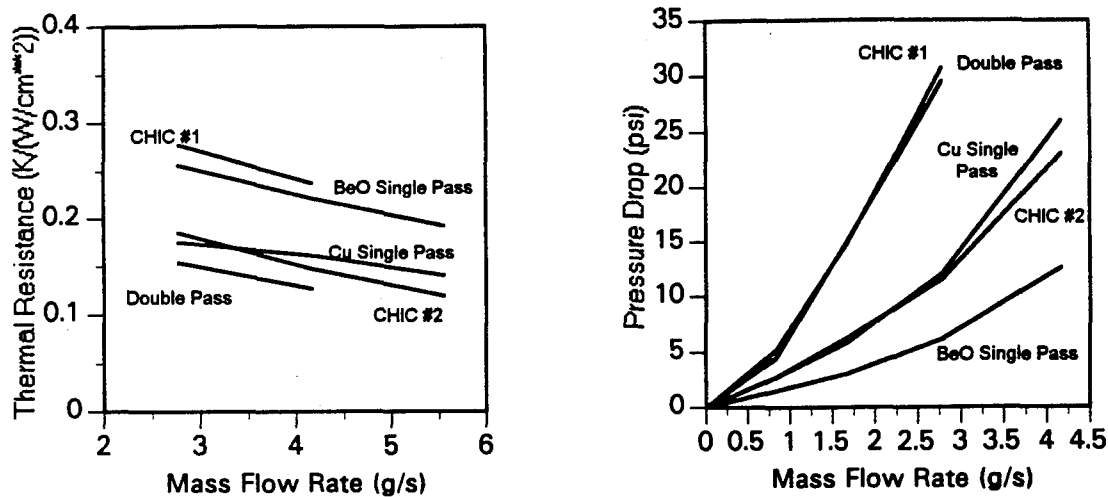


Figure 7. Heat transfer and pressure drop results from Reference 10.

The pressure drop performance is also shown in Figure 7, and is also taken directly from Reference 10 (Figure 17). The pressure drops for the double pass design are about 3X higher than predicted by McDonnell-Douglas, and the authors attribute this to possible channel deformation during diffusion bonding, or clogging due to soldering of the inlet/outlet manifold tubing. It will be noted in later sections that Saddleback experienced similar problems during the effort reported here, although the Saddleback pressure drops were significantly lower than those of Figure 7.

Sunstrand Corporation. Sunstrand has developed Compact High Intensity Coolers (CHICs) as described in Reference 22. Testing of two versions of CHICs was also described in Reference 10, in which both McDonnell-Douglas and Sunstrand coolers were examined. The CHIC was originally developed for the cooling of high power density space electronics, and so was designed for fairly low heat fluxes - 50 W/cm^2 . A later version performed well in testing up to 125 W/cm^2 . Because the coolers were intended for use in space, Freon-21 was selected as the primary coolant.

The CHIC concept is based on a staggered array of impingement jets. The jets are formed by small ($200 \mu\text{m}$) circular orifices etched in $100 \mu\text{m}$ copper plates. The jets were spaced $100 \mu\text{m}$ from the faceplate, with a total of 3 rows of jets and spacers in a cooler. The fabricated coolers had heated surface areas of 1 cm^2 , and versions built for side-mounting of laser diodes have been built with thicknesses as low as 1mm. A second design (CHIC #2) was fabricated for the testing reported in Reference 10; this design had fewer, larger rectangular orifices for reduced pressure drop, and improved internal thermal conduction paths.

The performance of the two designs was illustrated in Figure 7, presented in the McDonnell-Douglas discussion. As mentioned in that discussion, the tests were conducted so as to provide accurate measurements of the cooler thermal resistances. The tests were conducted with water, rather than Freon-21. The original cooler design demonstrated a thermal resistance of $0.25 \text{ }^\circ\text{C}/(\text{W/cm}^2)$, and a pressure drop of 30 psi at a flow rate of 2.8 g/s. The improved design (CHIC #2) had half the thermal resistance of CHIC #1, and a pressure drop of only 11.5 psi at a flow rate of 5 g/s. These results showed that a fairly coarse array of jets could provide superior performance to any of the other configurations tested in the MDEC effort (Ref. 10).

Cornell University/Argonne & Brookhaven National Laboratories. Cornell's efforts have focussed mainly on cooling of silicon x-ray monochromator crystals. Most of their work has involved relatively large channels etched or machined in silicon, and cooled with water or

liquid gallium (in conjunction with Argonne National Laboratory). The heat fluxes for monochromator crystals can be of the order of several kW/cm², with very little temperature rise allowed (to prevent thermostructural deformation of the crystal). Most of their data is for channels of the order of 0.2 cm x 0.6 cm (References 23 - 25), although more recent efforts have used 0.076 cm x 0.3 cm channels (Reference 26), and 0.004 cm x 0.04 cm channels (Reference 8).

The latter effort was performed in concert with LLNL investigators, with a heat flux of 100 W/cm² over an area of approximately 2.5 cm². The entire cooled area was 16 cm², so thermal spreading effects could have had a large influence. The measured thermal resistance was about 0.05 °C/(W/cm²), but flow conditions and pressure drops were not reported. Independent flow testing showed a 50 psi pressure drop at a flow rate of 16.7 g/s. The results of this testing were consistent with previous LLNL test results.

North Carolina State University. North Carolina State has investigated two "microchannel" configurations, although the channels they use are quite large when compared to those of LLNL. These channels are used to cool electronic devices with fairly low heat fluxes (42 W/cm² local heat flux), so large channels can provide adequate performance. Two channel configurations were tested in Reference 7: the first, the deep channel design, had dimensions of 1 mm x 5.87 mm; the second, the shallow channel design, had dimensions of 0.1 mm x 5.87 mm. The layout of the designs was somewhat unusual for microchannels. Normally the long dimension of the channels is perpendicular to the heated surface, to permit conduction down the metal channel walls. NCSU has used the opposite orientation, which is easier to manufacture but has much worse performance. Our conclusion is that the work described in Reference 7 has little relevance to the problem of microchannel cooling at high heat fluxes.

Nippon Telephone and Telegraph. The authors of Reference 27 and Reference 9 have developed and tested microchannels fabricated from silicon and alumina, respectively. These structures are intended for cooling of VLSI chips, with heat fluxes of the order of 10 W/cm²,

although excursions as high as 200 W/cm^2 were considered. While channels of many sizes were evaluated in these studies, thermal resistance values were provided only for the case of $400 \mu\text{m} \times 800 \mu\text{m}$ alumina channels. The thermal resistance varied between 2 - 4 $^\circ\text{C}/(\text{W/cm}^2)$, depending upon flow conditions.

In Reference 28, two of the authors report fabricating a staggered micro-pin fin array, using diamond-shaped fins machined in silicon. The fins were $150 \mu\text{m}$ wide, $500 \mu\text{m}$ long, and $300 \mu\text{m}$ high. They were spaced on $300 \mu\text{m}$ centers in the lateral direction, and $1000 \mu\text{m}$ centers in the flow direction. This design was not tested, but was predicted to have 1/3 the resistance of $300 \mu\text{m} \times 300 \mu\text{m}$ microchannels. This advantage would be greatly reduced for closer lateral spacings of the fins, since the advantage of the fins in this case is the interruption of the insulating boundary layer in the channel.

Others. TRW fabricated silicon microchannel coolers for laser diode arrays (Reference 29), but Saddleback has been unable to locate any test data for these designs. The TRW cooler test data is of interest for two reasons. First, because they etched very thin channels, with very thin fins, as listed below in Table 2. This provides more heat transfer area per unit heated area than a "standard" $25 \mu\text{m} \times 25 \mu\text{m}$ microchannel design, although at the sacrifice of pressure drop and mechanical strength. The second interesting feature was the manifolding. The manifold design produced effective channel lengths of only $333 \mu\text{m}$ - much shorter than any other channels, and only 50% longer than the combined inlet and outlet widths. Such a design might be expected to have unusual hydraulic and heat transfer characteristics; Saddleback's conjecture is that it would provide high average heat transfer, but with local hot spots and higher-than-predicted pressure drops.

Reference 30 describes work conducted at Sperry Corporation, which involved air-cooled microchannel structures. Copper microchannels with channel widths of $125 \mu\text{m}$, $250 \mu\text{m}$, and $625 \mu\text{m}$ were fabricated and tested. Fin widths were equal to channel widths, and the channel heights for all three models were 1.27 cm, with 0.5 cm faceplates. At an air flow rate of $500 \text{ cc}^3/\text{s}$, the thermal resistances for the three models were approximately 0.524,

0.645, and 1.37 °C/(W/cm²), respectively. This represents an order of magnitude improvement over conventional laminar flow air-cooled heat sinks.

Table 2. Comparison of TRW designs to other configurations

	Channel Width	Fin Thickness	Channel Height	Channel Length
TRW	9.3 μm	5.7 μm	200 μm	330 μm
	14.3 μm	5.7 μm	200 μm	330 μm
	20 μm	10 μm	200 μm	330 μm
	25 μm	15 μm	200 μm	330 μm
LLNL	25 μm	25 μm	150 μm	1400 μm
Saddleback Aerospace	25 μm	25 μm	225 μm	775 μm

2.2 ANALYSIS/OPTIMIZATION OF MICROCHANNEL DESIGNS

While almost every effort described in the preceding section involved at least some analytic and design optimization work, some studies either focussed on analytic technique, or spent relatively large resources on design optimization. There are two major questions in this area: first, what are the optimal dimensions of a microchannel structure, given a design heat flux and flow rate; and second, how significant are thermal spreading effects in the microchannel faceplate? Another issue that has arisen is the question of flow regime - the original microchannel concept was based on operation exclusively in the laminar flow regime, while other authors have claimed that operating in turbulent flow will have better net performance. The following paragraphs describe some of the analytic and design optimization efforts which have addressed these questions, and which are relevant to the current or to future programs.

MIT/LL. The author of the Reference 4 report wrote a 2D analytic design code, called MICROHEX, specifically for microchannel coolers. The code has been compared to test data generated by MIT/LL and by Lawrence Livermore, and has been very successful in matching thermal test results. The code is capable of handling laminar, turbulent and developing flows, and channels with smooth and roughened walls. The code computations are based largely upon experimental correlations collected and adapted in Reference 4. It includes 8 material models (including copper), and three fluid models (including water), and so is a versatile, accurate means of predicting thermal performance of microchannel coolers. The hydraulic performance predictions have not been as successful, with inaccuracies as high as 50%. Saddleback recently obtained a copy of MICROHEX, though too late to perform any comparative calculations for the Phase I program. In future efforts MICROHEX predictions should be compared to Saddleback predictions, other analytic methods, and experimental results.

In analytic design trades, the author concluded that turbulent flow operation could provide reduced thermal resistance at equivalent pressure drop. No tests have yet been conducted in this regime, however, so this conclusion is not yet experimentally verified. In the case of turbulent flow predictions, experimental verification is crucial - even scaling results for one fluid to a fluid with a different Prandtl number is difficult.

Auburn University. A microchannel sizing optimization methodology is presented in References 31 and 32. The optimization methodology uses 1D empirically-based predictions of heat transfer and flow performance, including turbulent and developing flow correlations. Using this methodology, they established an optimal microchannel channel for conditions comparable to those in Reference 11. The design differences were very slight, however, and the performance improvement was only about 10%.

A larger advantage was calculated when the microchannels are designed for turbulent flow. A 30% reduction in thermal resistance was predicted if the microchannels are made approximately three times as wide, and the flow rate was increased by 2 1/2. This provided

turbulent flow within the channels. The increased flow rate reduced the capacity resistance (i.e., the equivalent resistance due to the temperature rise in the coolant) and the turbulence increased the convective heat transfer coefficient. The conclusion that turbulent flow offers superior performance is consistent with the findings in Reference 4, but this might be expected, since the Auburn authors used many of the correlations listed in Reference 4.

The analytic optimization scheme was evaluated in experiments reported in Reference 33. In this study, predictions of the performance of three air-cooled aluminum alloy fin systems were prepared, and compared to experimental results for the same systems. The fins were relatively large: 7.62 cm in length, 1.27 cm in height, and varying in width, but never less than 0.3175 cm. The three fin systems had 6, 9, and 12 fins with predicted thermal resistances of 21.66, 20.50, and 22.47 °C/(W/cm²) - the 9-fin design having the optimal value by a margin of about 6%. The experimental results first showed a large underprediction of the pressure drop through the fins; the flow rate was about 1/2 of the predicted value. The thermal resistances were about twice the predicted values, although the 9-fin design did have the lowest thermal resistance. Though the authors claim that this is a successful demonstration of the optimization method, the large discrepancies between the predictions and the test conditions and results underline a need for further evaluations of this method.

TRW. TRW performed an extensive set of design optimization trades in a contracted effort for the USAF Phillips Laboratory (Reference 29). They restricted their analysis to laminar flow, and in fact claimed to operate in a Hele-Shaw flow regime. Hele-Shaw flow is a flow between parallel plates where inertial effects can be neglected in the fluid equations of motion, leaving a greatly simplified version of the steady-state Navier-Stokes equation:

$$u_i \approx -\frac{1}{2\mu} \frac{\partial p}{\partial x_i} x_3(d-x_3)$$

where $i = 1,2$ are the velocity components parallel to the channel walls, and $i = 3$ is the velocity component normal to the channel walls (with the channel width = d). The use of this reduced form allows one to derive an exact solution to the Navier-Stokes equations, and

this is how TRW obtained their velocity streamlines and pressure contours. There is some question, however, as to whether the Hele-Shaw approximation is applicable to the case of microchannels.

Batchelor (1967) notes that the Hele-Shaw form of the momentum equation can be used when the inertial forces are small compared to the viscous forces, i.e., when:

$$d \left(\frac{\rho d^3 |\nabla p|}{\mu^2} \right) < L$$

where L is the channel length, or a length in the flow direction over which the velocity change occurs. In the TRW configuration, the short channels turn the flow at the entrance and exit ports, so that either the channel height of 200 μm or the inlet/outlet port widths of 100 μm are probably the best choice for L . For typical microchannels, $d = 25 \mu\text{m}$, $\rho = 1 \text{ g/cm}^3$ (for water), $\nabla p \approx (20 \text{ psi})/L$, and $\mu = 0.0085 \text{ poise}$ (for water). This requires that L be greater than 330 μm , if L must be at least 10X the value on the left hand side of the equation.

This simple analysis shows that inertial effects can be important, particularly in the entrance and exit regions of the microchannels. There are several possible risks in neglecting the inertial terms in the momentum equation. First, one may overlook the possibility of flow separation and recirculation, which can cause the development of hot spots in the design. Second, one can expect to underpredict the pressure drop along the channels. Finally, trade studies conducted using the reduced form of the equations may mislead the designer in terms of selecting an optimized design. For these reasons, Saddleback did not make use of the TRW derivations and results in the Phase I trade studies, opting instead to use experimental correlations and numerical solutions of the Navier-Stokes equations.

Others. In Reference 34, transient finite element calculations were carried out for 50 μm x 250 μm copper microchannels with 50 μm fins. The microchannel cooled a heated area of 1cm x 1 cm using 4 layers of channels. An AlN layer was placed between the

microchannels and the high power chip running at 1.5 kW/cm^2 . The AlN served as a heat spreader and to match the thermal expansion of the silicon chip. Calculations were performed with water flow rates of 7.5 g/s per layer, which corresponded to a pressure drop of about 44 psi. The predicted thermal resistance between the chip and the coolant was approximately $0.067 \text{ }^\circ\text{C}/(\text{W/cm}^2)$. This is one of the few numerical calculations conducted at a heat fluxes of this level.

References 35 and 36 both proposed analytical optimization schemes, which are beyond the scope of this work to cover. In work funded by USAF Wright Laboratories, the Reference 35 paper concludes that channel height/width ratios "as large as possible" (> 10) provide optimal performance, and that a 30% reduction in thermal resistance can be achieved if the ratio of channel width to fin thickness is optimized (about 2). Sample calculations in Reference 36, concur with this overall conclusion, although there are differences in the numerical results. In future efforts it would be useful to examine these methods in detail and compare their predictions to experimental results.

3.0 DESIGN REQUIREMENTS

The problem of semiconductor laser diode cooling falls into the broader class of electronics cooling, though SLDAs are generally more sensitive to temperature and have higher heat dissipation requirements than other electronic components. In this section we describe general considerations for electronics cooling. In Section 3.1 we focus on problems specific to laser diodes, and in Section 3.2 we present the specific SLDA configuration and design requirements addressed in the Phase I program. The technology demonstrated during the Phase I study is applicable, however, to thermal management of most electronic components.

Predicted trends toward densely-packed multi-chip modules (MCMs) and high speed, high power devices indicate the common occurrence of heat dissipation levels of 100 W/cm^2 by the late-90's. These trends are symptomatic of the increasingly severe thermal management problems that pervade the electronics industry. Traditional methods of heat dissipation, such as heat sinking and mounting on cold plates, are incapable of addressing these problems. Air cooling, for example, is now expected to be inadequate for micro-computers within 5 years.

Thermal dissipation requirements for military systems are even more stressing. Power transistors used in radar systems can generate heat fluxes from $100 - 500 \text{ W/cm}^2$, which lie well beyond the capabilities of conventional thermal management technology. Thermal management is critical for the majority of electronic components, since component lifetime is directly related to operating temperature.

A variety of means of cooling electronics have been addressed. Figure 8, adapted from Reference 37, compares the performance of several approaches including immersion cooling and microchannel cooling. As shown, microchannel cooling offers far better performance than any of the other candidates, and the Saddleback copper microchannels are predicted to have superior performance to conventional silicon microchannels. It is this degree of performance that suggests its use for the severe heat fluxes produced in semiconductor laser diode arrays.

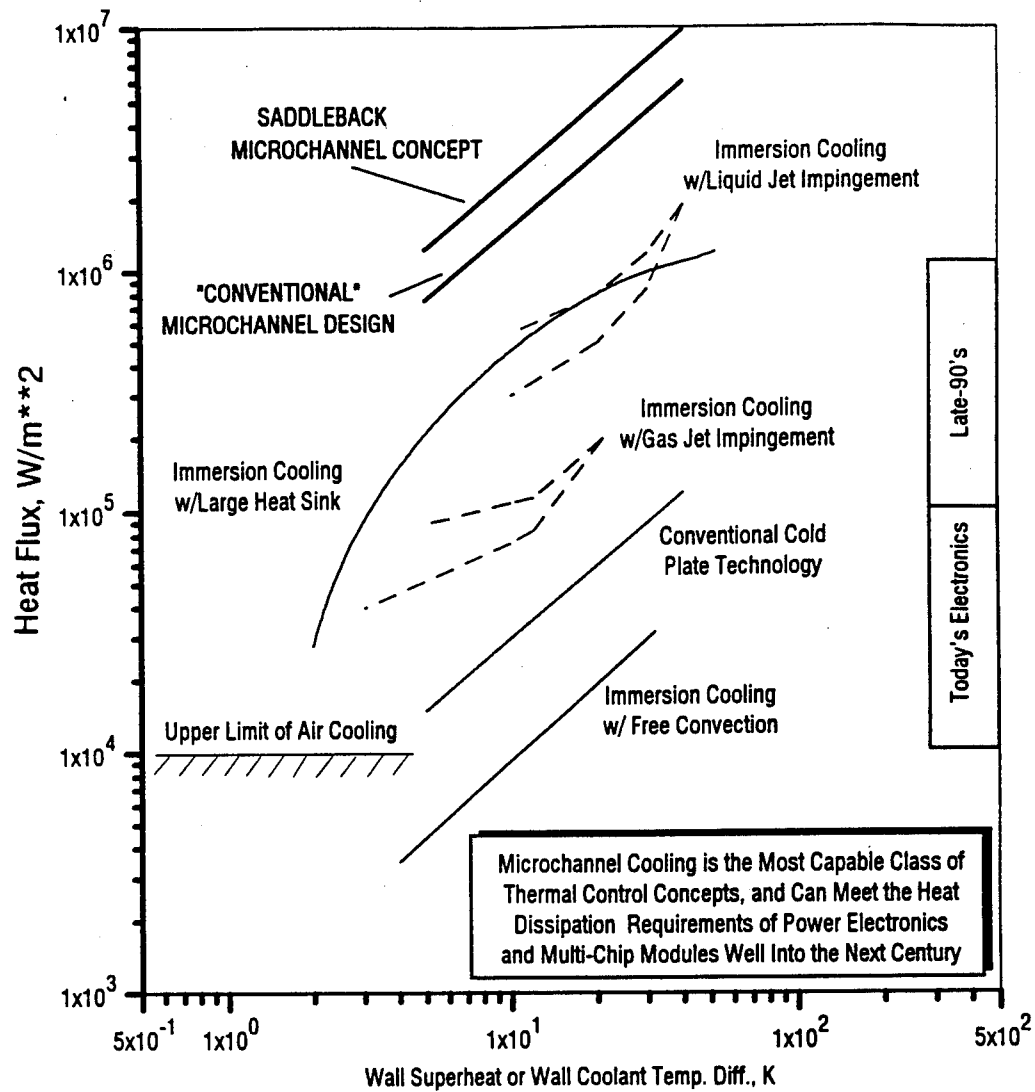


Figure 8. Comparison of electronics cooling techniques

3.1 DESCRIPTION OF THE SLDA COOLING PROBLEM

Semiconductor laser diodes have a variety of potential applications, including the pumping of solid-state lasers, service as medical lasers, and a variety of uses in optical communications. Most of these applications, particularly pumping solid-state lasers, require large optical output from the laser diode. The SLDA cooling problem is thus more severe than most electronics cooling cases because achieving these high optical output powers requires driving large powers through very small volumes in semiconductor materials. The waste heat from this process generates extremely high local heat fluxes, greater than 10 kW/cm^2 in some instances, and the material conductivity is usually low (for instance, $k_{\text{GaAs}} = 0.45 \text{ W/cm/K}$).

To alleviate this problem, several diodes are used in an array, with each diode contributing its portion to the total output power, and dissipating only a fraction of the total waste heat. Array spacing can therefore be limited by thermal concerns, since high heat flux devices must be spaced more widely apart than low heat flux devices. Heat dissipation can also affect the selection of the laser diode configuration itself. The investigators in Reference 38, for example, fabricated very small cylindrical diodes to allow 3D thermal conduction rather than fabricating diode bars, which have a 2D conduction geometry.

In addition to the dissipation of high heat fluxes, high power SLDA's also require an unusual degree of temperature stability. The temperature cannot change either across the array or in time, because the diode output wavelength is a sensitive function of temperature. In fact, LLNL, MIT/LL, and Perkin-Elmer (see discussions in Section 2) have all used the output wavelength as a measure of junction temperature in their thermal performance experiments. A typical value from these experiments is 3 angstroms wavelength shift for every degree Celsius. The efficiency of the device is also a function of temperature.

Diode laser require electrical contacts, with the heatsink components serving as a ground plane. For silicon heatsinks metallization of the surface is required, but for copper heatsinks such as developed in this Phase I study, no additional surface preparation is required. This

simplifies attachment, unless a diamond heat spreading layer is required between the laser and the cooler. One of the benefits of the stringent temperature control requirements is that thermal stresses at the joints are virtual eliminated - the assembly is essentially kept at room temperature, with no lateral thermal gradients.

3.2 PHASE I DESIGN GOALS

In the Phase I study, Phillips Laboratory provided thermal design requirements for a specific array design to Saddleback Aerospace - these are shown in Figure 9. The figure shows a $100\ \mu\text{m} \times 1000\ \mu\text{m}$ semiconductor laser diode bars on $900\ \mu\text{m}$ centers. The active layer is $1\ \mu\text{m} - 2\ \mu\text{m}$ thick, and the GaAs substrate is $100\ \mu\text{m}$ thick. A typical array would have 10 of these diode bars, spanning approximately 1 cm. The bars are expected to be 0.5 mm - 1 mm in length. Each bar dissipates 10 W, giving an average heat flux over the array of about $1000\ \text{W}/\text{cm}^2$, and a local heat flux at the bar of $10000\ \text{W}/\text{cm}^2$. The junction design temperature is 300 K, and the junctions across the array must be maintained within $\pm 1\ \text{K}$. It was assumed that the diodes are mounted in an inverted configuration with the active layer against the SLAC so that the thermal resistance of the device itself is negligible.

The Phillips Laboratory requirements also included packaging constraints. Minimal volume configurations were desired, to facilitate eventual operational implementation. A second requirement was to provide manifolding and coolant supply lines without intruding laterally beyond the frontal area of the cooler. This specification is intended to allow eventual tiling of individual arrays, to form arrays of arrays.

The approach in the Phase I study was to take the detailed thermal requirements provided by Phillips Laboratory, and to design a microchannel cooler to the thermal specifications only. No consideration was given in the Phase I study to issues such as details of SLDA mounting, electrical/optical interfaces, and general integration of the cooler into optical systems. Instead the program focussed on meeting the stringent thermal requirements in a compact package, and providing a simple flat surface upon which the SLDA could be eventually

mounted. In future studies, a variety of integration architectures, such as the low, intermediate, and high integration architectures discussed in Reference 39, may be examined.

No special environmental constraints, such as unusual temperature ranges or chemical compatibility requirements, were levied during the Phase I study. For this reason copper was selected as the microchannel material, and water was selected as the coolant. These selections were made, by agreement with USAF/PL, for convenience and to take advantage of the obvious performance benefits of these materials. Alternative materials and coolants could be used if the need arises. For example, in the event that operation in a space environment becomes of interest, a coolant with a lower freezing temperature than water (such as freon) could be employed.

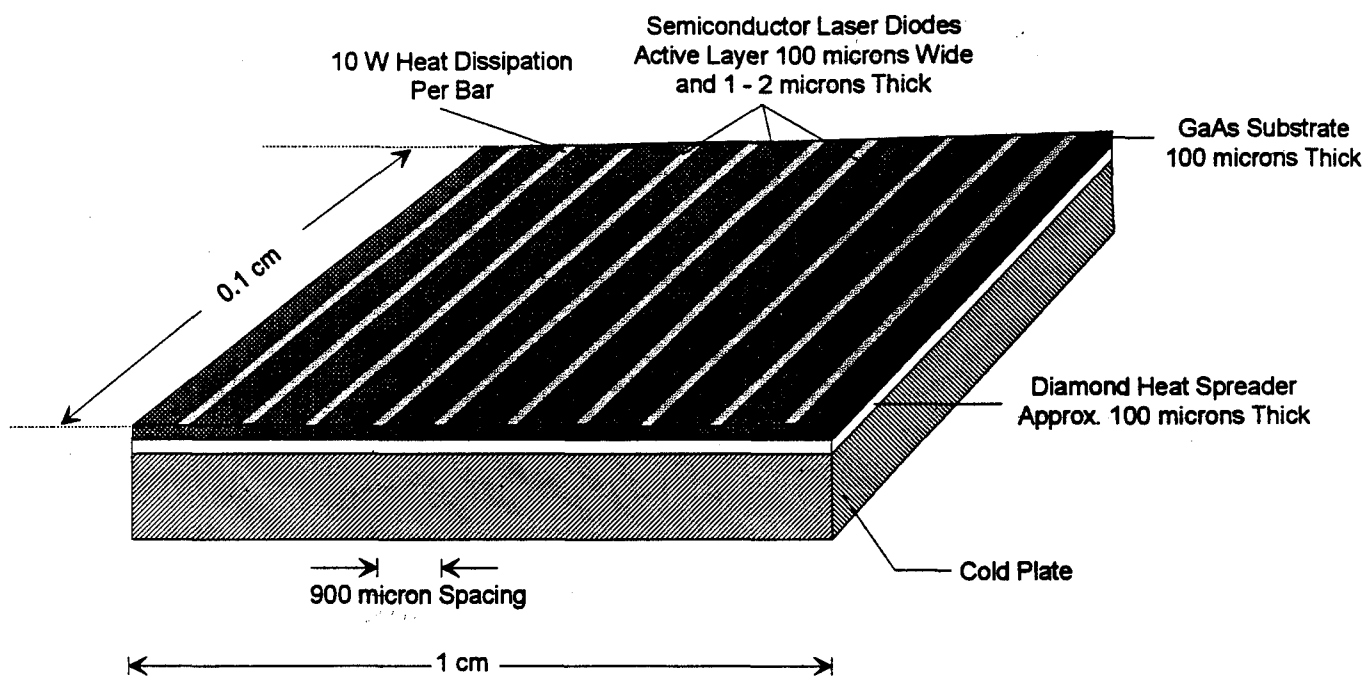


Figure 9. Phase I design requirements - 1D SLDA configuration

4.0 ANALYTIC TRADE STUDIES

Analytic trade studies were performed to identify design sensitivities and to support the prototype design task. At the beginning of the optimization studies, parametric 1D analyses were used to evaluate performance trends and to predict the best-performing designs. The 1D analyses used empirically-derived formulas to predict heat transfer coefficients and friction factors for pressure loss. Subsequently 2D numerical analyses were performed to provide a more detailed look at specific design areas. One set of numerical analyses examined the flowfield characteristics within the microchannels to determine when and where recirculation and stagnation zones might develop. The second set evaluated the performance of a diamond heat spreader to aid in sizing the required heat spreader thickness.

The results of the trades showed that a copper microchannel structure with a diamond heat spreader could dissipate the 10 kW/cm^2 required by the Phillips Laboratory design specifications. The sizing information provided in the trades was then used to design the Phase I prototype models, as described in Section 5. The three sections directly below describe the details of the 1D, 2D flowfield, and 2D heat spreader analyses.

4.1 1D MICROCHANNEL SIZING STUDIES

As mentioned in Section 3, copper was selected for the SLAC material, and water was chosen as the coolant. In all calculations conducted in the Phase I study, contact thermal and internal laser diode resistances were neglected. Thus, the heat-generating active region of the diode is assumed to be in perfect contact with the outer surface of the copper faceplate. This should not provide much error in the analyses: typical thermal resistances for the diode interior and an indium solder interface are 0.0002 and $0.002 \text{ }^\circ\text{C}/(\text{W}/\text{cm}^2)$, respectively, while the thermal resistance values of interest (between the heated surface and the coolant) in this program range from $0.04 - 0.1 \text{ }^\circ\text{C}/(\text{W}/\text{cm}^2)$.

The minimum faceplate thickness is currently fixed at a 125 μm due to manufacturing constraints. At the design heat flux, the temperature drop through even the minimum thickness face plate is very high, and can exceed the allowable temperature difference between the device (@ 300 K) and the coolant (liquid water with $T_{\text{min}} = 273.2 \text{ K}$). This effect is shown in Figure 10, which presents the temperature drop vs. faceplate thickness for several materials of interest. The design conditions given above, taken with the desirability of using water as a coolant, led to the conclusion that a heat spreader must be used to distribute the heat flux over a larger area at the SLAC interface.

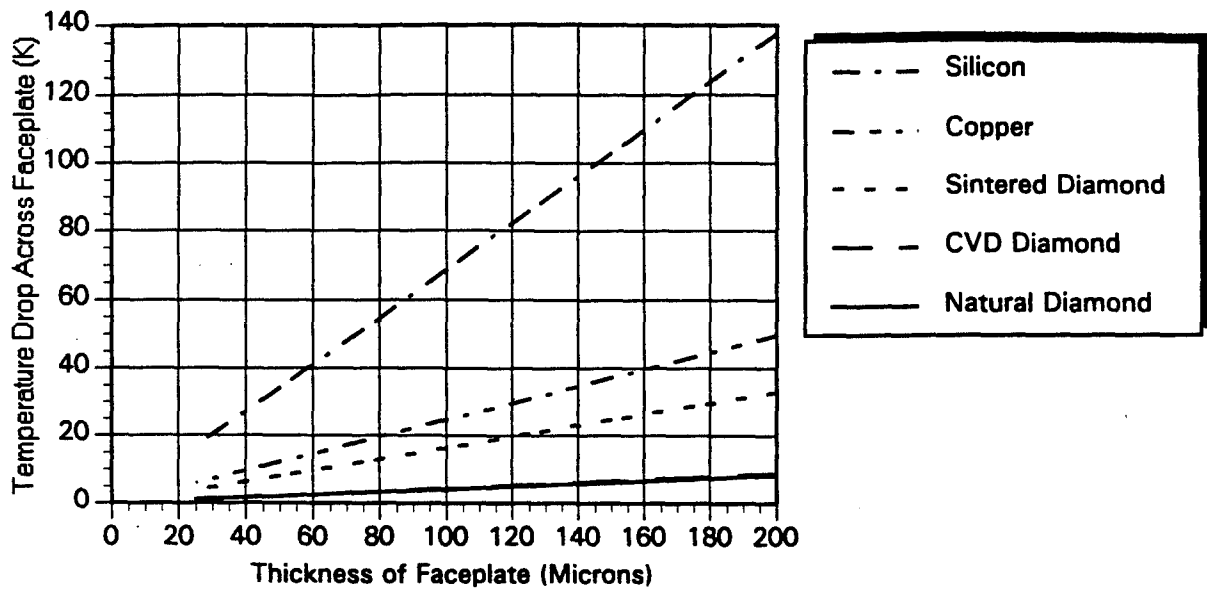


Figure 10. 1D calculations of temperature drop across the microchannel faceplate.

Initially, a simple set of calculations were performed to examine the required characteristics of a heat spreader. One-dimensional fin effectiveness calculations were performed to provide a rough sizing for the spreader. The copper face plate itself serves to distribute the heat flux laterally; the effective heat transfer area is increased by approximately a factor of 4. This also reduces the average temperature drop across the face plate thickness by roughly a factor of 4, from 31°C to about 8°C. The resultant average heat flux is still too high, however, to be accommodated by microchannels with or without fins. It was determined during the course of the 1D trades (described in Section 4.1) that the average heat flux would have to be

reduced to less than about 1700 W/cm^2 in order for microchannel structures of reasonable dimensions (e.g., $\sim 25 \mu\text{m}$ channel width) to be used.

Figure 11 compares the required thicknesses for Chemical Vapor-Deposited (CVD) diamond and natural diamond heat spreaders. The calculations are based on 1D fin effectiveness, with adiabatic walls on the air side and at the ends of the spreader. The excess temperature calculated using this approach compared well with the 2D calculations presented for an axisymmetric body in Reference 40. The thermal conductivity for CVD diamond was taken from Reference 40 as 2170 W/m/K through the thickness and 1300 W/m/K in the direction parallel to the interface. The conductivity for natural diamond (Type IIA) was taken as 2400 W/m/K . The figure shows that the average heat flux can be reduced by a factor of 7 (to about 1400 W/cm^2) using either a CVD diamond spreader with a thickness of $250 \mu\text{m}$, or a natural diamond spreader with a thickness of $150 \mu\text{m}$. The temperature drop across the $250 \mu\text{m}$ CVD diamond layer would be about 1.6 K , which is added to the drop across the faceplate of 4.5 K . These values were used in the remainder of the 1D trade studies.

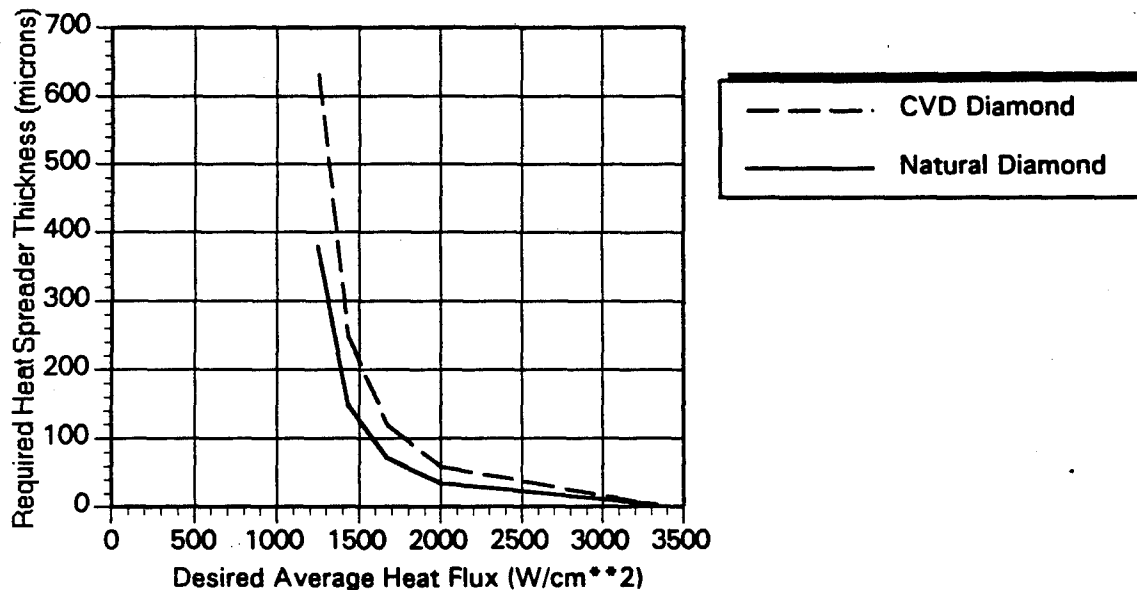


Figure 11. 1D heat spreader sizing analysis.

The thermal performance and pressure drop were computed for microchannels with no secondary fins. The results are shown in Figure 12. The figure presents comparisons of the performances of copper and silicon microchannels of varying dimensions. The microchannels are assumed to run perpendicularly to the laser diode bar to reduce the pressure drop and thermal gradients in the diode. The total water flow rate was kept constant for all the calculations at 1 g/s, giving a temperature rise of about 2 K (from an inlet temperature of 275.2 K). The channel width and primary fin thickness were kept constant for each curve (with the values shown in the legend), and the channel height was varied.

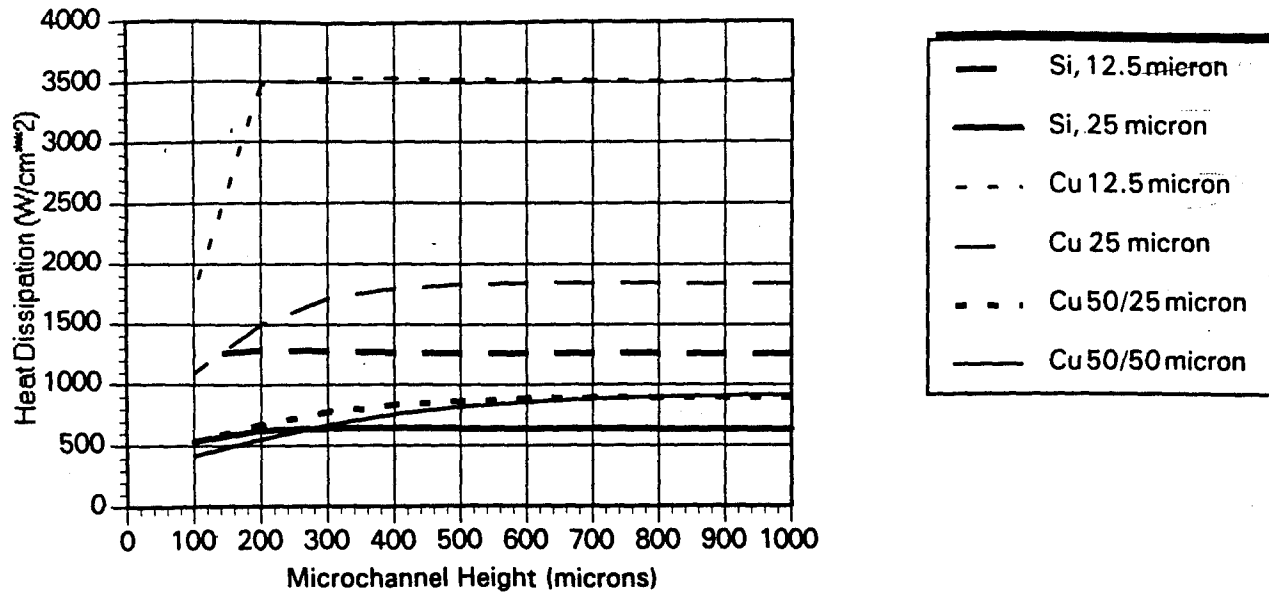
As the figure illustrates, the copper microchannel structures are much more effective for a given geometry than are the silicon structures. In fact, only the 12.5 μm and 25 μm copper microchannels meet the heat dissipation requirement ($= 1400 \text{ W/cm}^2$ on the y-axis of Figure 12a). All the curves level off with channel height ($=$ primary fin length) as the primary fin effectiveness goes to zero; the effect is more rapid for thinner fins and for the lower conductivity material. The pressure drops shown are reasonable, with the exception of the 12.5 μm channel case. As Figure 12a shows, the channel height should be about 200 μm for the 12.5 μm channel, but the corresponding pressure drop shown in Figure 4b is about 350 psi. A practical limit for microchannel use is probably in the range of 50 - 100 psi, with pressure drops of 25 - 30 psi being more desirable.

Similar calculations were then performed for the case of 25 μm copper microchannels with secondary fins - these results are presented in Figures 13 - 15. In Figure 13, circular secondary fins of diameter $= 100 \mu\text{m}$ were used at various fin spacings. The results are compared to the 25 μm copper case (no secondary fins) presented in Figure 12. This comparison should be treated with caution, since different correlations are used for finned and unfinned microchannels. The thermal performance for the finned microchannels is calculated using a Reynolds number-dependent correlation based on Reference 2 results, while that for the unfinned channels is independent of Reynolds number. Thus, at high

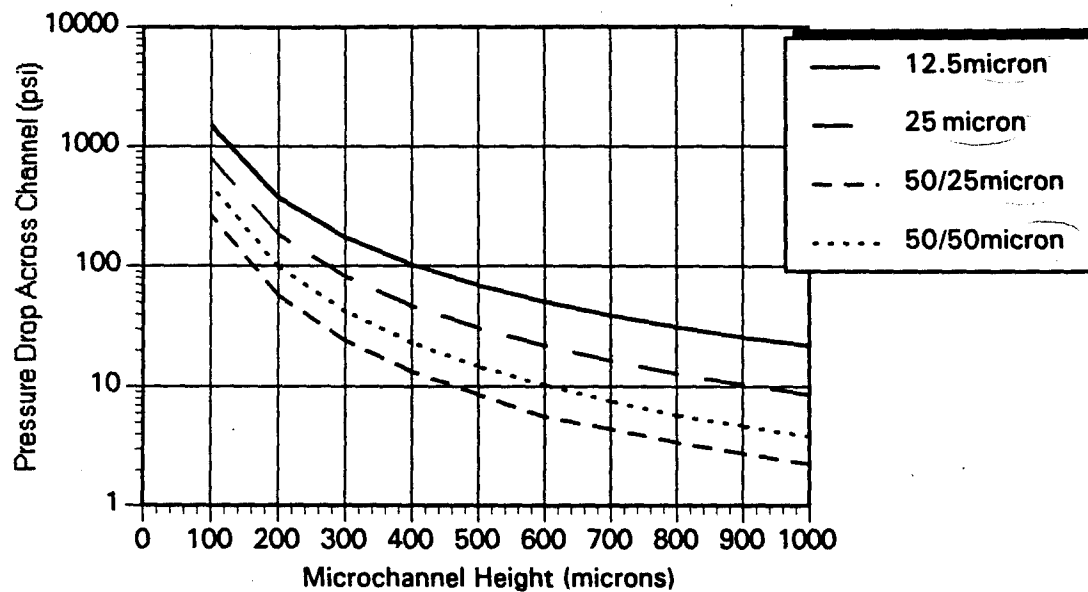
Reynolds numbers (i.e., small channel heights since the flow rate is fixed), the heat transfer coefficient is much higher for the finned channels than for the unfinned channels.

An interesting feature of the Figure 13 calculations is that the secondary fins actually reduce the available heat transfer area, so that the largest fin spacing yields the best thermal performance. This is because the secondary fin height (= channel width) is much smaller than the fin diameter, so that the fin footprint is larger than its exposed surface area. The microchannels maintain superior thermal performance (compared to microchannels with no secondary fins) due to the increased heat transfer coefficient, which is due in turn to the interruption of the boundary layer due to the presence of the fins. Figures 14 and 15 show a reversal of the order of performance, with the densest fin arrays yielding the highest thermal performance. This is due to the smaller fin diameters for those cases - Figure 14 = 50 μm , and Figure 15 = 25 μm . The fin height is constant at 25 μm in all cases.

Overall, the microchannel thermal performance appears to be insensitive to fin diameter and fin spacing, with the exception of the 120 μm fin spacing cases shown in Figures 14 and 15. In those cases, the heat transfer area and Reynolds number have increased substantially in comparison to the other spacings, yielding higher thermal performance, but high pressure drops as well. For a constant 50 psi pressure drop, the best thermal performances for each fin radius are within 5% of one another, dissipating about 1800 W/cm² at the given design conditions. This is nearly 30% higher than the requirement for the SLAC, but will be reduced with the addition of solder joint thermal resistances, and other real-world considerations.

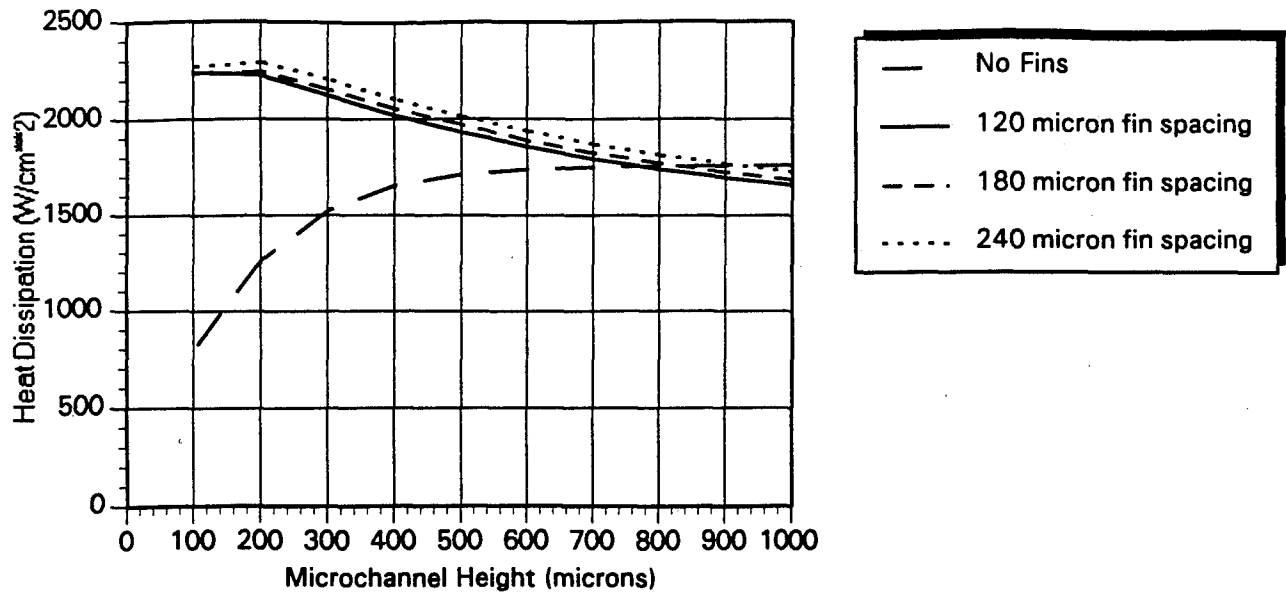


(a) comparison of silicon and copper microchannel performance for a range of channel widths and heights

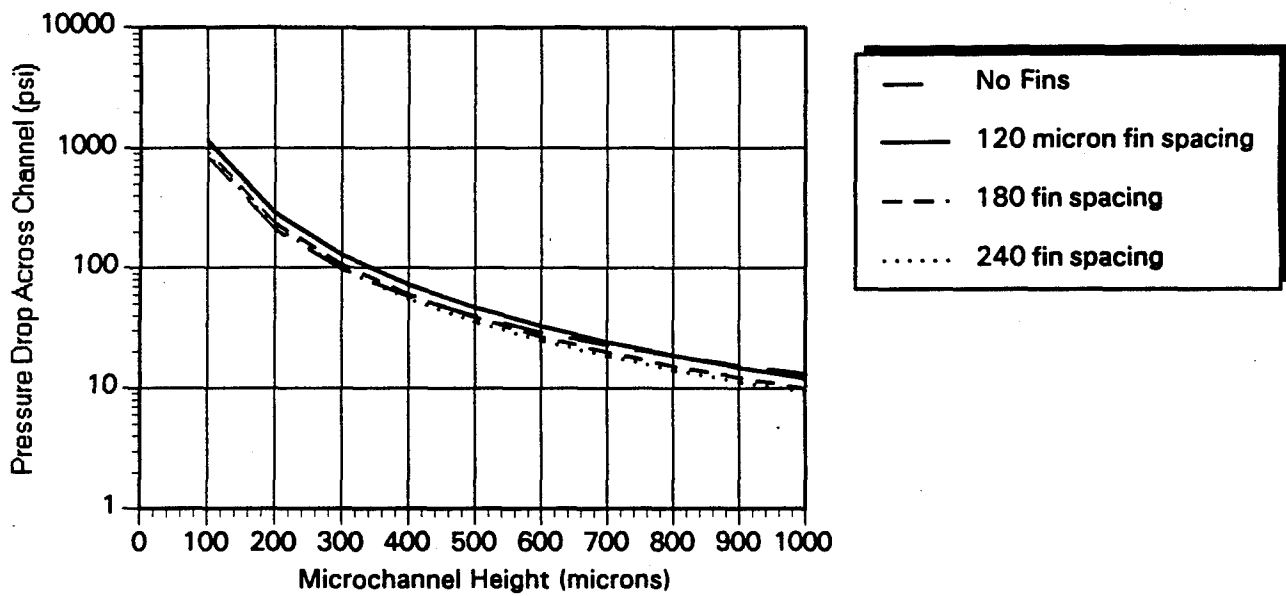


(b) comparison of pressure losses for the channel geometries considered in (a)

Figure 12. Comparison of silicon and copper microchannel performance

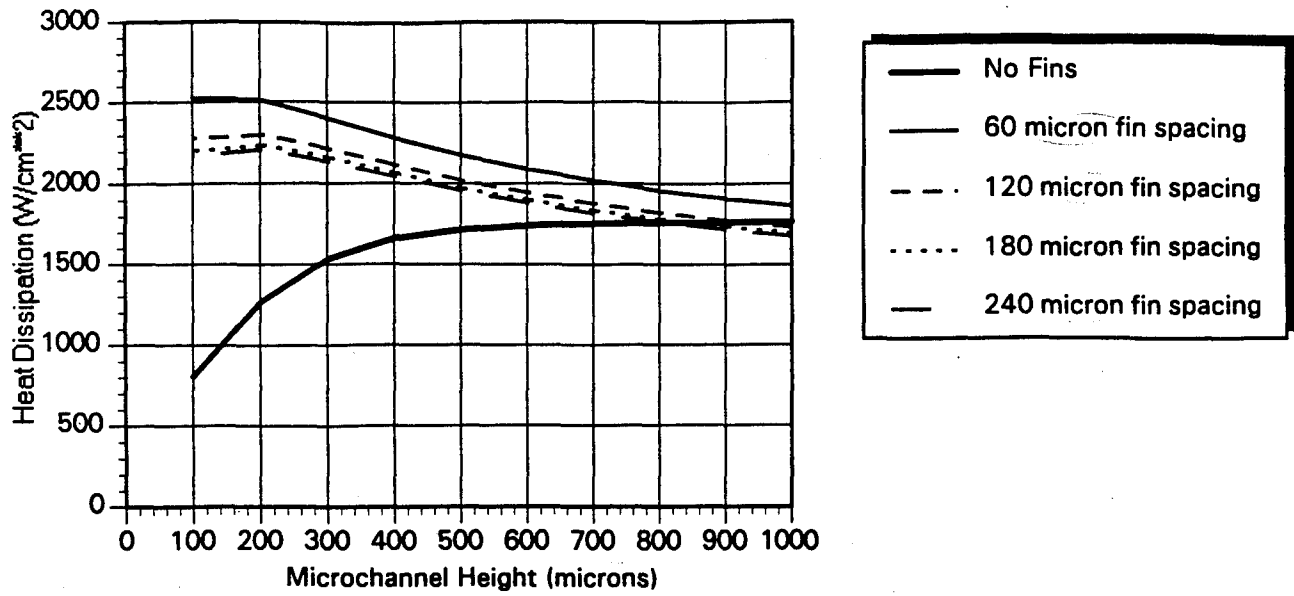


(a) heat dissipation for microchannels with secondary fins

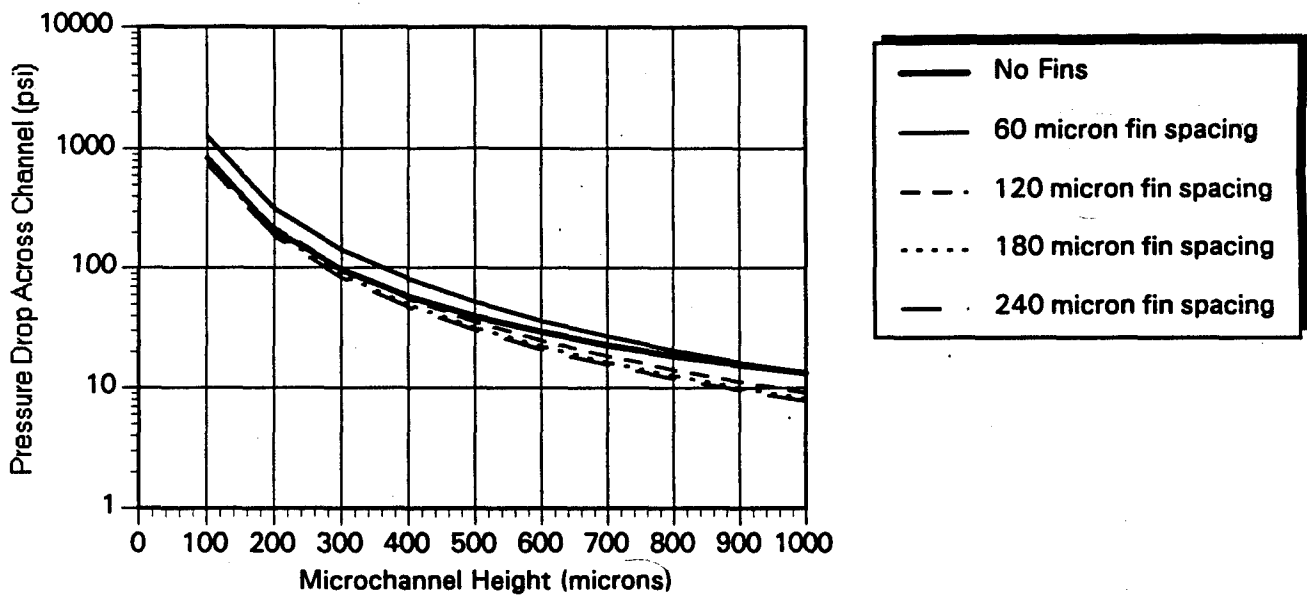


(b) pressure losses across microchannels with secondary fins

Figure 13. Performance of 25 micron microchannels with 100 micron secondary fins

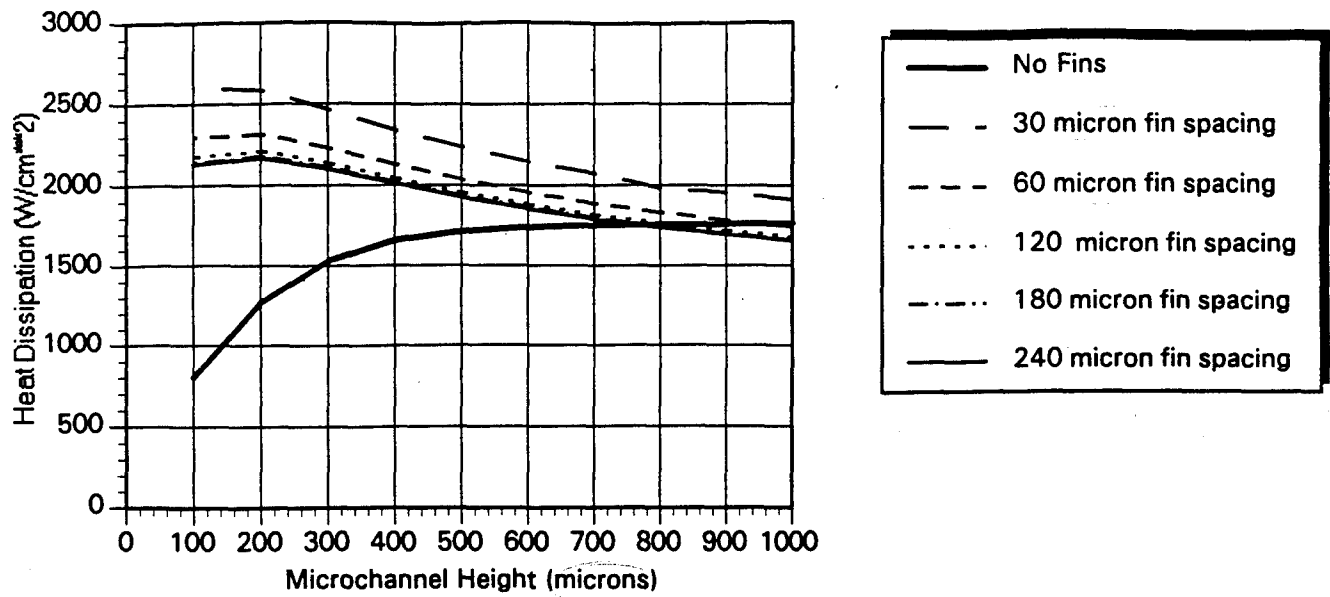


(a) heat dissipation for microchannels with secondary fins

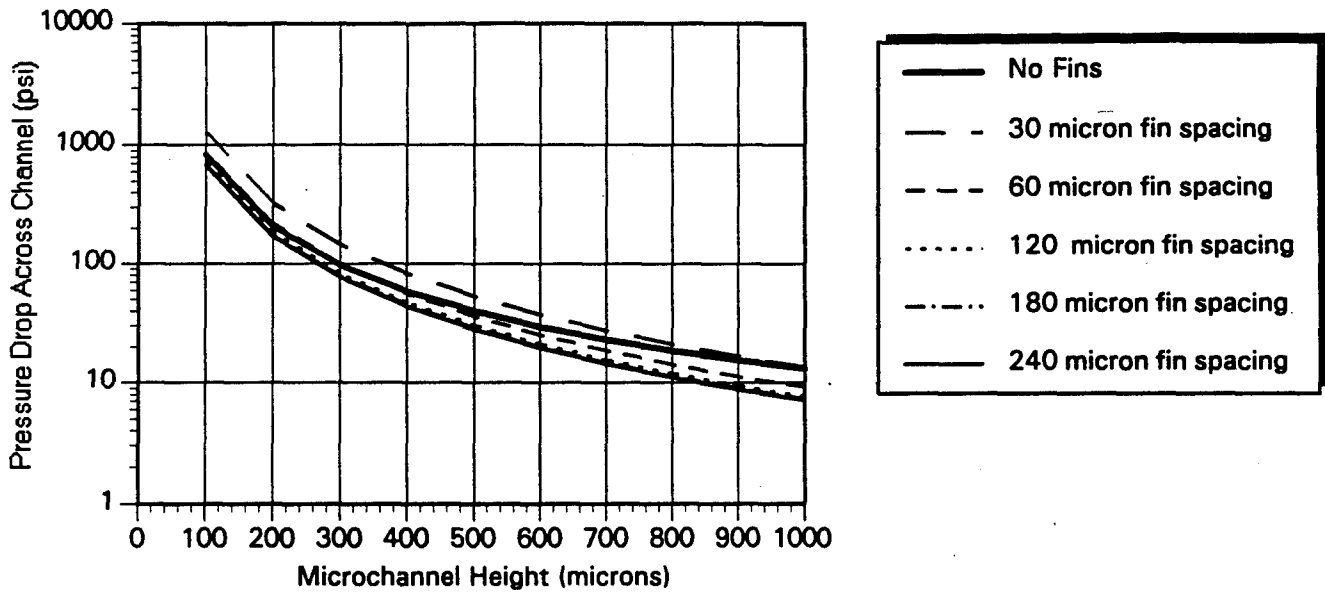


(b) pressure losses across microchannels with secondary fins

Figure 14. Performance of 25 micron microchannels with 50 micron secondary fins



(a) heat dissipation for microchannels with secondary fins



(b) pressure losses across microchannels with secondary fins

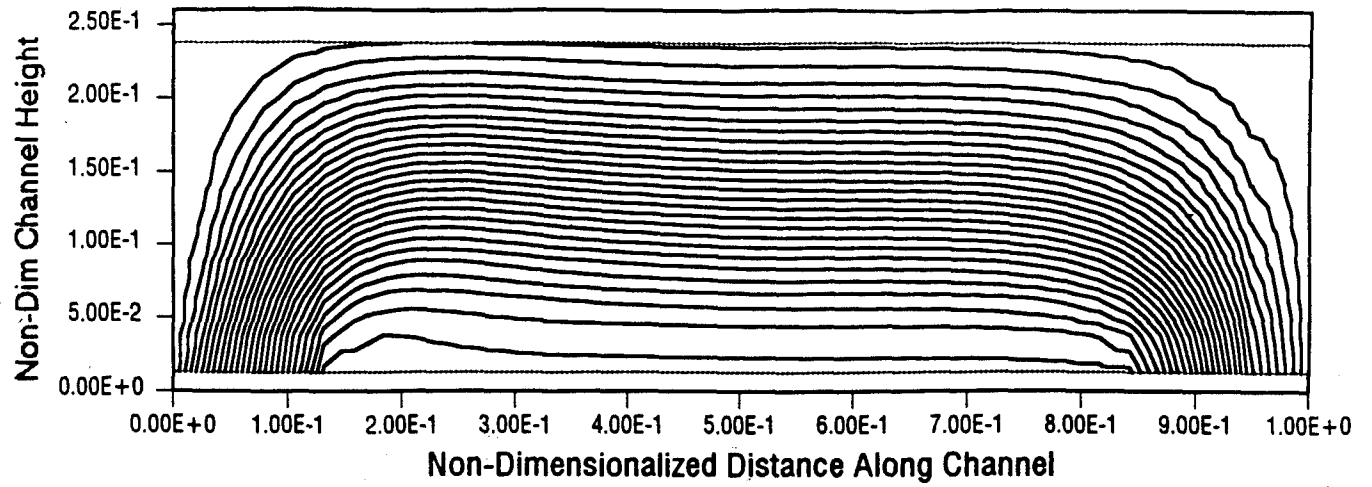
Figure 15. Performance of 25 micron microchannels with 25 micron secondary fins

4.2 2D MICROCHANNEL FLOW STUDIES

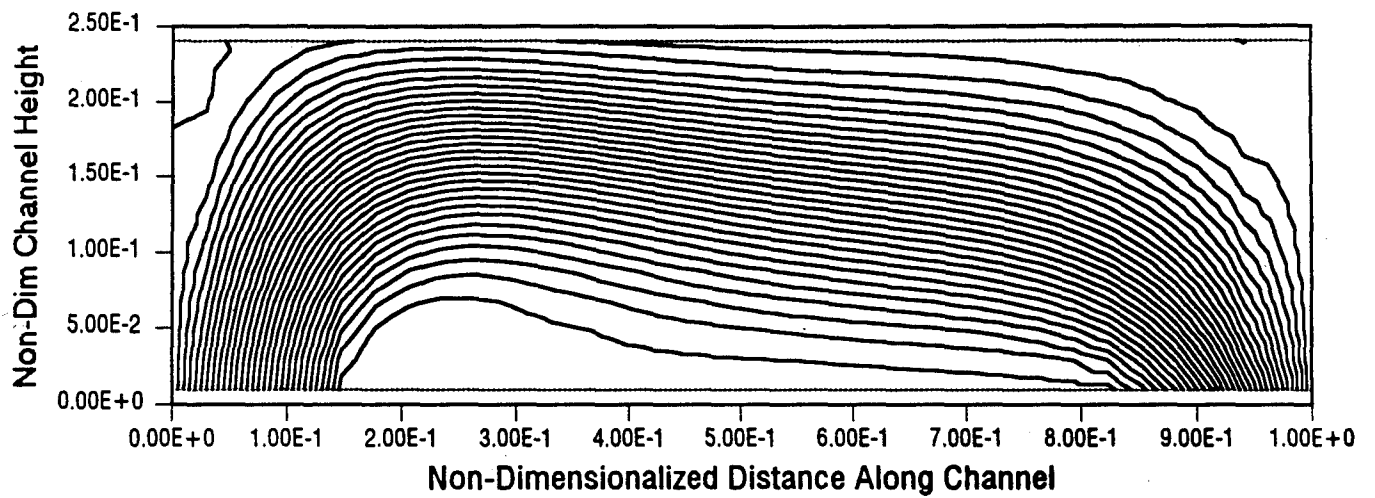
Flow performance calculations were also conducted, to determine the likelihood of development of "hot spots"; i.e., regions of stagnant or recirculating flow within the microchannel. Finite difference predictions for 2D steady-state flow along the microchannel centerplane (the plane between the primary fins) are shown in Figures 17 and 18. All calculations are for laminar flow conditions; microchannels typically operate at Reynolds numbers in the low hundreds, and for stressing heat flux levels can be forced to a range of $700 < Re < 1000$.

This range of Reynolds numbers implies that inertial effects are significant, and regions of separation and recirculation can occur within the flow. The finite difference calculations performed here include inertial effects, and the result on the flowfield solution can be seen immediately in Figures 17b - 17d, as the streamlines of the entering flow separate from the lower wall, forming a region of recirculation. As the subsequent plots in Figure 17 show, at higher Reynolds numbers the effects become even more significant, with the recirculation region occupying more than a third of the lower wall area, and additional recirculation regions forming in the upper corners of the microchannel (see Figure 17d, $Re = 200$). The low Reynolds number ($Re = 10$) calculation shown in Figure 17a compares well on a qualitative basis with comparable calculations in Reference 38 (pp. A-4 and A-5, Ref. 38).

The inertial effects are more significant in the Figure 18 series of computations, where the passage height has been doubled from $1/4$ the passage length (as in Figure 17) to $1/2$ the passage length (all Figure 5 plots). This corresponds to passage heights of approximately $200 \mu\text{m}$ in Figure 17, and $400 \mu\text{m}$ in Figure 18. The $Re = 100$ and $Re = 200$ cases show that about a quarter of the heat transfer area of the passage is eliminated due to the formation of recirculation regions. One of the reasons for the aggravated recirculation is that the passage entrance and exit are poorly matched to the channel size - that is, the entrance into the Figure 17 channels is about $1/2$ the size of the channel, while the entrance into the Figure 18 channels is about $1/4$ the channel size. Geometric and structural integrity concerns make

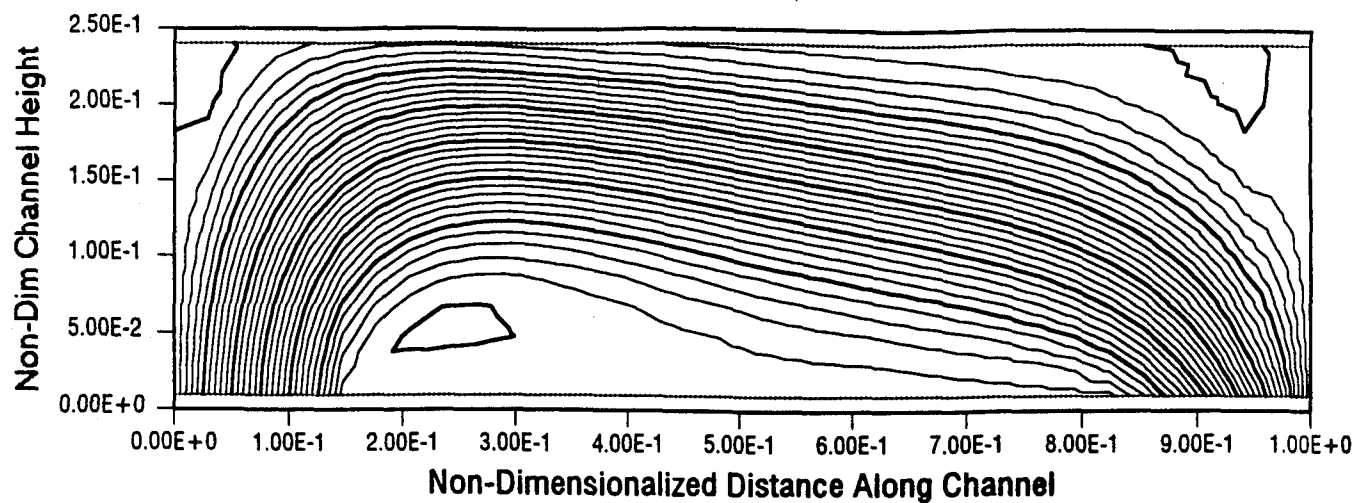


(a) streamlines for $Re = 10$

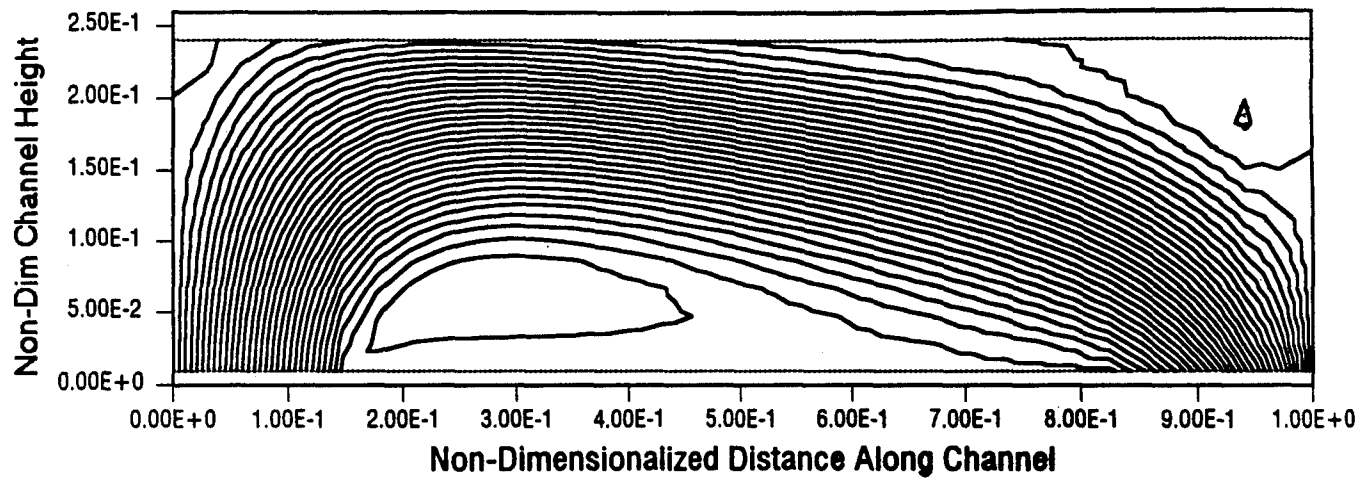


(b) streamlines for $Re = 50$

Figure 17. Streamlines for simple microchannel with 1/4 aspect ratio

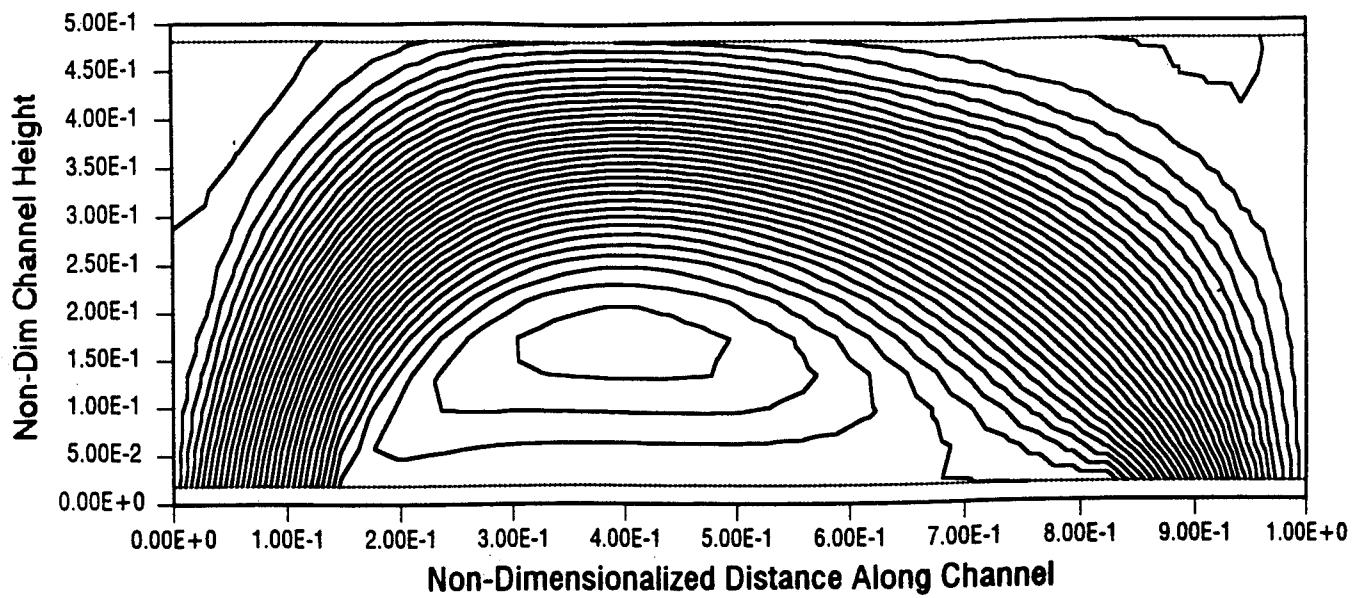


(c) streamlines for $Re = 100$

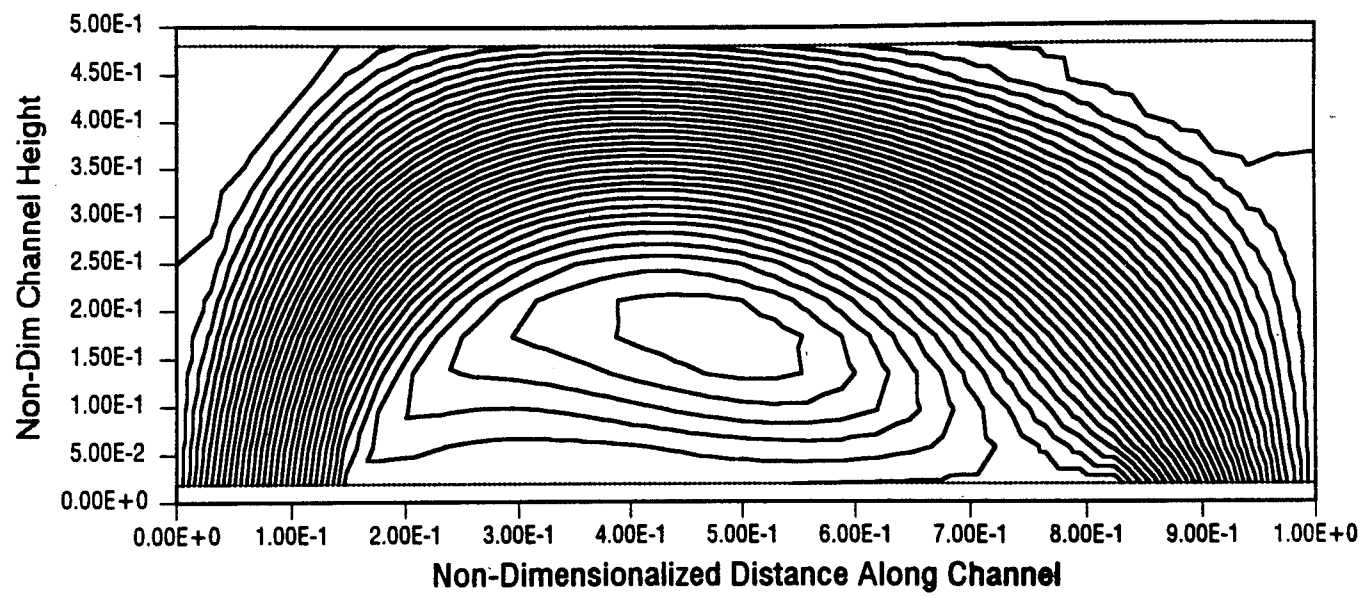


(d) streamlines for $Re = 200$

Figure 17 (cont.). Streamlines for simple microchannel with 1/4 aspect ratio

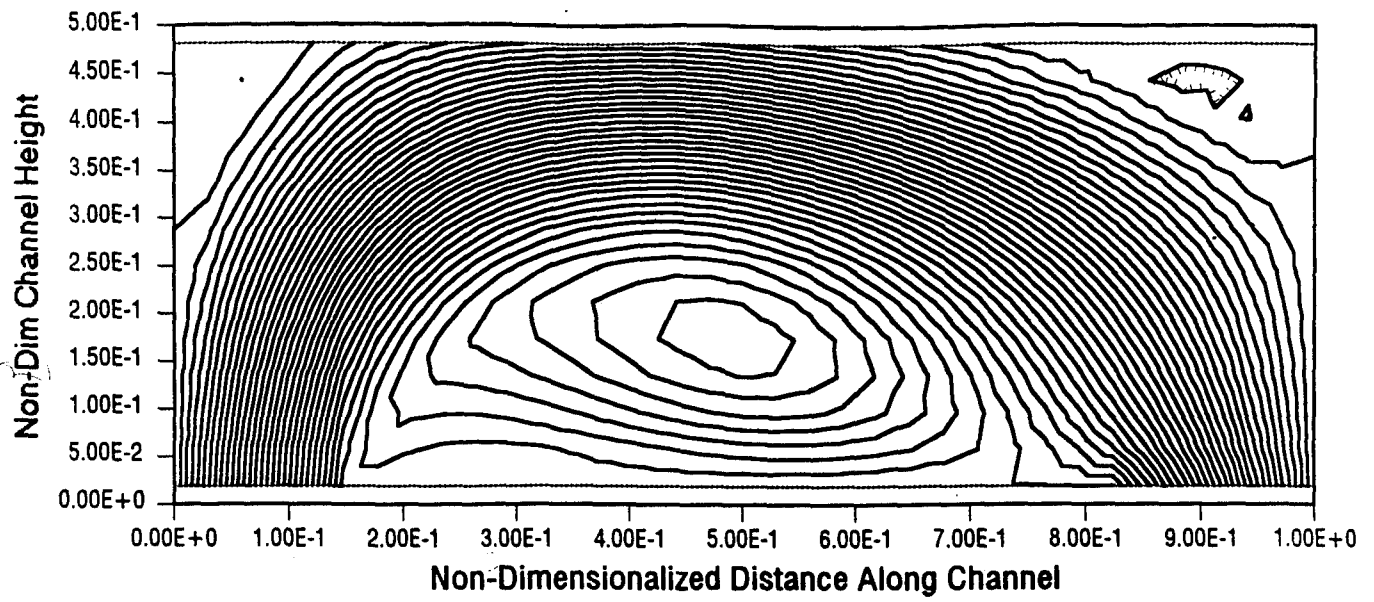


(a) streamlines for $Re = 50$



(b) streamlines for $Re = 100$

Figure 18. Streamlines for simple microchannel with 1/2 aspect ratio



(c) streamlines for $Re = 200$

Figure 18 (continued). Streamlines for simple microchannel with 1/2 aspect ratio

it desirable to minimize the size of the entrances and exits, since the area available to accommodate the inlet and outlet passages is limited.

The viscous effects due to the proximity of the channel walls were not included in these 2D calculations. [The analysis was conducted in the x-y plane, and the viscous effects act on the z faces of the fluid elements (i.e., on faces parallel to the page)] They can be important, serving to damp out some of the separation effects. A full 3D analysis should be conducted in future efforts to assess the magnitude of the viscous effects.

4.3 2D FACEPLATE/HEAT SPREADER DESIGN STUDIES

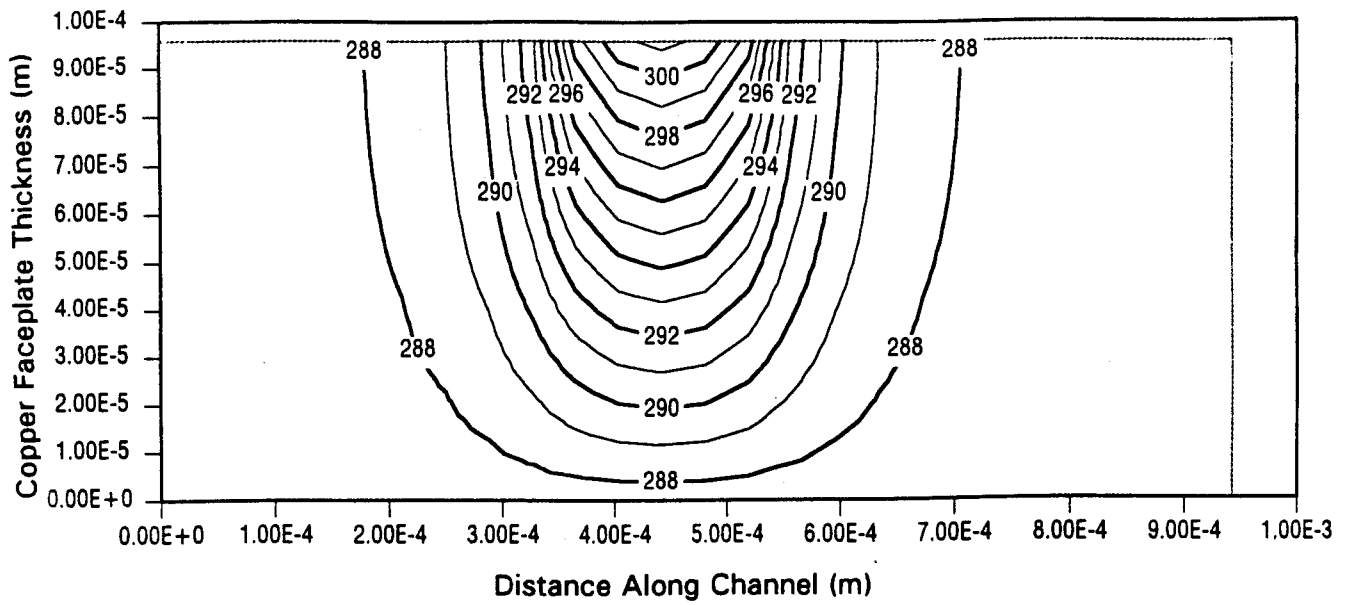
As illustrated in the figures, the thinnest faceplate had the lowest overall thermal resistance. This, combined with the observation that the 1D fin results show lower overall resistance than the 2D results, led to the conclusion that the thermal constriction in the interface area is dominating the thermal resistance of the faceplate. This led in turn to the requirement for a higher conductivity heat spreader to reduce the overall thermal resistance.

The results of the thermal trade studies are illustrated in Figures 19 -21. Figures 19a - 19d show 2D steady-state finite difference computations for the copper faceplate region of the microchannel cooler. Thermal profiles for faceplate thicknesses ranging from 100 μm to 200 μm (with 125 μm considered to be the minimum fabricable thickness) are presented. The laser diode occupies the center 100 μm of this 900 μm wide analysis region, and supplies a heat flux of 10^4 W/cm^2 at this location. The interface between the diode and the faceplate was kept at approximately 300 K in the analysis, though the heat flux is used as the actual boundary condition in this area. As mentioned previously, the thermal resistance between the active region of the laser and the copper faceplate was assumed to be negligible. No radiation is considered, and the upper and side boundaries of the faceplate are treated as adiabatic. The bottom surface is kept at a fixed temperature, with the temperature specified as that required to keep the diode/faceplate interface near 300 K.

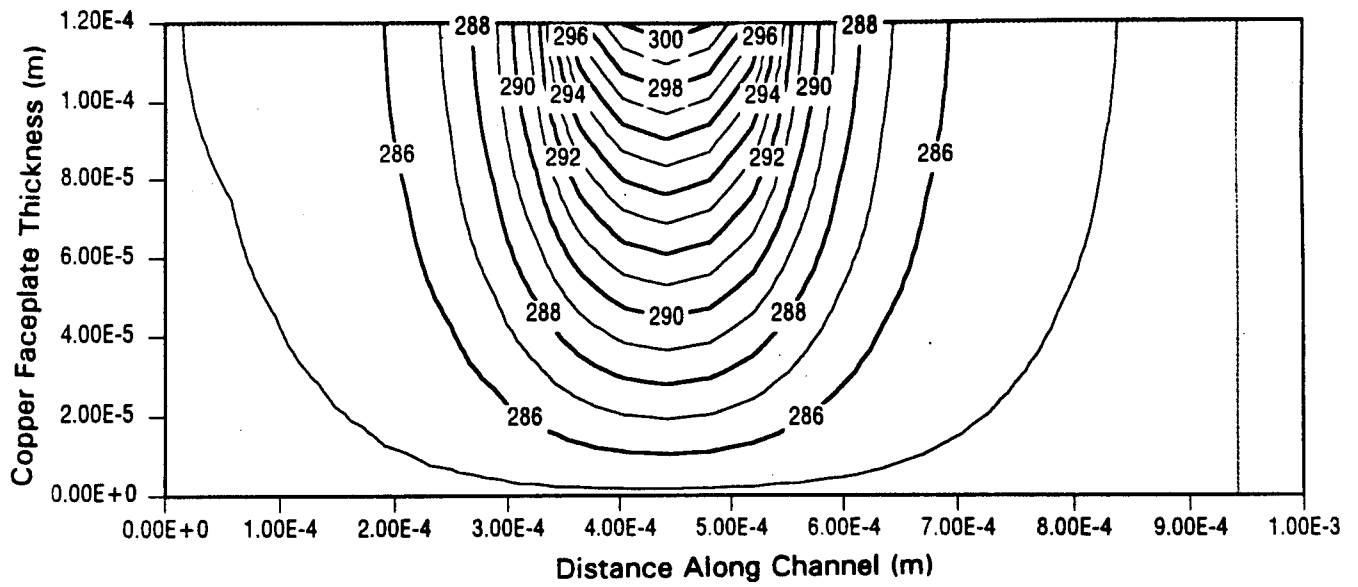
The effectiveness of an isotropic diamond heat spreader is demonstrated in Figure 20, where diamond heat spreaders ranging in thickness from 25 μm to 175 μm were examined, with a fixed copper faceplate thickness of 125 μm . The boundary conditions were the same as described above, with the assumption of no thermal resistance between the copper and diamond. In all cases, the thermal constriction effect was reduced substantially over the copper faceplate used alone. The 125 μm thickness appears to offer the best overall performance - the thinner spreaders have significant lateral thermal resistance, while the thicker spreaders do not offer substantial performance improvements.

This analysis was supplemented by computations for the more realistic case of a CVD diamond heat spreader with anisotropic heat conduction properties. The thermal conductivity for CVD diamond was taken from Reference 1 as 2170 W/m/K through the thickness and 1300 W/m/K in the direction parallel to the interface. The copper faceplate was assumed to be isotropic. The results are shown in Figure 21, for the same heat spreader thicknesses and boundary conditions as used in the Figure 20 calculations.

The results showed that, as expected, the anisotropic heat spreader is slightly worse than the isotropic heat spreader, with temperatures 1 - 1.5 K lower along the back face of the copper faceplate. Again, there is little difference between the performance of the two larger thicknesses, while the lateral resistance of the two smaller thicknesses is aggravated by the reduction in lateral conductivity. The performances of the 125 μm and 175 μm heat spreaders are adequate for a typical 25 μm -wide microchannel. The 125 μm heat spreader, for instance, permits the use of a cooler with a thermal resistance as high as 0.018 $^{\circ}\text{C}/(\text{W}/\text{cm}^2)$, with 10% of that resistance attributed to the copper faceplate. This is still a very low value, but it is attainable. Without the heat spreader, the required thermal resistance (neglecting the faceplate) is 0.009 $^{\circ}\text{C}/(\text{W}/\text{cm}^2)$, as opposed to 90% of 0.018, which is 0.162 $^{\circ}\text{C}/(\text{W}/\text{cm}^2)$. The heat spreader clearly provides a significant benefit.

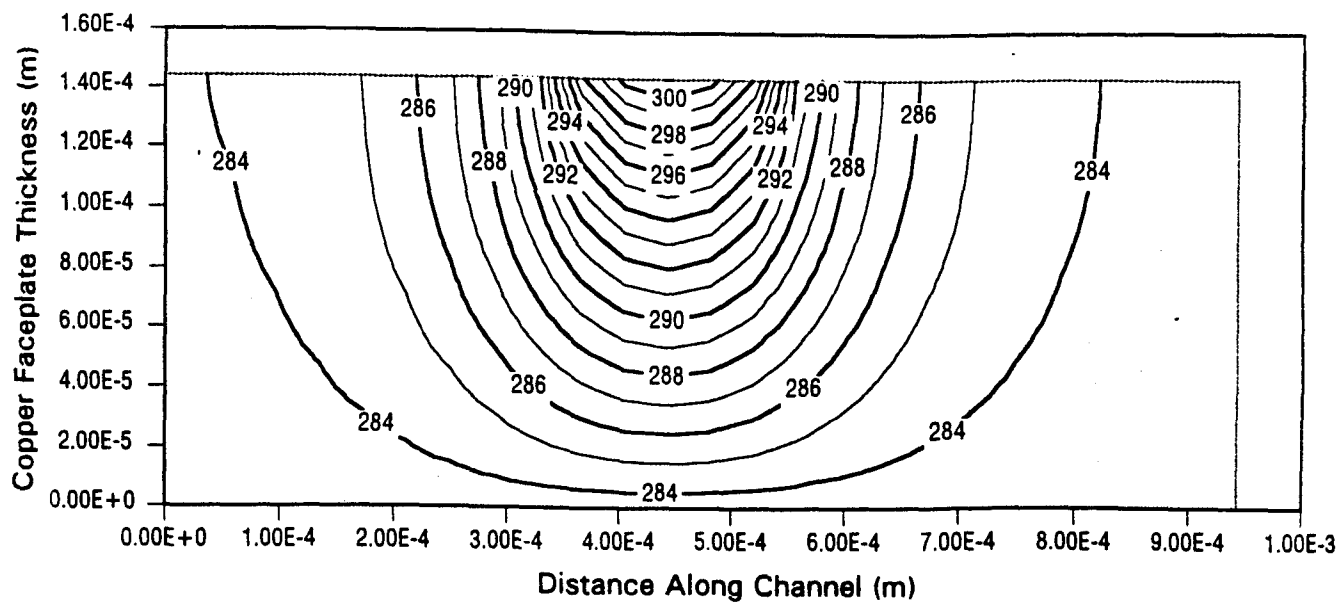


(a) thermal profiles for a 100 μm Cu faceplate

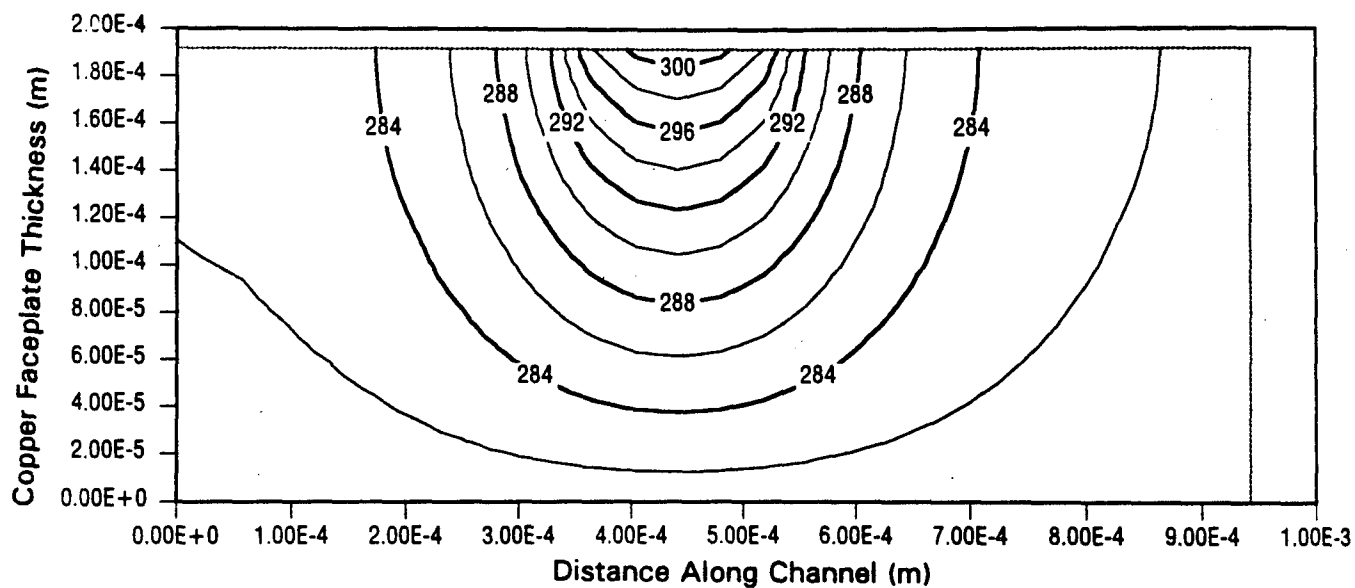


(b) thermal profiles for a 125 μm Cu faceplate

Figure 19. Thermal profiles for copper faceplate for several copper thicknesses

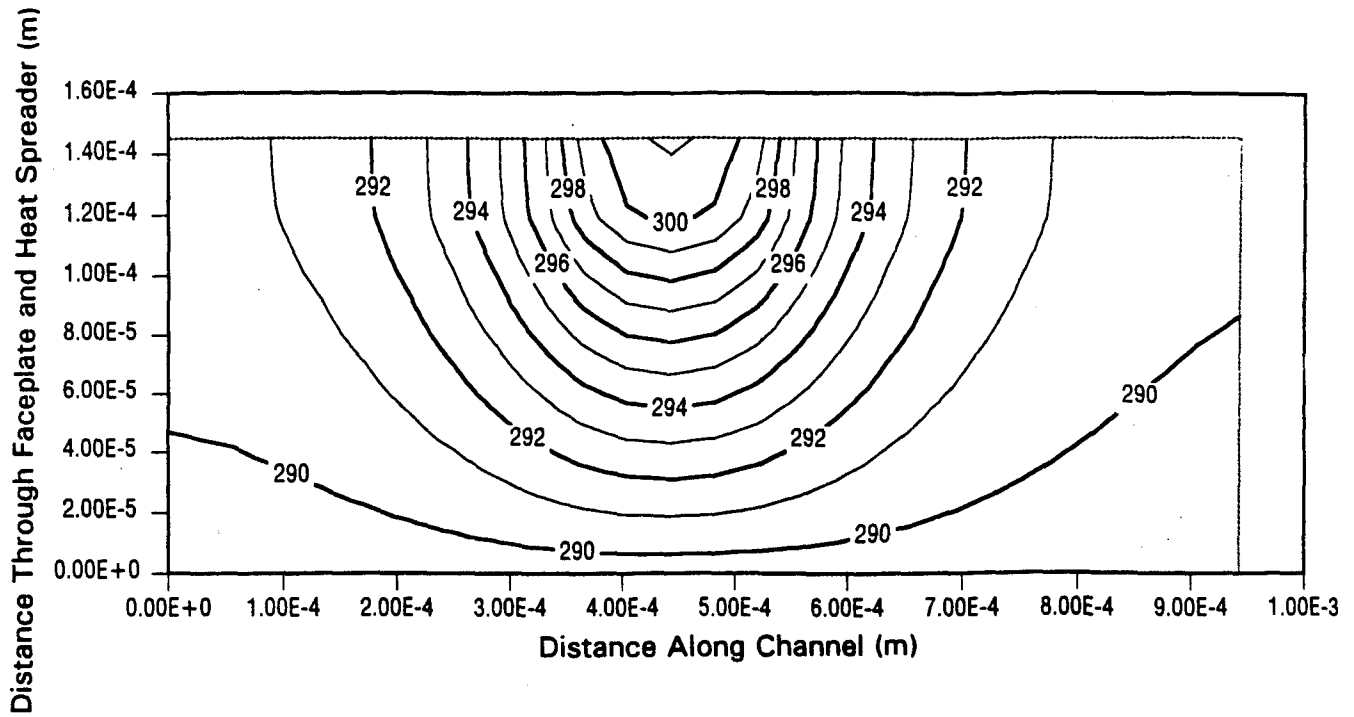


(c) thermal profiles for a 150 μm Cu faceplate

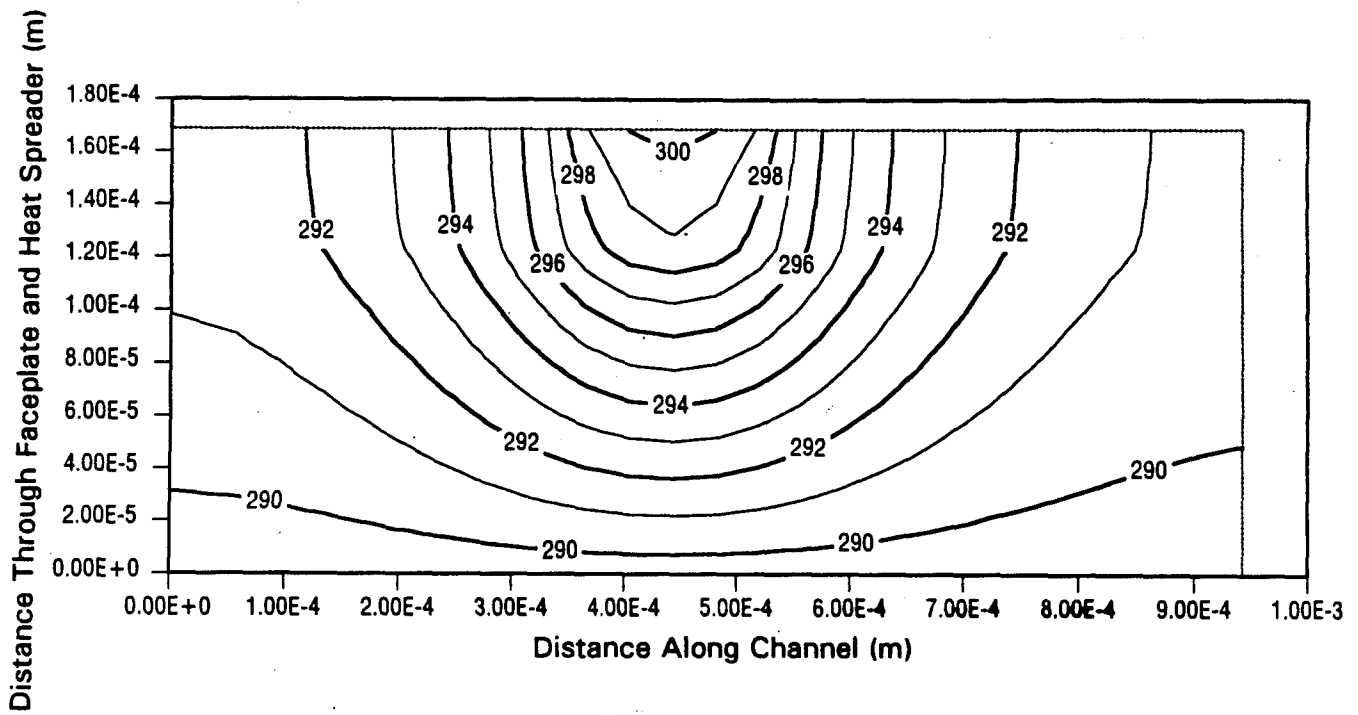


(d) thermal profiles for a 200 μm Cu faceplate

Figure 19 (cont.). Thermal profiles for copper faceplate for several copper thicknesses

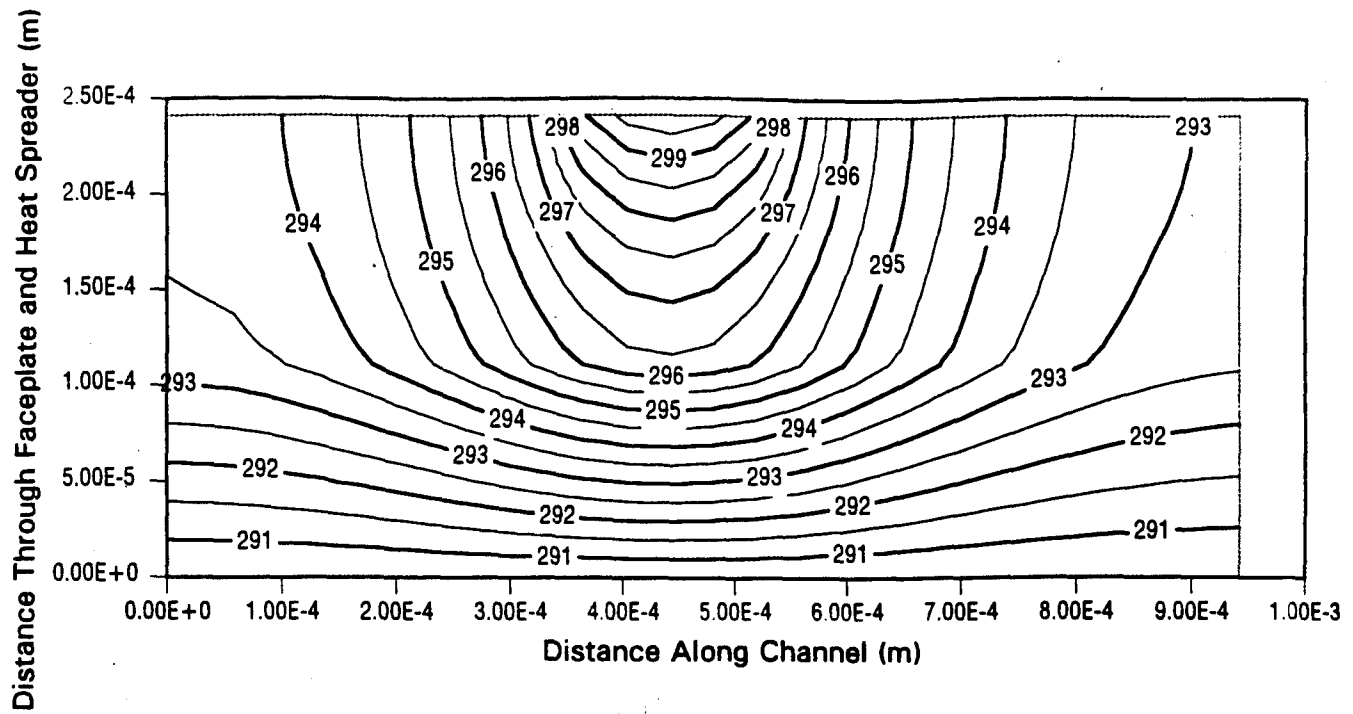


(a) thermal profiles for a 125 μm Cu faceplate with a 25 μm diamond heat spreader

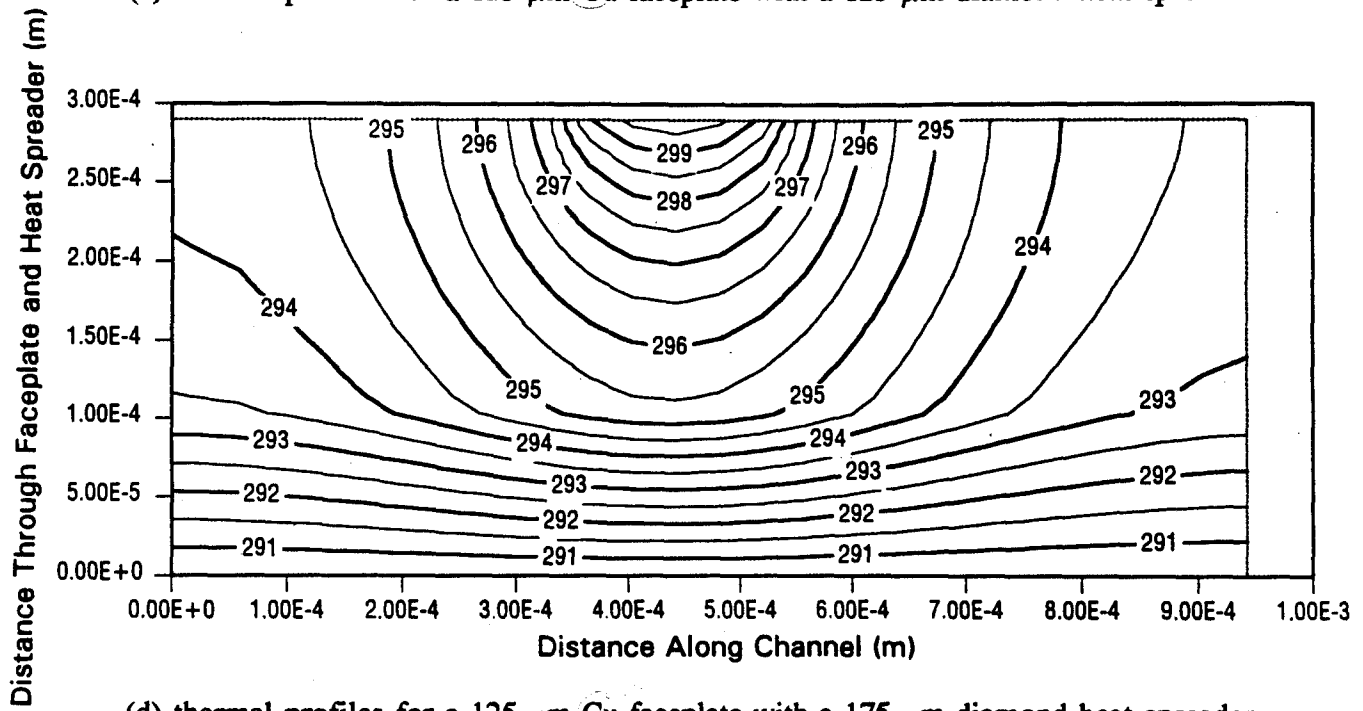


(b) thermal profiles for a 125 μm Cu faceplate with a 50 μm diamond heat spreader

Figure 20. Thermal profiles for copper faceplate with isotropic diamond heat spreader

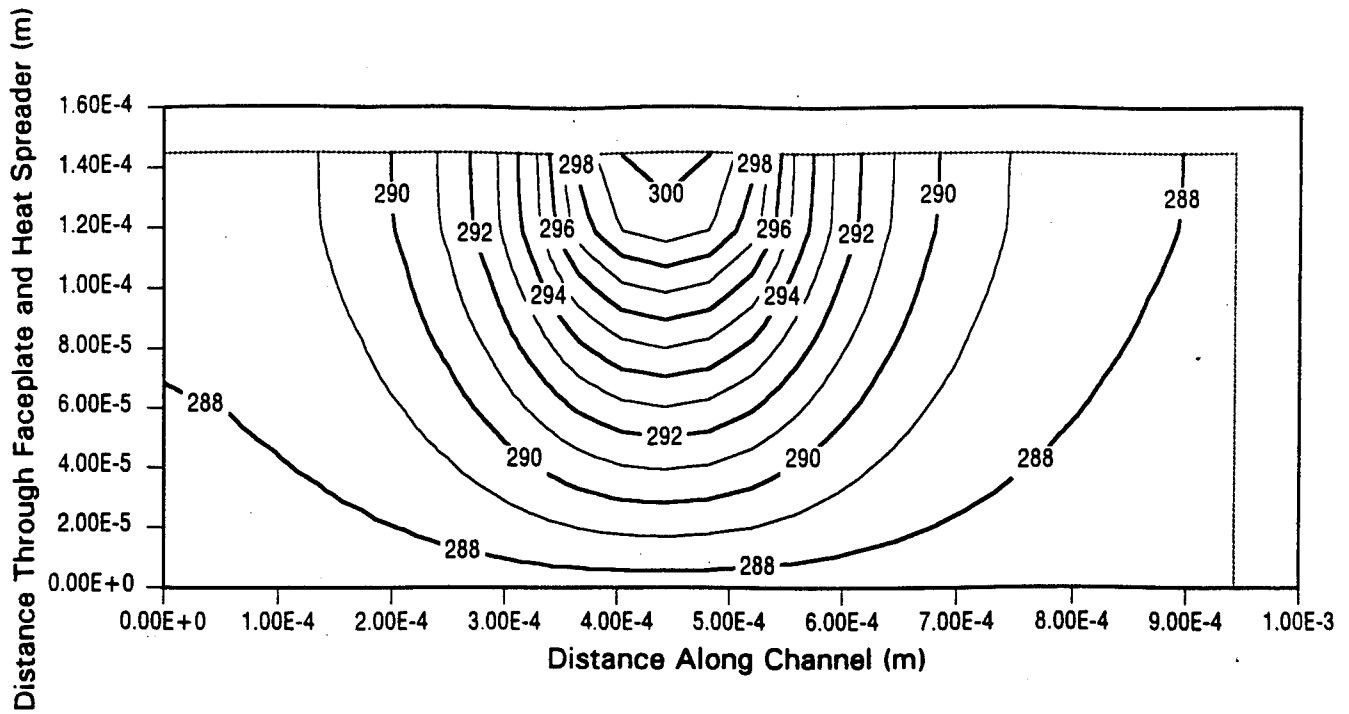


(c) thermal profiles for a 125 μm Cu faceplate with a 125 μm diamond heat spreader

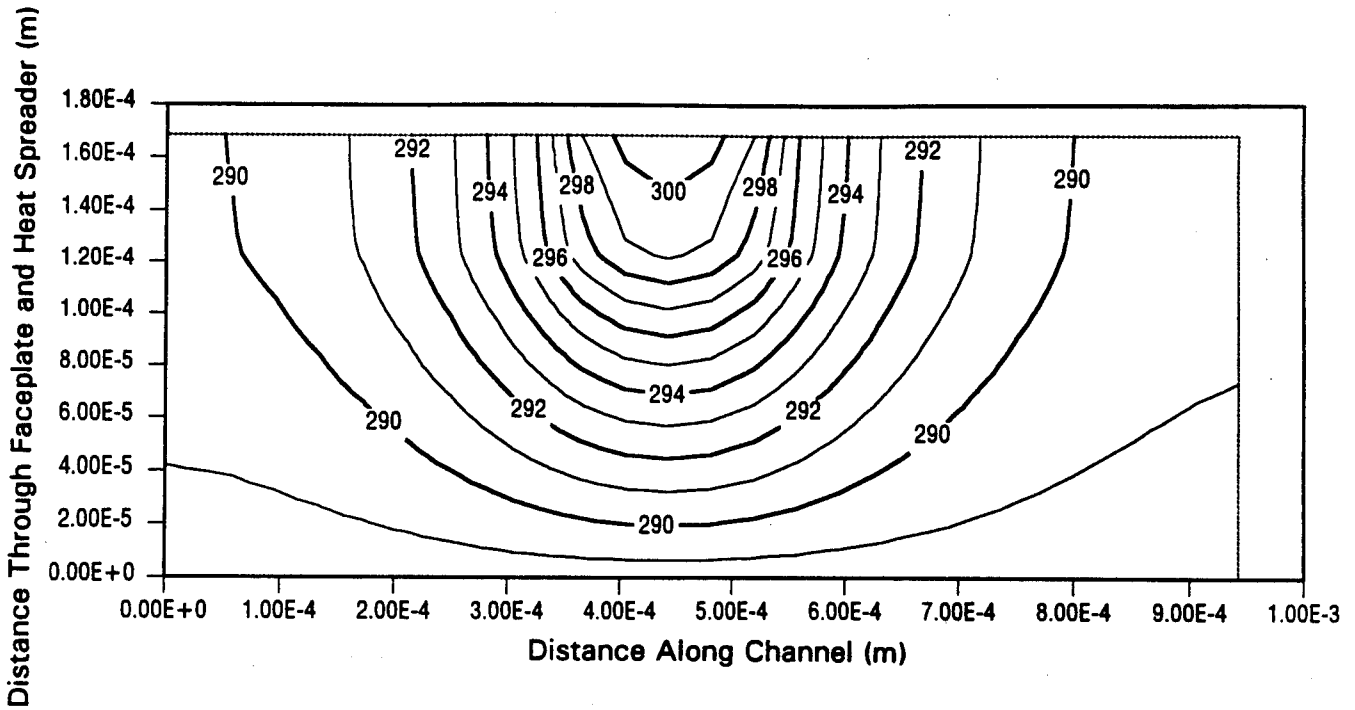


(d) thermal profiles for a 125 μm Cu faceplate with a 175 μm diamond heat spreader

Figure 20 (cont.). Thermal profiles for Cu faceplate with isotropic diamond heat spreader

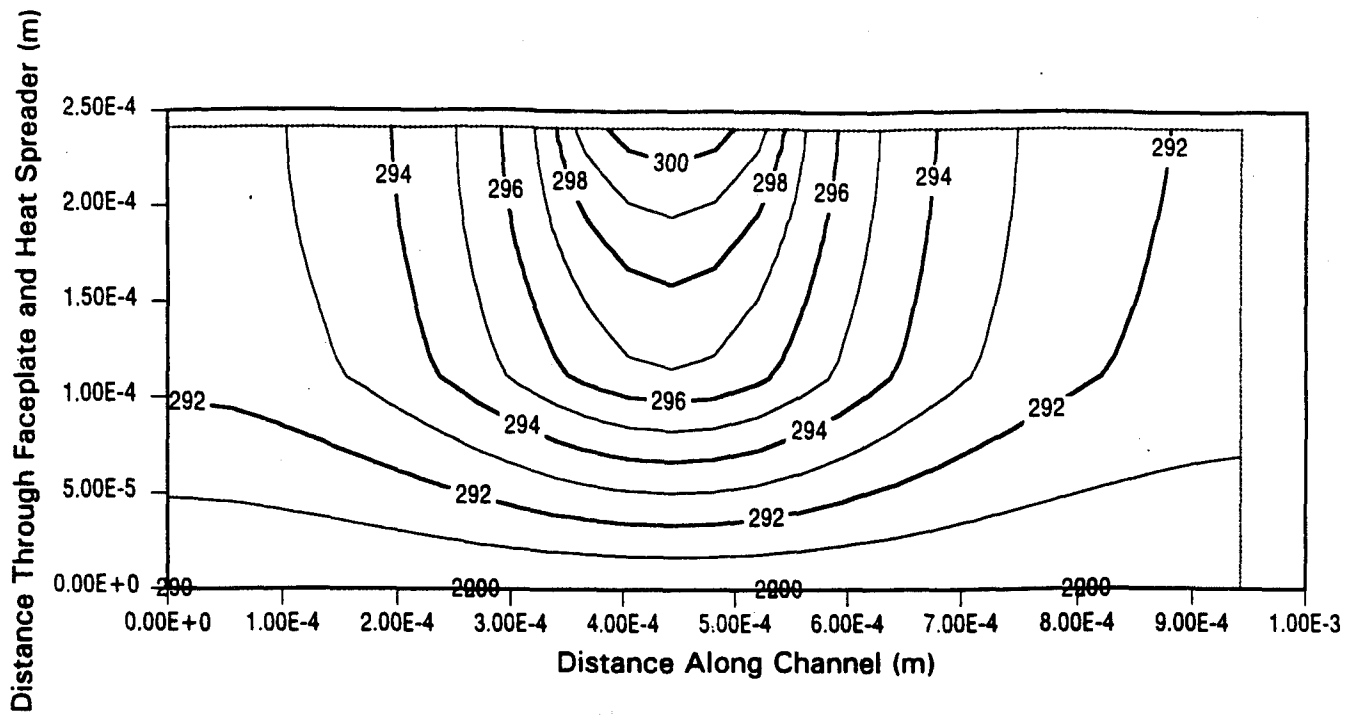


(a) thermal profiles for a 125 μm Cu faceplate with a 25 μm diamond heat spreader

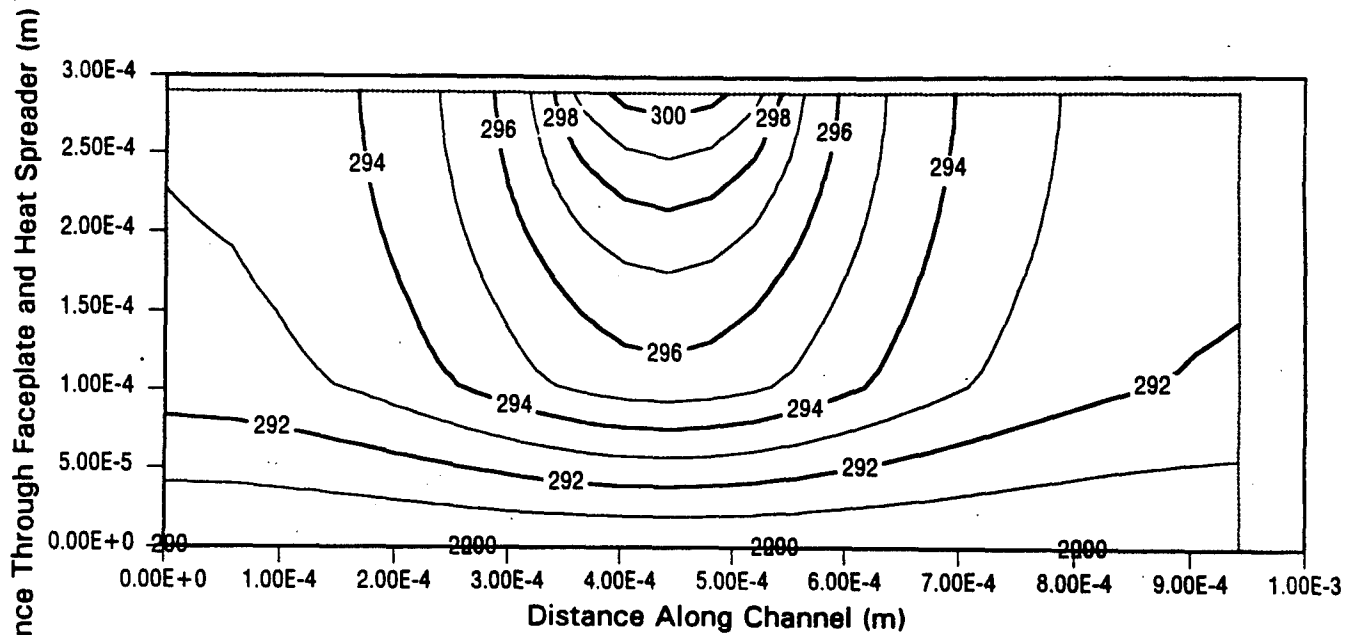


(b) thermal profiles for a 125 μm Cu faceplate with a 50 μm diamond heat spreader

Figure 21. Thermal profiles for copper faceplate with CVD diamond heat spreader



(c) thermal profiles for a 125 μm Cu faceplate with a 125 μm diamond heat spreader



(d) thermal profiles for a 125 μm Cu faceplate with a 175 μm diamond heat spreader

Figure 21 (cont.). Thermal profiles for copper faceplate with CVD diamond heat spreader

5.0 PROTOTYPE MODEL DESIGN AND FABRICATION

The observations resulting from the flowfield analyses were incorporated into the prototype design. It was decided to prepare designs for three prototypes. The first was a standard microchannel with rounded corners, to reduce recirculation along the heated wall. The second was a microchannel with secondary fins in the passage, to interrupt recirculation along the bottom wall. The third was an unconventional impingement jet design which sought to avoid the pitfalls of simpler passage designs. All three designs are described in more detail below.

The impingement design was given the highest priority, because it was expected to have the best thermal performance. The goal, however, was to build prototypes of all three designs if program resources allowed. Although several fabrication obstacles were encountered during the study, a prototype of each of the designs was fabricated. The fabrication process and results are discussed in Sections 5.2 and 5.3.

5.1 PROTOTYPE MODEL DESIGNS

The prototype designs were all based on 25 μm microchannel widths and 25 μm primary fins. This was a result of the trade studies, which indicated that very narrow channels were required, and as a result of fabricability concerns, which dictated that the copper foil thickness be at least 50 μm . Approximately 100 foils are used in each design, forming a 1 cm long cooler. The foils are stacked with the plane of the foils perpendicular to the laser diode axis, and each foil is 1 cm wide to accommodate the ten diode bars.

Each design is comprised of six different foil patterns: inlet, outlet, spacer, and 3 end cap designs. There are approximately 40 inlet foils, 40 outlet foils, 5 spacer foils, and 6 end cap foils. The microchannel sections for the inlet, outlet and spacer foils are identical; only the manifolding section is changed. The end cap foils have no microchannels. Specifics of the microchannel designs are discussed in the paragraphs below, followed by a description of the

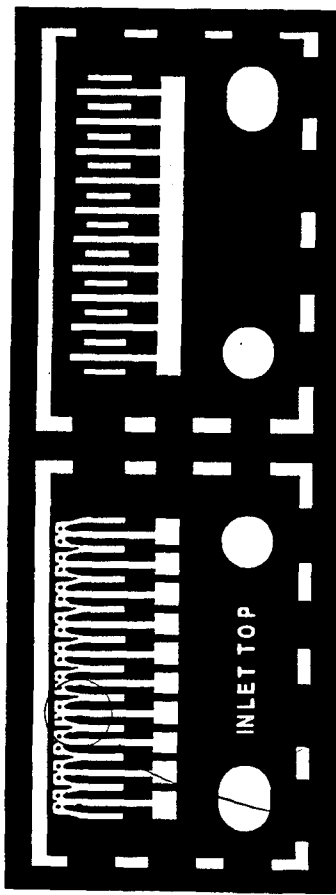
manifolding system. The manifolding discussion also includes conceptual drawings of the inlet, outlet, and space foils (Figure 23).

"Conventional" Microchannel Design. The "conventional" microchannel design had simple $25\ \mu\text{m} \times 400\ \mu\text{m}$ channels with $25\ \mu\text{m}$ fins. The channels were originally $775\ \mu\text{m}$ in length, but about $200\ \mu\text{m}$ was taken up on either end of the channel so that the inlet and outlet ports could be extended into the channel. This can be seen in Figure 25 in Section 5.3. The inlet and outlet extensions were included to minimize the pressure drop at those locations. In this design, the laser diode bar would be located at the midpoint of the channel.

"Conventional" Microchannel Design With Fins. A "conventional" finned design was prepared to allow comparison of the finned model performance to that of the model without fins. The fins were included to interrupt boundary layer formation along the channel walls, and to inhibit the formation of a recirculation zone on the channel "bottom". Due to the confined geometry of the microchannels, it was only possible to place about half of a unit cell of the fin array in the channels. This meant that the 1D predictions in Section 4.1 (which are based on analysis of a unit cell) would probably not be very accurate. The benefits of using fins, however, should still be measurable.

The channels sizes were identical to those for the unfinned microchannel design. Three fins were placed in each channel. Each fin was $50\ \mu\text{m}$ in diameter, and was placed in a staggered grid approximately $200\ \mu\text{m}$ from the other fins. The fins could have been designed with non-circular profiles, but for simplicity it was decided to use a standard pin fin shape. The etched channel with fins can be seen in Figure 25 in Section 5.3.

Impingement Design With Fins. The impingement design was prepared in an attempt to improve thermal performance without substantial pressure drop penalties. Jet impingement is a well-known means of augmenting heat transfer by a factor of 2 to 3 at the impingement point. As shown in Figure 22, the flow emerges from the inlet passages and impinges at the location of the laser diode bar. A stagnation region would normally form at the impingement



Front Side of Inlet Foil

Back Side of Inlet Foil

ACTUAL FOIL DESIGN

SKETCH OF MICROCHANNEL SECTION

Flow Travels Up the Inlet Secondary Manifold, Strikes the Flow Deflector, and is Split Toward the Outlet Secondary Manifolds on Either Side. The Laser Diode Bar Would be Centered at the Flow Deflector Location.

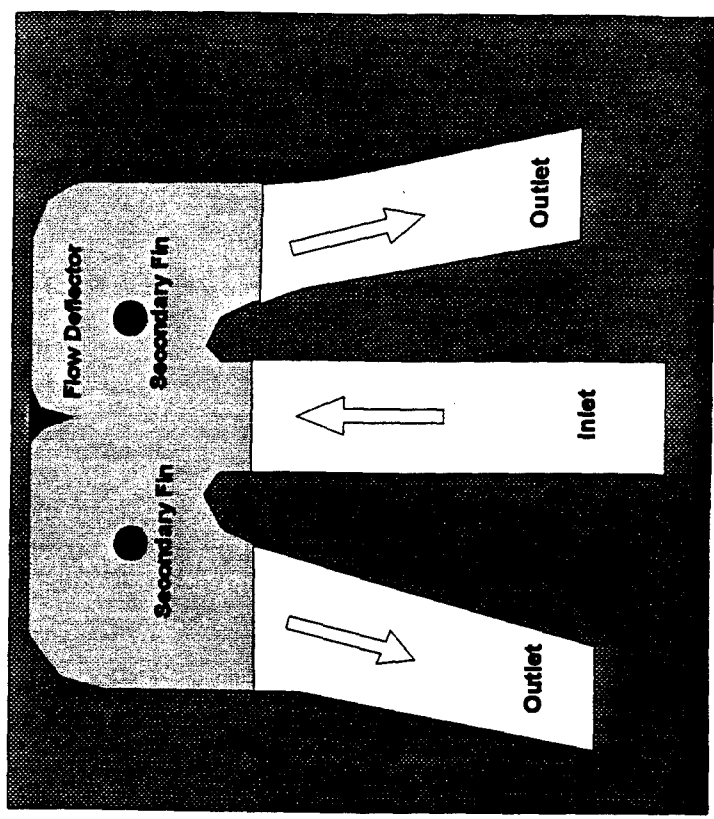


Figure 22. Sketch of impingement microchannel prototype design (inlet foil).

point, so a flow deflector has been placed there to improve heat transfer. Secondary fins and rounded channel corners are also included to reduce the formation of "dead" zones in the channel. The flow exits symmetrically about the inlet through the two outlets. Impinging jets are generally thought to increase the convective heat transfer coefficient at jet Reynolds numbers above 500, and especially past jet transition (at $Re = 1000$). An etched impingement foil is shown in Section 5.3 (Figure 25).

Manifolding design. The design of the manifolds is somewhat complex, but has distinct advantages compared to other approaches. The major benefit is that the manifolds are built right into the foil stack; a second advantage is distribution at low pressure losses to each of the 1000 microchannels in a typical design. The concept is shown in Figures 1 and 23.

In Figure 1 the end cap foils have been removed so that we can see the interior of the cooler. A large cavity at the bottom of the cooler, labelled "Main Inlet Manifold", serves as the interface between the secondary manifolds and the exterior plumbing. A coolant fitting provides coolant to the main manifold, which extends nearly halfway through the foil stack. At the midpoint in the stack, spacer foils block off the main inlet manifold, as can be seen in Figure 23, where the spacer foil is shown without the main manifold section. All the foils between the end cap foils and the spacer foils are of the "inlet" type, and all the foils after the spacer foils (except for the end cap foils at the opposite end) are "outlet" foils.

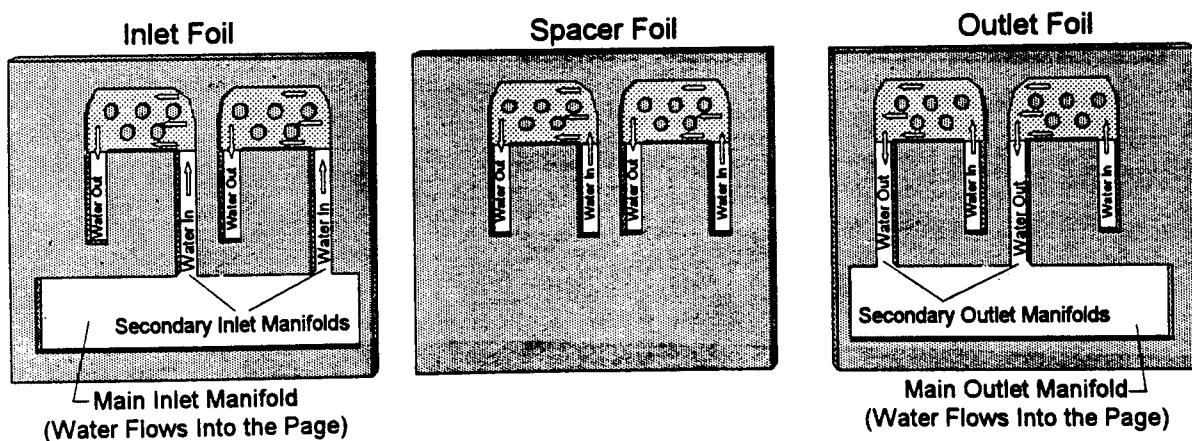


Figure 23. Flow concept for inlet, outlet and spacer foils.

The difference between the inlet and outlet foils is in the secondary manifolding. In the inlet foil in Figure 23, the main inlet manifold is connected to the secondary inlet manifold, which extend up to the microchannel. Note that the secondary manifolds are etched all the way through the foil, so that they form a continuous channel of their own (perpendicular to the page) as the foils are stacked up. This channel extends through all of the inlet foils, the spacer foils, and then on through the outlet foils. It is the means by which coolant is provided to the microchannels on the outlet foils. As shown in the figure, the outlet foil secondary inlet manifold is cut off from the main manifold, so it must receive coolant from secondary manifolds on adjacent foils.

The design is simply reversed for the outlet secondary manifolds. On the inlet foil, the main manifold provides coolant to the secondary manifold, which carries it to the microchannel. The coolant passes through the microchannel, absorbing energy from the heated surface, and then exits through the secondary outlet manifold. The outlet coolant is passed through the secondary outlet manifolds on adjacent foils until the outlet foils are reached, and the coolant can access the main outlet manifold.

The main manifolds have side access ports - this was for convenience during the Phase I work. In operational implementations, the main manifolds would be sealed at the ends and opened at the bottom, to allow coolant access directly behind the cooler. More spacer foils (~ 10) would be used to aid providing a good seal between the inlet and outlet manifolds. This configuration would permit coolers to be mated together in larger arrays, without interference from the coolant supply system.

5.2 FABRICATION PROCESS OVERVIEW

Saddleback Aerospace has developed an alternative microchannel design and fabrication approach, which is an outgrowth of prior high performance cooling research performed by Saddleback employees in support of semiconductor laser diode array coolers and advanced ICBM reentry vehicle development. The Saddleback approach is shown in Figure 24, where

a series of copper (or alternative metal) foils are soldered, brazed or diffusion bonded together in a transverse layup. As the figure shows, high aspect ratio channels are created by etching shallow surface features in individual metal laminates. This approach results in increased heat dissipation capabilities, simplified fabrication, and more robust microchannel structures compared to the conventional microchannel approaches described in Section 2. With the exception of porous matrix heat exchangers, microchannels of this type should provide the highest heat dissipation performance ever obtained for a single-phase forced convection cooling system.

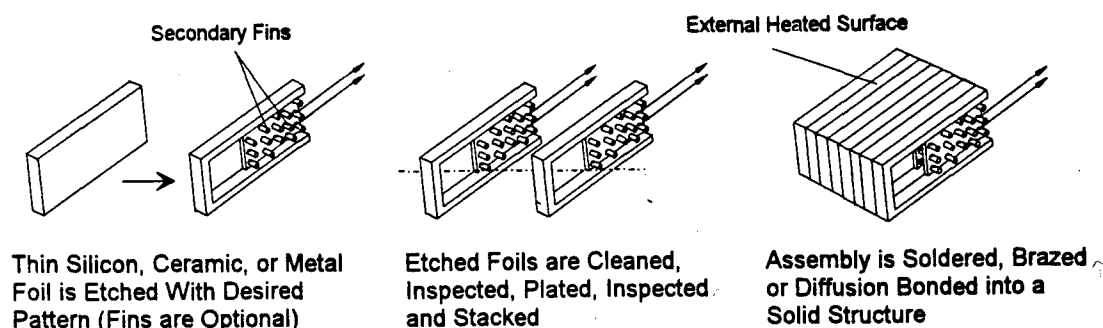


Figure 24. Laminated foil microchannel fabrication process.

As shown in Figure 24, the passages can be designed with secondary fins etched on the surfaces of the laminates, and the shapes and orientations of these fins can be tailored to increase heat transfer with minimum perturbation of the natural channel streamlines. Inclusion of secondary fins is not possible with conventional microchannels, but is straightforward with the Saddleback approach. Phase I calculations showed that the heat dissipation capability can be increased by more than 60% using secondary fins. The fins not only enhance the thermal performance, but they contribute to the structural integrity of the heat sink as well.

In addition to their thermal performance, these coolers offer several other advantages. Their all-metal construction makes them extremely rugged, facilitating handling and hardening them to use in environments with high shock and vibration levels. The use of a laminated foil approach makes the routing of coolant inlets and outlets very simple (as in Figure 1). The manifolds are actually built into the stack, unlike current silicon microchannel designs, where a separate glass manifold is bonded to the microchannel section.

5.3 FABRICATION OF THE PROTOTYPE MODELS

The fabrication of the prototype models followed the processes described in Section 5.2. ETP (electrolytic tough pitch) copper foil in 0.002" ($\sim 50 \mu\text{m}$) and 0.004" ($\sim 100 \mu\text{m}$) thicknesses was procured. OFHC (oxygen-free, high conductivity) copper was desired, but was unavailable in the requisite thicknesses. An R&D-scale photochemical etching capability was established at Saddleback, including artwork preparation, photoresist application and exposure, and chemical etching. All etching described in this report was conducted in the Saddleback facility.

The fabrication began with the impingement design, since it had been given the highest priority. Artwork for the impingement microchannel design was prepared by Saddleback using photographic processes. There were 6 different foil designs used in each cooler design, with 2 pieces of artwork for each design (for the front and back of each foil). For economy, and due to the small size of the cooler, 18 foils were included on each piece of master artwork. Before etching, each copper master sheet (i.e., 6.35 cm x 7.62 cm copper piece which would produce 18 individual foils) was cleaned and coated with photoresist. A fine-line electronics-grade resist was used (as opposed to a PC-board or machining-grade resist) to obtain the high resolution necessary for the fine features of the impingement design. The resist-coated sheet was placed between the two requisite pieces of artwork, and exposed to high-intensity near-UV light. Exposed resist was removed with a developer, and the remaining resist was hardened in a mild bake cycle.

Trial etches on copper foil samples were attempted in a bubble etcher using FeCl (a standard etchant), and the ability to etch small features such as the flow deflectors and secondary fins was demonstrated. These designs were fairly challenging in terms of the photochemical etching process. The desired features are very small (the secondary fins were 50 - 75 μm in diameter), and the copper foils are very thin (50 μm). During the Phase I proposal period, it was assumed that 100 μm foils would be used, but the trade studies indicated that the performance gains obtained by using thinner foils warranted the additional fabrication risk.

The predicted etch factors were verified (etch factors account for undercutting of etched features) on the 50 μm foil and on scrap pieces of 150 μm copper. Several lessons were noted during the trial etching, however. The first was that the 50 μm foils are exceedingly delicate, and this prompted a redesign of the manifold area to include support struts for cantilevered portions of the original design. Retention tabs (to keep individual foils within the master sheet during processing) were strengthened along the periphery of each foil, but removed from the heated surface side to avoid burrs or foil deformation along that critical boundary. The outlets were enlarged slightly to avoid the possibility of clogging during the soldering process, or fouling during operation.

As a result of the investigations described above, it was decided to generate new artwork. It had been noted during processing, however, that the accuracy of the photographic process required improvement. For this reason it was decided to use laser photoplotting to generate the artwork, rather than photographic processes. A file of the necessary photoplotter instructions was generated and sent to a local vendor, and new artwork was generated. Artwork was generated for all three designs.

Foils of the impingement design were etched and sent to a vendor for solder plating. The requested solder thickness was 2.5 μm , but it was found that the vendor had applied as much as 10 μm on the foils. Some trial soldering experiments demonstrated that this amount of solder completely clogged the microchannels, and in most cases the secondary manifolds as

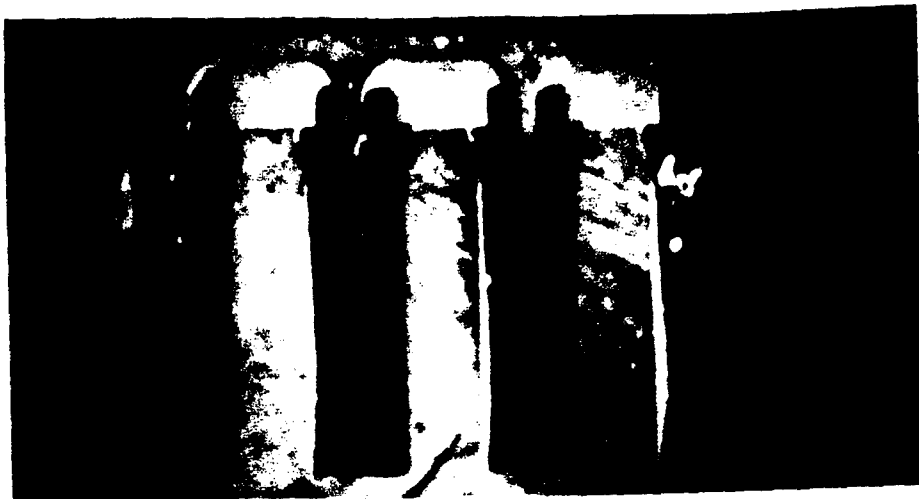
well. There being no means of removing the excess solder, the batch of foils was discarded and more foils were etched.

Foils for all three designs were etched using the same process described above. The microchannel sections etched very well; a portion of the microchannel section of each foil is shown in the photographs in Figure 25, where some of the details of the microchannels can be seen. The foils shown in Figure 25 were actually rejected as being unsuitable for inclusion in a cooler. The foils were again sent to the vendor for solder plating, and were returned with solder thicknesses of approximately $5 \mu\text{m}$. Trial soldering experiments indicated that this amount of solder was marginal, but time and resource limitations led to a decision to proceed with the fabrication process.

A model was fabricated for each design. The etched foils were inspected, and the best were selected for use in the models. Seventy good foils were selected for the conventional finned model, and ninety foils were selected for the other two models. The models were thus approximately 5 times the required length, but the larger size facilitated thermal testing and represented a more stressing fabrication case. The foils for each model were soldered together using the soldering fixture shown in Figure 26. The soldering was completed successfully, a picture of the three completed models is shown in Figure 27.

The first two prototypes fabricated, the conventional channel with fins, and the conventional channel without fins, encountered some difficulties, due to the developmental nature of the fabrication process and the excess solder applied to the foils. These two models are suspected to have a large amount of internal foil deformation and solder movement. These models were considered unsuitable for thermal performance testing, due to excessive pressure losses.

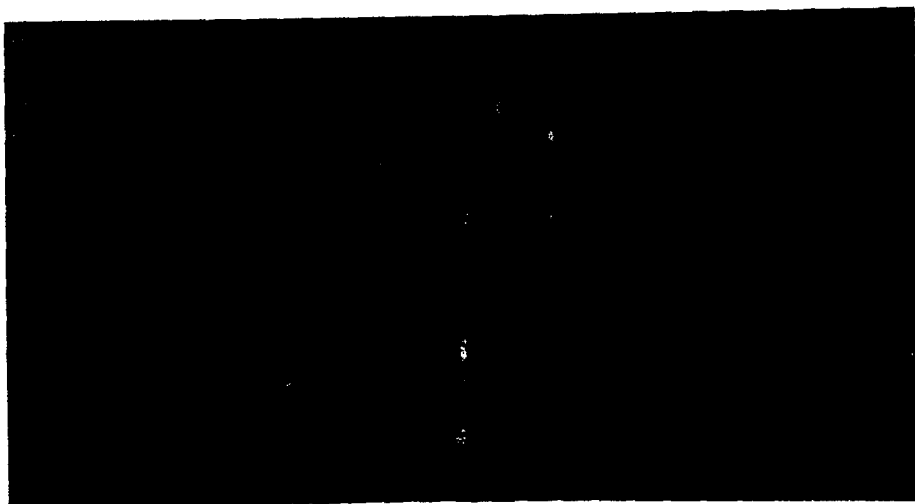
The fabrication process for the third prototype, the impingement model, took advantage of the lessons learned from the first two models, and internal foil deformation was eliminated. There was still the possibility of some solder movement within the stack, however, which



(a) conventional microchannel



(b) conventional microchannel with fins



(c) impingement foil

Figure 25. Microchannel section of etched foils (approximately 32X).

could have resulted in total or partial clogging of the microchannels. As discussed below, it is suspected that partial clogging did occur, although the model was still testable and showed excellent thermal performance.

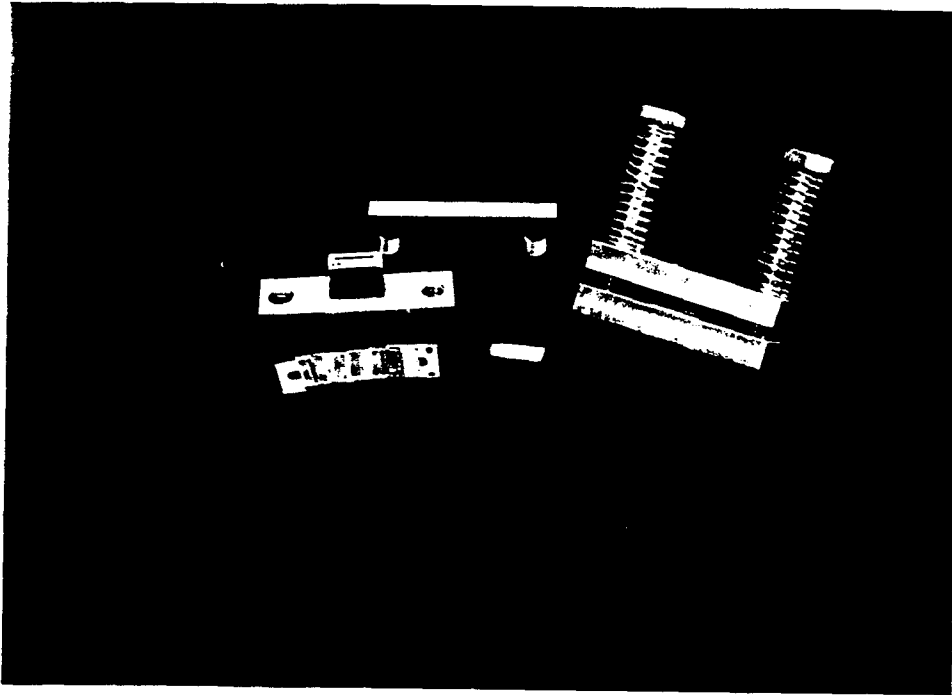


Figure 26. Soldering fixtures used in the Phase I study.

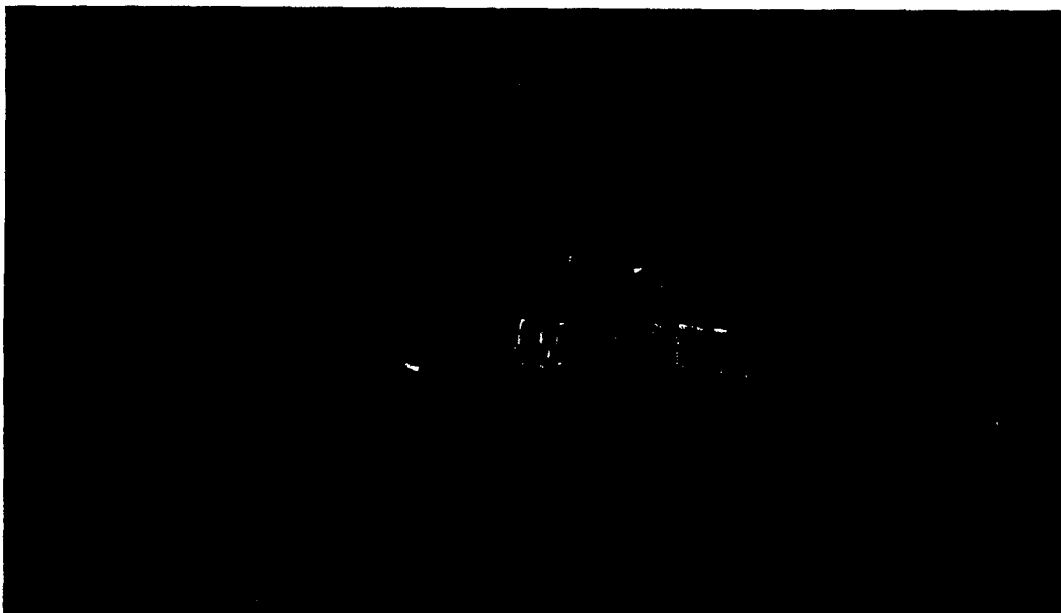


Figure 27. The three microchannel models fabricated in this program.

6.0 TESTING OF THE PROTOTYPE MODELS

A simple test setup was assembled to measure the flow and thermal performance of the models. A water supply system was assembled; it is designed to be able to supply chilled, room temperature, or heated water at supply pressures up to 200 psi. Peak testing pressures were less than 100 psi. Thermocouples were installed on the upstream and downstream water lines to measure the inlet and outlet coolant temperatures. A pressure gauge was placed just upstream of the thermocouples to provide inlet pressure measurements. The outlet pressure was atmospheric, since the coolant ran out of the model and into an open receptacle. Water flow rates were measured by collecting water during the test and dividing by the test duration.

The models were placed in a model holder, as shown in Figure 28. The small silicone rubber seals served to both seal the cooler/holder inlet and outlet, and to thermally isolate the cooler from the holder. The estimated thermal resistance of the seals is about $6\text{ }^{\circ}\text{C}/(\text{W}/\text{cm}^2)$, while the thermal resistance of the cooler is less than $0.1\text{ }^{\circ}\text{C}/(\text{W}/\text{cm}^2)$. The results of the testing using this arrangement are discussed below.

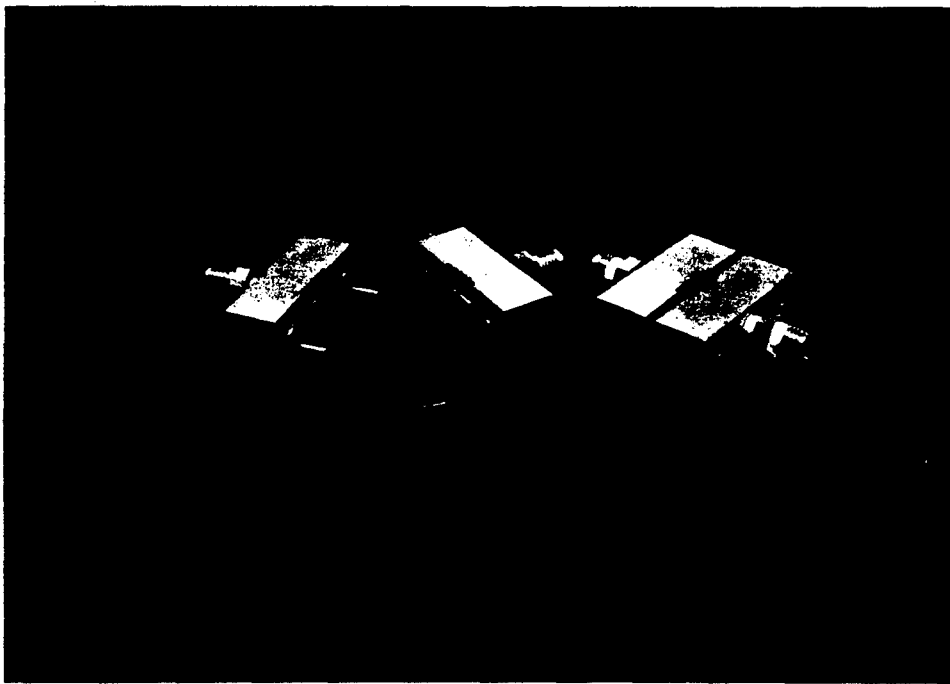


Figure 28. Model holders for flow and thermal performance testing.

6.1 FLOW PERFORMANCE TESTING

The pressure drop across all three models was measured as a function of flow rate. The results of these tests are shown in Figure 29, which compares the measured pressure drops for each model. As shown, the first two models fabricated, the finned and unfinned "conventional" microchannel designs, had substantially higher pressure drops for the same mass flow rate than the pressure drops for the impingement design. The high pressure losses in the conventional designs made testing at higher flow rates both more difficult and less interesting, so they were only tested until their trends became evident. The "system" measurements included on the chart represent the pressure drop measured with no model present. That is, this was a measurement of the pressure losses due to the inlet and exit tubing, the model holders, fittings and seals. To obtain true pressure drops for the models, the system pressure drop should be subtracted from the measured model pressure drop (at the same flow rate).

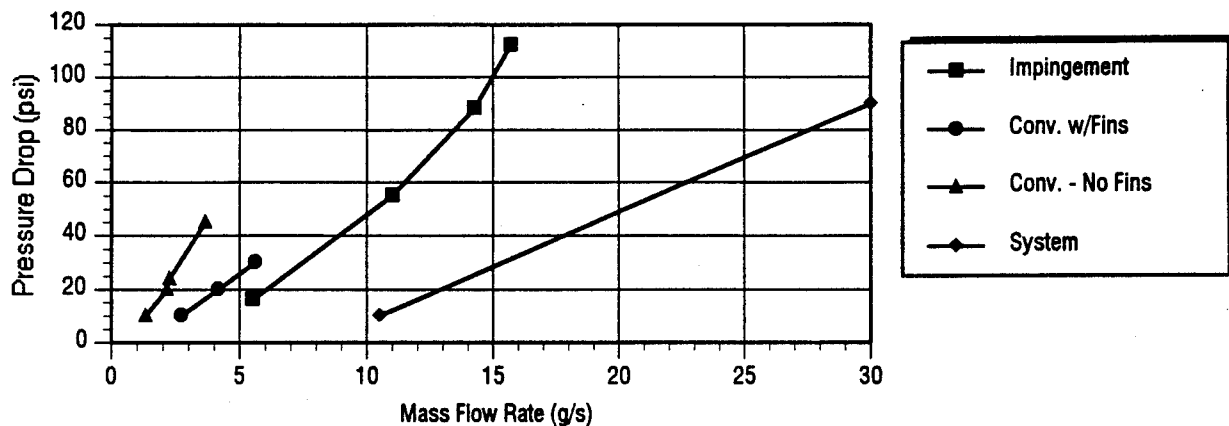


Figure 29. Pressure drop performance of prototype models.

The flow performance was found to be repeatable after a 2 μm filter was installed upstream of the model. Prior to that time there was a fair degree of clogging due to dirt in the model, solder flux, metallic particles and teflon tape particles. Since the models were changed out quite frequently during the testing, it was fairly easy for contaminants to enter the system.

Prior to testing, the models were boiled in a solvent to remove solder flux and other particles. It is not clear, however, that the solder flux was completely removed, and this surviving flux could be partly responsible for internal blockage.

The measurements of the pressure drops for the models are consistent with laminar flow conditions in the microchannels. The Reynolds numbers are less than 100, so the hydrodynamic development lengths are very short, and the flow is essentially unperturbed by the presence of fins. The measured pressure drops for the impingement design are about a factor of 3-4 higher than predicted - it is suspected that this was due to clogging in the microchannels. As mentioned previously, solder and solder flux are the most likely sources of this clogging. It was calculated that if half of each channel were blocked, the pressure drops would correspond to the measurements.

6.2 THERMAL PERFORMANCE TESTING

As was shown in the photograph in Figure 2, the impingement model was subjected to thermal testing up to nearly 500 W/cm^2 . The thermal performance testing was conducted using a heat gun to provide a heat flux of about 85 W/cm^2 , and a propane torch to provide heat fluxes of about 225 and 490 W/cm^2 . As can be seen in Figure 2, the high heat flux torch test is a severe thermal environment, where poor heat transfer performance can quickly result in model failure.

The heat flux level was calculated by measuring the water mass flow rate and inlet and outlet water temperatures. The water measurements are considered the absolute measurement of the effectiveness of the cooler; the only way to measure the effectiveness of the cooler in transferring energy into the coolant is to measure the energy absorbed by the coolant. The heat flux measurements were verified in independent testing using a slug calorimeter. It is felt that the heat flux measurements are accurate to within $\pm 5\%$.

The surface temperature was measured by pressing two thermocouple wires against the heated surface. The wires were spaced approximately 2 mm apart, so thermal gradients in the material could have influenced the measurement. Unless substantial clogging is present, however, thermal gradients on the surface should have been small. This measurement is very difficult to make reliably at higher heat fluxes - in future efforts internal thermocouples located close to the heated surface will be used. It is difficult to make an estimate of the accuracy of this measurement, since the largest sources of error do not lie in the measurement devices. We estimate that $\pm 5\%$ is a reasonably conservative value, particularly given the consistency of the test results.

The data from the tests are shown in Figure 30, which plots the total heat absorbed by the water versus the temperature difference between the water and the heated surface. The straight line suggests that the heat transfer coefficient was the same during all the tests, and this is borne out in the data plotted in Figure 31, which shows that the heat transfer coefficient based on the heated surface area was about $12 \text{ W}/^\circ\text{C}/\text{cm}^2$, regardless of the mass flow rate. The behavior of the heat transfer coefficient with respect to mass flow rate is typical of laminar pipe flows, and this is also consistent with the flow performance measurements.

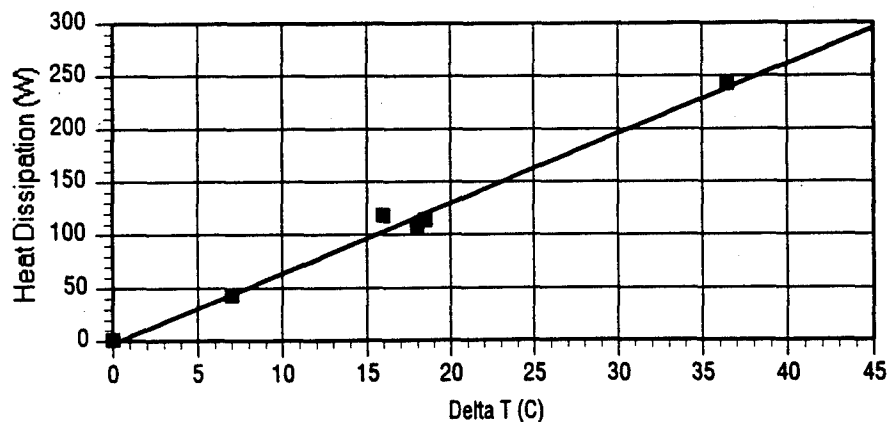


Figure 30. Thermal performance of impingement prototype.

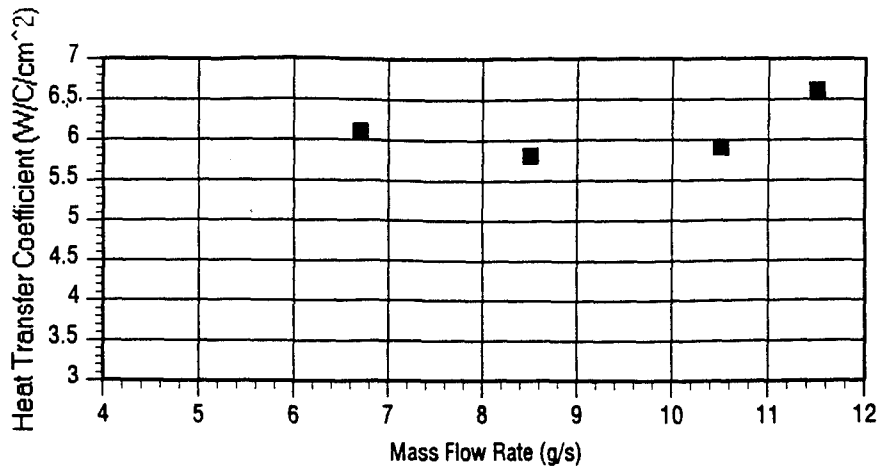


Figure 31. Heat transfer coefficient as a function of mass flow rate

The thermal resistance based on the measured heat transfer coefficient is then $0.083 \text{ }^{\circ}\text{C}\text{-cm}^2/\text{W}$. This can be compared to results reported in the literature, tabulated in Table 1. As discussed in Section 2, the thermal resistance numbers should be used with caution, since thermal spreading effects make comparisons among tests with different geometries very difficult. After reviewing the Table 1 data, much of which is discussed in detail in Section 2, it appears that only the 1st entry in the table has superior performance to that measured in this program. Our estimate of the 1D thermal resistance of the LLNL silicon microchannel cooler is $0.048 \text{ }^{\circ}\text{C}/(\text{W}/\text{cm}^2)$.

Phase I Performance Summary. Having accounted for thermal spreading effects, the Saddleback thermal resistance is still more than 40% larger than the Lawrence Livermore results, and this is inconsistent with the predicted thermal resistance of $< 0.02 \text{ }^{\circ}\text{C}\text{-cm}^2/\text{W}$. The discrepancy is thought to be due to two effects:

- 1) The model was operating at reduced flow rates, and thus reduced Reynolds numbers, due to the excessive pressure losses. The fins begin to be effective at Reynolds number of 400 - more than 4 times the maximum Reynolds number during the tests. Similarly, the impingement design would expect to

show advantages at $Re > 500$. At higher Reynolds numbers, the heat transfer coefficient would be expected to increase, and the caloric resistance (i.e., the effective resistance due to the coolant temperature rise) would also drop.

- 2) If the channels in the model were half-clogged, as described above in the flow performance discussion, the heat transfer area would be reduced, further increasing the total thermal resistance.

When these two effects (due to a single cause \Rightarrow clogging of the flow passages) are taken into account, the predicted heat transfer coefficients are consistent with the measurements. As mentioned above, the clogging can also explain the flow performance results, and the thermal and flow measurements can both be predicted by assuming 50% clogging in the microchannels.

Of course, the thermal resistance value of $0.083 \text{ }^\circ\text{C-cm}^2/\text{W}$ measured in the tests is itself very low, and unequalled except by the silicon microchannel coolers built by Lawrence Livermore. It should be noted that the absolute capacity of the Saddleback cooler was larger than any of the other coolers listed - the Saddleback cooler absorbed 245 W, while the next largest capacity was demonstrated by LLNL, with 160 W. There are prospects for improvement, however, are apparent and significant - motivating further study of this approach.

7.0 CONCLUSIONS AND RECOMMENDATIONS

The Phase I program had two major objectives: first, to show that it was possible to fabricate a microchannel cooling device by soldering thin copper foils together; and second, to show that the fabricated device could dissipate large amounts of heat while maintaining a low surface temperature. These objectives were satisfied, serving to demonstrate the feasibility of the laminated foil approach, and motivating further work in this area. Though the Phase I results were very promising, although several areas of design and fabrication improvements were identified.

The thermal resistance of the prototype model, measured as $0.83 \text{ }^{\circ}\text{C}/(\text{W}/\text{cm}^2)$, was about 4 times the expected value, and this was attributed to internal clogging from solder and solder flux. It is anticipated that if these problems were eliminated, the thermal resistance would drop to a much lower value, and the microchannel cooler would be capable of meeting Phillips Laboratory's stringent heat dissipation requirements. Regardless, the thermal resistance measured here was one of the lowest ever measured for a single-phase forced convection system.

The experiences of the Phase I program have resulted in the identification of four distinct areas for further research and development:

- 1) Developing an understanding the detailed heat transfer and flowfield physics of microchannel configurations, and using this understanding to improve analytic tools and optimize the design,
- 2) Addressing thermal managment needs for a broader range of laser diode arrays, in addition to the single configuration examined in the Phase I study,
- 3) Refining the fabrication process to eliminate difficulties encountered in the Phase I, and to lower the fabrication costs for larger quantities of coolers.

- 4) Examining implementation requirements: electrical connections, mounting, plumbing, pumps, seals, etc., to aid in placing coolers into service as quickly as possible.

A variety of specific tasks suggest themselves, including: 1) comparing various analytic methods against test data, 2) upgrading the MICROHEX code, 3) establishing basic flow and heat transfer coefficients for simple micro-flow configurations, 4) establishing detailed understanding of the fluid and thermal performance of the Phase I prototype designs, examining several alternate design concepts to address a greater variety of user needs, 5) improving the joining process using soldering and diffusion bonding, 6) etching larger sheets, with more parts per sheet, with fewer defects per sheet, 7) demonstrating the low thermal resistance physical attachment of a laser diode to a cooler, and 8) building an integrated, compact cooling system to demonstrate use of microchannel coolers with minimal system impact.

A key question for future studies is the performance of turbulent flow designs. Several authors have claimed that turbulent flow microchannels can provide decreased thermal resistance at increased passage sizes, thus improving performance while reducing manufacturing tolerances. No test data to support these predictions is yet available, however. Future studies should make resolution of this issue a priority, since this can substantially change the design philosophy of microchannel systems.

REFERENCES

1. R. Beach, et al., "Modular microchannel cooled heatsinks for high average power laser diode arrays," IEEE Journal of Quantum Electronics, Vol. 28, No. 4, pp. 966-976, April 1992.
2. D. Munding, et al., "High average power edge emitting laser diode arrays on silicon microchannel coolers," Appl. Phys. Lett., Vol. 57, No. 21, pp. 2172 - 2174, 19 November 1990.
3. R. Beach, et al., "High-reliability silicon microchannel submount for high average power laser diode arrays," Appl. Phys. Lett., Vol. 56, No. 21, pp. 2065 - 2067, 21 May 1990.
4. R. J. Phillips, "Forced-Convection, Liquid-Cooled Microchannel Heat Sinks," AD-A193-337, MIT/LL Technical Report 787, 7 January 1988.
5. L. J. Missaggia, et al., "Microchannel heat sinks for two-dimensional high-power-density diode laser arrays," IEEE Journal of Quantum Electronics, Vol. 25, NO. 9, pp. 1988 - 1992, 9 September 1989.
6. S. H. Macomber, et al., "recent developments in surface emitting distributed feedback arrays," SPIE Vol. 1219, p. 228 - 232, 1990.
7. D. Nayak, et al., "A high-performance thermal module for computer packaging," J. of Elec. Matls., Vol. 16, No. 5, pp. 357 - 364, 1987.
8. J. Arthur, et al., "Microchannel water cooling of silicon x-ray monochromator crystals," Rev. Sci. Instrum., Vol. 63, No. 1, pp. 433 - 436, January 1992.
9. T. Kishimoto and T. Ohsaki, "VLSI packaging technique using liquid-cooled channels," IEEE Transactions on Components, Hybrids, and Manufacturing Technology, Vol. CHMT-9, No. 4, pp. 328 - 335, December 1987.
10. M. G. Grote, et al., "Test results of wafer thin coolers at heat fluxes from 5 to 125 W/cm²," SAE No. 880997, 18th Intersociety Conference on Environmental Systems, 11 - 13 July, 1988.
11. D. B. Tuckerman and R. F. W. Pease, "High-performance heat sinking for VLSI," IEEE Electron Device Letters, EDL-2, pp. 126-129, 1981.
12. D. B. Tuckerman, "Heat-transfer microstructures for integrated circuits," Ph.D. Thesis, Stanford University, 1984.

REFERENCES (continued)

13. E. A. Foumeny and P. J. Heggs, "Heat Exchange Engineering, Vol. 2 compact heat exchangers: techniques of size reduction," Ellis Horwood, New York, NY, 1991.
14. J. Goodling, "Microchannel heat exchangers - a review," SPIE Vol. 1997, Paper No. 1997-06, High Heat Flux Engineering II, 12-13 July 1993.
15. R. Beach, et al., "Modular microchannel cooled heatsinks for high average power laser diode arrays," IEEE J. of Quantum Electronics, Vol. 28, No. 4, pp. 966 - 976, April 1992.
16. "High-Repetition-Rate, Diode-Pumped, Solid-State Slab Lasers," Energy and Technology Reviews, June 1992.
17. A. F. Bernhardt, N. J. Colella and R. J. Contolini, "Microchannel Cooling of RF Amplifiers," UCID-21953, Informal report to document work on a DOE contract, January 15, 1990.
18. D. Munding, et al., "Demonstration of high-performance silicon microchannel heat exchangers for laser diode array cooling," Applied Physics Letters, Vol. 53, No. 12, pp. 1030 - 1032, 19 September 1988.
19. W. J. Bennett, et al., "Microchannel-cooled heatsinks for high-average-power laser diode arrays," SPIE Vol. 1997, Paper No. 1997-09, High Heat Flux Engineering II, 12-13 July 1993.
20. L. J. Missaggia and J. N. Walpole, "A microchannel heat sink with alternating directions of water flow in adjacent channels," SPIE Vol. 1582, Integrated Optoelectronics for Communication and Processing, 1991.
21. R. E. Hendron, et al., "Stackable wafer thin coolers for high power laser diode arrays," SPIE Vol. 1219, Laser-Diode Technology and Applications II, 1990.
22. T. J. Bland, R. E. Niggemann, and M. B. Parekh, "A compact high intensity cooler (CHIC)," SAE Technical Paper Series #831127, presented at the 13th Intersociety Conference on Environmental Systems, July 11 - 13, 1983.
23. D. H. Bilderback, "Fabricating rectangular internal cooling channels for silicon x-ray monochromator optics," Rev. Sci. Instrum., 60(7), pp. 1977 - 1978, July 1989.

REFERENCES (continued)

- 73 24. T. Oversluizen, et al., "Performance of a directly water-cooled silicon crystal for use in high-power synchrotron radiation applications," Rev. Sci. Instrum., 60(7), pp. 1493 - 1496, July 1989.
- 21 25. R. K. Smither, et al., "Liquid gallium cooling of silicon crystals in high intensity photon beams," Rev. Sci. Instrum., 60(7), pp. 1486 - 1492, July 1989.
26. R. K. Smithers, et al., "Recent experiments with liquid gallium cooling of crystal diffraction optics," Rev. Sci. Instrum., 63(2), pp. 1746 - 1754, February 1992.
27. S. Sasaki and T. Kishimoto, "Optimal structure for microgrooved cooling fin for high-power LSI devices," Electronics Letters, Vol. 22, No. 25, pp. 1332 - 1333, 4 December 1986.
28. T. Kishimoto and S. Sasaki, "Cooling characteristics of diamond-shaped interrupted-cooling fin for high-power LSI devices," Electronics Letters, Vol. 23, No. 9, pp. 456 - 457, 23 April 1987.
29. J. E. Eninger, et al., High-Intensity Heat Exchanger Program, PL-TR-91-1076, Phillips Laboratory, Kirtland AFB, NM, April 1992.
30. N. Goldberg, "Narrow channel forced air heat sink," IEEE Trans. on Component, Hybrids, and Manufacturing Technology, Vol. CHMT-7, No. 1, March 1984.
31. R. W. Knight, "Optimal thermal design of forced convection heat sinks - analytical," Journal of Electronic Packaging, Vol. 113, pp. 313 - 321, September 1991.
32. R. W. Knight, et al., "Heat sink optimization with application to microchannels," IEEE Transactions on Components, Hybrids, and Manufacturing Technology, Vol. 15, No. 5, pp. 832 - 842, October 1992.
33. R. W. Knight, J. S. Goodling, and B. E. Gross, "Optimal thermal design of air cooled forced convection finned heat sinks - experimental verification," IEEE Transactions on Components, Hybrids and Manufacturing Technology, Vol. 15, No. 5, pp. 754 - 760, October 1992.
34. K. Tsubouchi, et al., "Theoretical analysis for a new package concept: high-speed heat removal for VLSI using AlN heat-spreading layer and microchannel fin," Japanese Journal of Applied Physics, Vol. 30, No. 1B, pp. L88 - L91, January 1990.

REFERENCES (concluded)

35. V. K. Samalam, "Convective heat transfer in microchannels," Journal of Electronic Materials, Vol. 18, No. 5, 1989.
36. R. W. Keyes, "Heat transfer in forced convection through fins," IEEE Transactions on Electron Devices, Vol. ED-31, No. 9, pp. 1218 - 1221, September 1984.
37. W. Nakayama and A. E. Bergles, "Cooling electronic equipment: past, present, and future," Heat Transfer in Electronic and Microelectronic Equipment, ed. by A. E. Bergles, Hemisphere Publishing Corporation, 1990.
38. J. W. Scott, et al., "Modeling the current to light characteristics of index-guided vertical-cavity surface-emitting lasers," Applied Physics Letters, Vol. 62, No. 10, pp. 1050 - 1052, 8 March 1993.
39. J. G. Endriz, et al., "High power diode laser arrays," IEEE Journal of Quantum Electronics, Vol. 28, No. 4, pp. 952 - 965, April, 1992.
40. E. F. Borchelt and G. Lu, "Applications of diamond made by chemical vapor deposition for semiconductor laser submounts," SPIE Vol. 1851, Processing and Packaging of Semiconductor Lasers and Optoelectronic Devices, ed. by H. Temkin, 20 - 21 January 1993.

DISTRIBUTION LIST

AUL/LSE Bldg 1405 - 600 Chennault Circle Maxwell AFB, AL 36112-6424	1 cy
DTIC/OCC Cameron Station Alexandria, VA 22304-6145	2 cys
AFSAA/SAI 1580 Air Force Pentagon Washington, DC 20330-1580	1 cy
PL/SUL Kirtland AFB, NM 87117-5776	2 cys
PL/HO Kirtland AFB, NM 87117-5776	1 cy
Official Record Copy	
PL/VTPT/Larry Crawford	2 cys
Dr. R. V. Wick PL/VT Kirtland, AFB, NM 87117-5776	1 cy